1993

An investigation of electrorheologial material adaptive structures

David L. Don
Lehigh University

AUTHOR:

Don, David L.

TITLE:

An Investigation of Electrorheological Material Adaptive Structures

DATE: May 30, 1993

An Investigation of Electrorheological Material Adaptive Structures

by

David L. Don

A Thesis

Presented to the Graduate and Research Committee

of Lehigh University

in Candidacy for the Degree of

Masters of Science

in

The Department of Mechanical Engineering and Mechanics

Lehigh University

1993

CERTIFICATE OF APPROVAL

This thesis is accepted and approved in partial fulfillment of the requirements for the Master of Science.

May 21, 1993
Date

Thesis Advisor
Dr. John P. Coulter

Chairperson
Dr. Robert P. Wei

Acknowledgements

First, I would like to thank my parents, Dr. Sherman Don and Gloria Chang, for supporting me throughout my academic career. Without their never ending emotional and financial support through these years, the completion of this effort would not have been possible. I will forever be indebted.

Second, I would like to thank Dr. John P. Coulter for choosing me as your first graduate student. My confidence in my abilities and my understanding of the surrounding environment has forever benefited. As a friend and advisee - thank you.

I would also like to acknowledge my fellow graduate students who I have worked, played, and partied with. There are *so* many to recognize - My roommates Alejandro Martin Mayori, Edward I. Wolfe IV, Steven P. Wolfe, and Joe Towfigi for not only providing support but doing the dishes; Muge Demir (pronounced müge) and friends for keeping me entertained and well fed; My co-workers, William H. Umbenhaur III, Aki, and the rest of the gang for letting me think I was important; My drinking buddies Jin H. Kim, James Mitrano, Eric Brause, and the rest of the Thursday night crew for keeping me up all night and making the house smell like beer and cigarettes. I will remember the times.

I can't forget my *old* friends Parker M. Normann, Edward S. Regan, the rest of the Lehigh gang, and Glen S. Gregory. Guys, Parker is going to marry first. Thanks for hanging around.

I would like to also acknowledge a couple of undergraduates who worked on the project with me. Michelle Parker and Mike Butzkies, thanks for doing some of the grunt work. Your persistence and efforts are appreciated. Thanks goes to out Dr. Stanley H. Johnson for giving me the "spark" to pursue an engineering career. You made it look fun.

Finally, I would like to acknowledge and thank the sponsors for this project. Funding was provided by Lehigh University, the National Science Foundation (grant no. MSS-9110909), and the U.S. Army Research Office (grant no. DAAL03-92-G-0388). Materials and supplies were generously provided by Dr. Keith D. Weiss, and Dr. Ted G. Duclos from Lord Corporation, and Dr. Frank Arcella and Paul Biermann from Johns Hopkins Applied Physics Laboratory.

TABLE OF CONTENTS

LIST OF FIGURES

LIST OF TABLES

NOMENCLATURE

RHEOLOGLICAL INVESTIGATION

τ	Shear stress
G	Shear Modulus
γ	Shear strain
ω	Radial sinusoidal excitation frequency
ϕ	Phase angle

STRUCTURAL INVESTIGATION

$m(x)$	Mass per unit length
w	Displacement in the vertical direction
E_i	Tensile elasticity of the ith layer
I_i	Moment of inertia of layer ith layer
H_i	Height of ith layer
H_{ij}	Distance away of ith layer from the jth layer
H_{i0}	Distance away from ith layer to the new neutral plane constructed by the addition of the constraining and sandwiched layers
ϕ	Flexural angle
B	Effective Flexural Rigidity
D	Distance the neutral plane is adjusted by the addition of constraining and sandwiched layers
g	Geometric shear parameter
Y	Geometric parameter
G_2'	Real part of the shear modulus of the sandwiched layer
β	Loss factor of the sandwiched material

λ	Wave number for simply supported boundary condition
ω	Natural frequency of the structure
η	Damping of the structure

ABSTRACT

The investigation examined the application of electrorheological (ER) materials in adaptive or intelligent structural systems. The first phase of this investigation characterized the linear viscoelastic behavior of ER material 6533-30B obtained from Lord Corporation. The material behaved linear viscoelastically up to approximately 1% strain within an electric field range from 1.5 to 3.0 kV/mm and a frequency range from 0 to 50 Hz. The yield strain was dependent upon electric field and slightly dependent upon frequency. A positive correlation existed between electric field and yield strain and a negative correlation existed between frequency and yield strain. Within the linear regime, the material behavior, as quantified by the complex shear modulus, was dependent upon electric field. The modulus increased in a parabolic manner with increases in electric field. These experimentally determined properties were substituted into the Ross, Kerwin, and Ungar, and Mead and Markus models that predict dynamic response of 3 layer composite beam structures. The models predicted the resonance frequency of the experimentally fabricated structures, but was less effective in predicting the damping of those structures. In addition to simple beam structures, an experimental feasibility analysis of a multi-electrode ER based structure was done. The resonance frequencies of the structure changed dramatically when various electrodes were activated. The modal shapes changed less dramatically when different panels were activated.

CHAPTER 1: INTRODUCTION TO ELECTRORHEOLOGICAL MATERIAL ADAPTIVE STRUCTURES

1.1 What is an electrorheological (ER) material?

Electrorheological (ER) materials are suspensions of dielectric particles in non-polar liquids that exhibit dramatic reversible changes in rheological response when exposed to an electric field. A simple physical description of the behavior is that the material transforms from a liquid without an applied field to a solid like gel with an applied field. A mechanism for this transformation is the formation of particle chains aligned with the applied field as seen in Figure 1.1.1. Several papers have reviewed the causes of this phenomenon [1-4,50].

Before discussing possible mechanisms for the ER phenomenon, it is important to comprehend the physical restructuring of the ER material components that occurs when the material is exposed to an electric field. Winslow's early work demonstrated the formation of a fibrous mass when particles suspended in low viscosity oils were exposed to an electric field [5]. He suggested that the mutual attraction of spherical particles in regions of high electric field intensity leads to the formation of particle chains between electrodes. In the presence of a shear stress, the equilibrium that is established between the formation and breaking of the inter electrode chains corresponds to the yield strength defined in the Bingham plastic model described later in this section [6]. When the electric field is removed, the particles return to a random distribution allowing fluid flow to resume. Several microscopy studies have provided evidence for the existence of these fibrillated structures [5, 7-9].

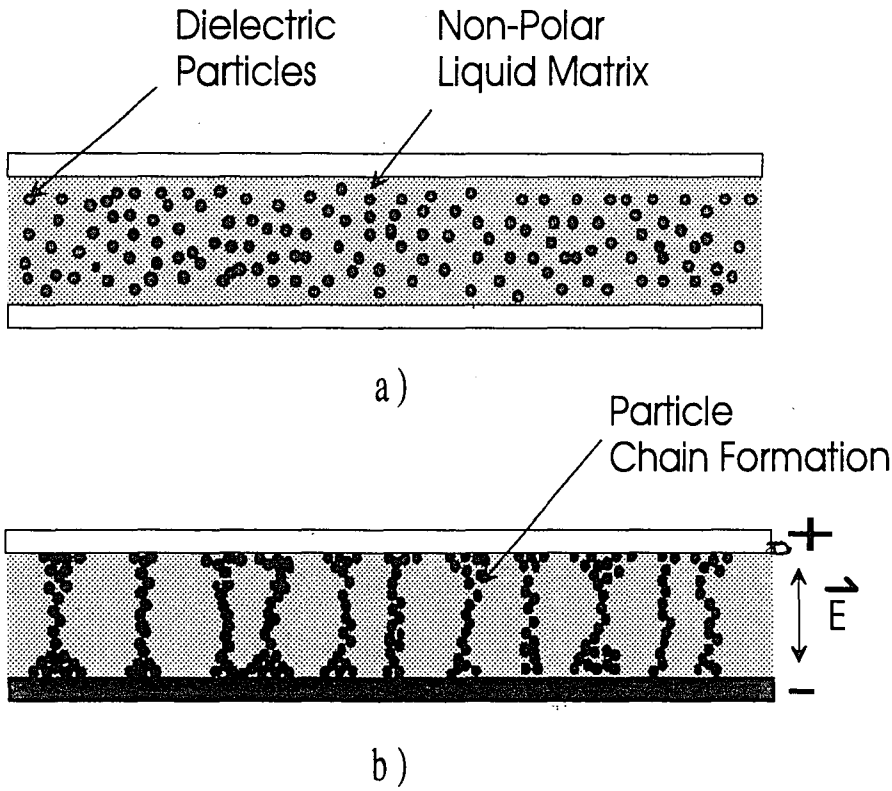

Figure 1.1.1 ER Phenomenon a)no electric field b)with electric field applied

The primary criticism of particle fibrillation has been that the amount of time required for mass migration does not correlate with the millisecond response time observed for the electrorheological effect. However, the question that needs to be answered is not so much as to whether particle fibrillation occurs, but rather what happens to these particle chains under shear? Most of the concern over the formation of a single fibril structure or the lack of this structure in an ER material is academic from an application point of view. Utilization of ER materials in any practical device requires such a high loading of particles that individual chains are not discernible. In this case, the formation of thick columns or three dimensional particle structuring is evident [9-11].

Although it is generally accepted that the electrorheological phenomenon originates from particle polarization induced by an electric field, no consensus regarding the mechanism for the observed effect has been reached. Klass and Martinek were the first to propose the induced polarization of the double layer surrounding each individual particle in the fluid as a plausible mechanism for the electrorheological phenomenon [12, 13]. This double-layer can be defined as the asymmetric distribution of charges caused by the influence of an external potential. The main criticism of this mechanism has been that the Debye length of the double layers surrounding the particles is too large. In fact, it can be argued that the extent of an individual double layer is often greater than the distance actually separating the electrodes. This inconsistency led Stangroom to propose that water acts as a bridge between particles through an electro-osmosis process [8, 14]. This mechanism assumes that ions trapped within the pores of the particle increase their mobility by dissolving in the water. In the presence of an electric field these mobile ions shift the water layer surrounding the particle toward the oppositely charged electrode. Thus one side of the particle becomes overly saturated with water. Overlap of the water between the particles is considered to be the bridge or glue that causes the ER effect.

Although it is possible that this mechanism is active in systems inherently containing water, the development of ER materials containing semiconducting particles [15], lithium hydrazinium sulfate [39], and substantially "anhydrous" alumino-silicates [16] has eliminated the possibility of the presence of water being a necessary prerequisite for the observation of the ER effect. A third mechanism that has been proposed to explain the ER phenomenon is simply particle polarization [1, 5, 17-19]. It has been suggested that the origin of polarization [1], such as charge migration through the bulk, on the surface or in the double-layer, does not matter. Once polarization has been established, the interaction of inter particle coulombic forces leads to the formation of a fibrillated network. Again, from an design engineering point of view, this is all academic. The **macroscopic,** rather than the microscopic, properties of the material are going to define how the engineer chooses the design. With this in mind, the macroscopic rheological characteristics of the material when exposed to different excitations - the two most prevalent being steady-state shear and dynamic excitations - have been investigated.

The electrorheological effect initially was defined as the apparent change in viscosity observed in the materials developed by Winslow. Although from a macroscopic point of view, a change in apparent or effective viscosity does occur, the actual plastic viscosity (η) of the material defined as the change in stress per unit change in shear strain rate remains approximately constant as the applied electric field is varied. In this situation the parameter that changes is the amount of shear stress needed to initiate flow. An example of the typical shear stress versus shear strain rate behavior observed for an ER material in the presence of an electric field is shown in Figure 1.1.2. A Bingham plastic model, as described by equation 1.1.1, can often provide a sufficiently accurate description of the observed behavior to be used for the designing of ER material devices;

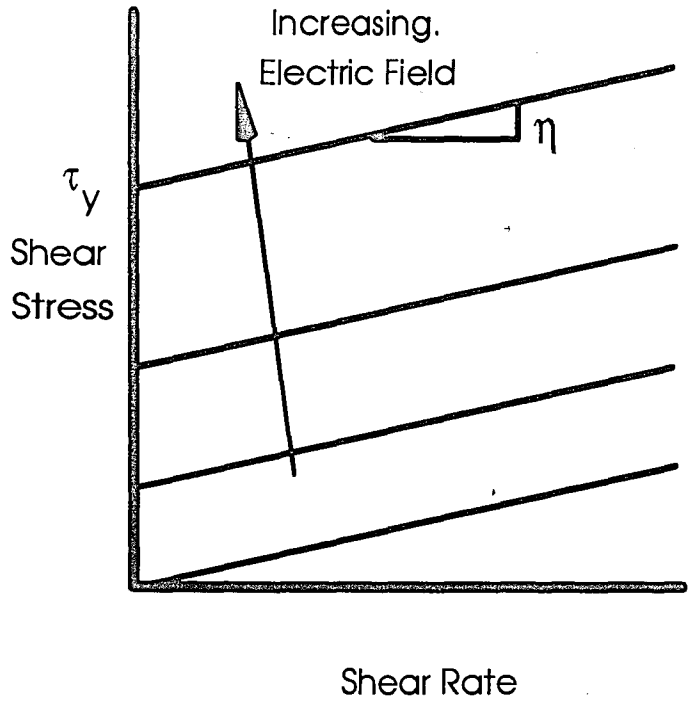

Figure 1.1.2 Idealized Constitutive Shear Behavior of ER Materials

$$\tau = \tau_y + \eta\dot{\gamma} \qquad (1.1.1)$$

This model recognizes that the property of an ER material generally observed to change with an increase in electric field is the yield stress (τ_y) defining the onset of flow. The electric field induced yield stress, τ_y, and viscosity, η, are the two most significant parameters used in designing electroactive devices where flow properties or post-yield properties are essential [20-22]. The dynamic yield stress ($\tau_{y,d}$) in a Bingham plastic modeled ER material can be defined as the zero-rate intercept of the linear regression curve fit. Naturally, the plastic viscosity of the material in the post-yield regime is accurately reflected by the slope of the linear regression curve fit used in the analysis.

Many scientists have reported observing a higher static yield stress than dynamic yield stress [1, 23] as shown in Figure 1.1.3. It is suggested that this apparent static yield stress is related to the transient fracture of the particle chains which is highly dependent upon particle size, particle shape, the prior electric field, and flow history of the material. In designing a device to utilize a particular ER material, it is necessary to consider the possible occurrence of this static yield. Upon returning to the flow regime from the static situation, the rheology for an ER material is observed to follow the more typical behavior exemplified by Figure 1.1.2.

The observed static regime is related to the pre-yield behavior observed in Figure 1.1.4. Several studies have investigated the behavior within this regime[23-26]. The pre-yield regime is defined by a yield strain, γ_y, and a static yield stress ($\tau_{y,s}$). In reality there is no such thing as static yield stress, there is always some shear rate, albeit very small. For primarily elastic materials, the static yield actually is an approximation for the steady-state dynamic yield characterized by the complex shear modulus G*. The complex shear modulus can be separated into its real, G', and imaginary, G", parts called

the storage modulus and loss modulus, respectively. The loss factor, tan δ, is obtained through the ratio G''/G'. For ER materials these properties are dependent upon the applied electric field. In the design of non-flowing devices, such as flexible or adaptive structures, control of the pre-yield complex shear modulus is essential.

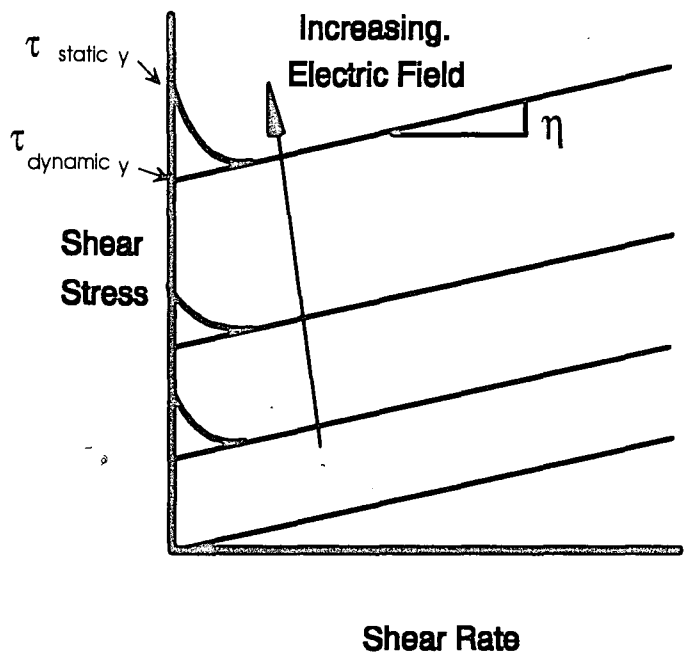

Figure 1.1.3 Observed Post-yield Shear Behavior

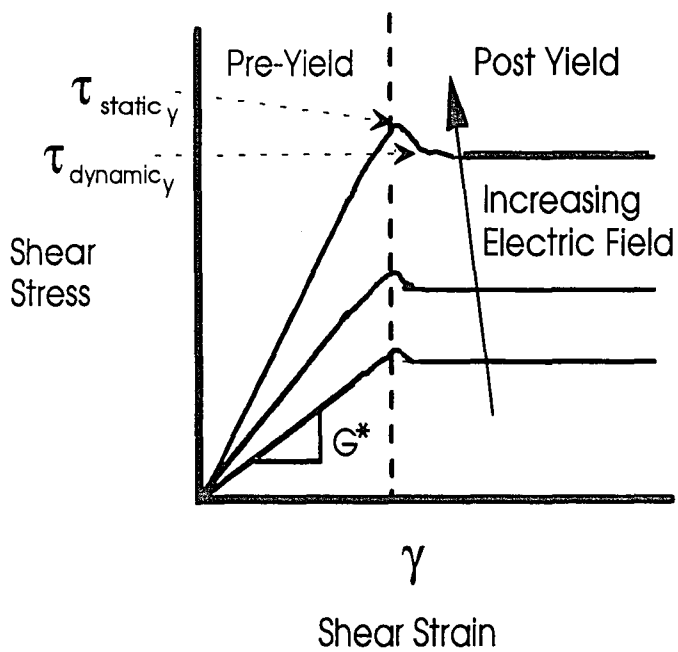

Figure 1.1.4 Pre-yield Shear Behavior of ER Materials

1.2 Engineering Applications for ER Materials

The controllable rheological behavior of electrorheological materials is useful in engineering systems and structures where variable performance is desired. When a tunable product based on electrorheological behavior is implemented so as to have sensory and control capabilities, the result is an intelligent material system or an adaptive structure. In general terms such systems or structures are those that can sense external stimuli and react appropriately to optimally meet pre-specified performance criteria

There have been many identified applications for ER materials in which there is research including dampers, clutches, valves, and brakes. Significant advancements related to these applications have recently been reviewed by Coulter et. al [27,50].

Controllable valves were among the original classes of ER material devices identified and investigated by Winslow [5]. Provided that the material flowing through the device is an ER suspension, the pressure drop across and flow rate through the device can be controlled by the application of an electric field. Benefits of ER valves include fast response time and an absence of mechanical moving parts.

Another class of devices that have been made controllable through the incorporation of ER material valve technology is machinery and engine mounts. A schematic diagram of a possible controllable mount configuration is shown in Figure 1.2.1. Traditional fluid filled mounts, which are configured much like that shown in Figure 1.2.1, are designed to have fluid inertia track characteristics, as well as top and bottom compliance values, appropriate for specific force transmission applications. The number, size, and shape of fluid inertia tubes is application specific, and in traditional mounts is fixed once the mount is fabricated. The introduction of ER valves as inertia

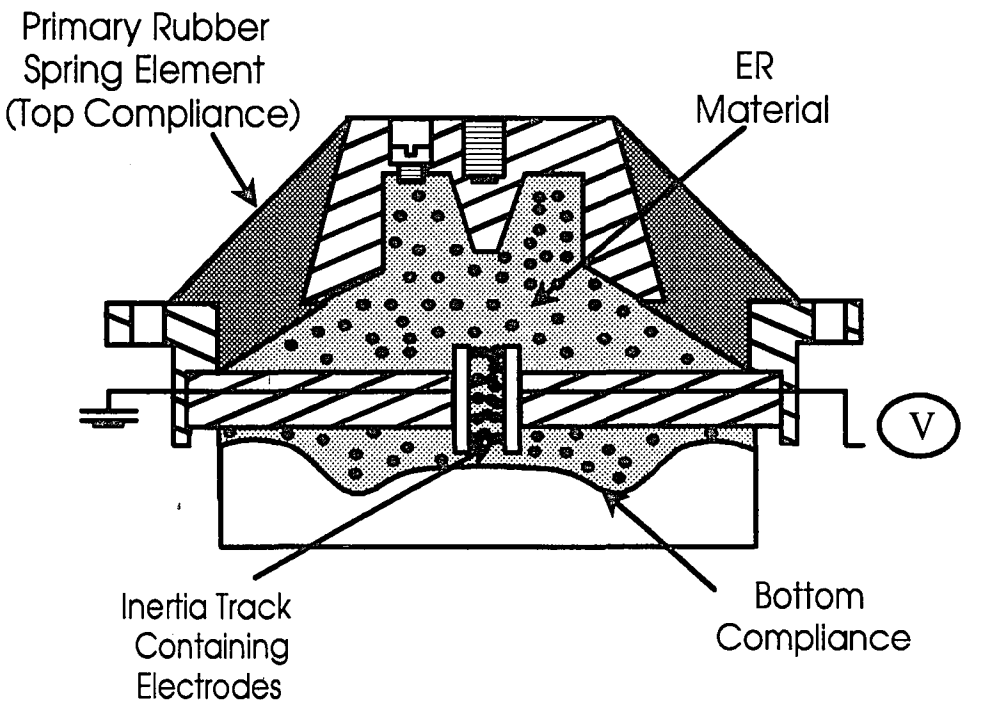

Figure 1.2.1 ER Engine Mount

track components brings with it a capability for temporal fluid inertia variation, and as a result overall mount performance control.

Like ER valves, controllable ER clutches and brakes were originally investigated by Winslow and reported in his 1949 disclosure [5]. Little was done to further the development these devices over the next three decades. Since the early 1980's, however, ER clutches and brakes have received much attention. ER clutches are based on sliding plate configurations. They can be set up in either concentric cylinder or parallel disk configurations as shown in Figure 1.2.2.

Example configurations for the two damper type devices, known as fixed plate and sliding plate dampers, respectively, are shown in Figure 1.2.3. In a fixed plate damper, the damping force on a piston is realized by the control of the pressure drop across valve-like channels through which the ER material is forced to flow. In a sliding plate damper, the damping force originates from the controlled shear resistance between the moving piston, which acts as one electrode, and adjacent parallel surfaces, which remain motionless and act as the other electrode. In both types of damping devices, accumulators are often required to account for volume variations due to the travel of the piston rod into and out of the damper cavity.

The inherent advantage of using ER materials in all of these devices is the ability to alter almost instantaneously their rheological behavior by controlling an applied electric field giving the device the ability to change it's performance in real time.

One of the latest ER technology applications is in adaptive or smart structures. Adaptive or smart structures are structures that contain their own sensors, actuation, or computational and/or control capabilities [28]. There are three classifications of general structures; passive, semi-active, and active controlled structures. Passively controlled structures offer no ability to change the already present mechanical system. The design

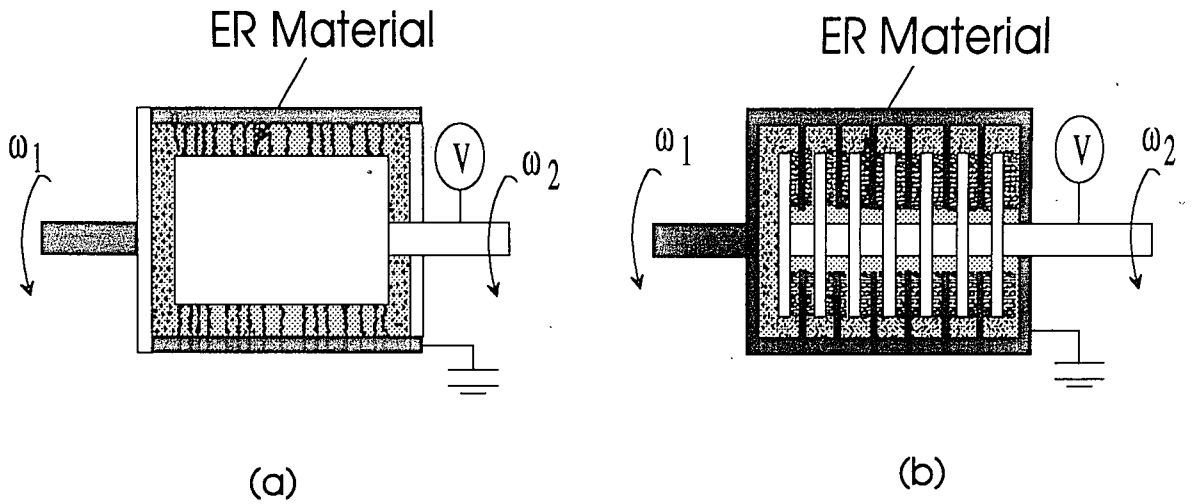

Figure 1.2.2 ER Clutch and/or Brake
(a) Concentric Cylinder Configuration (b) Parallel Plate Configuration

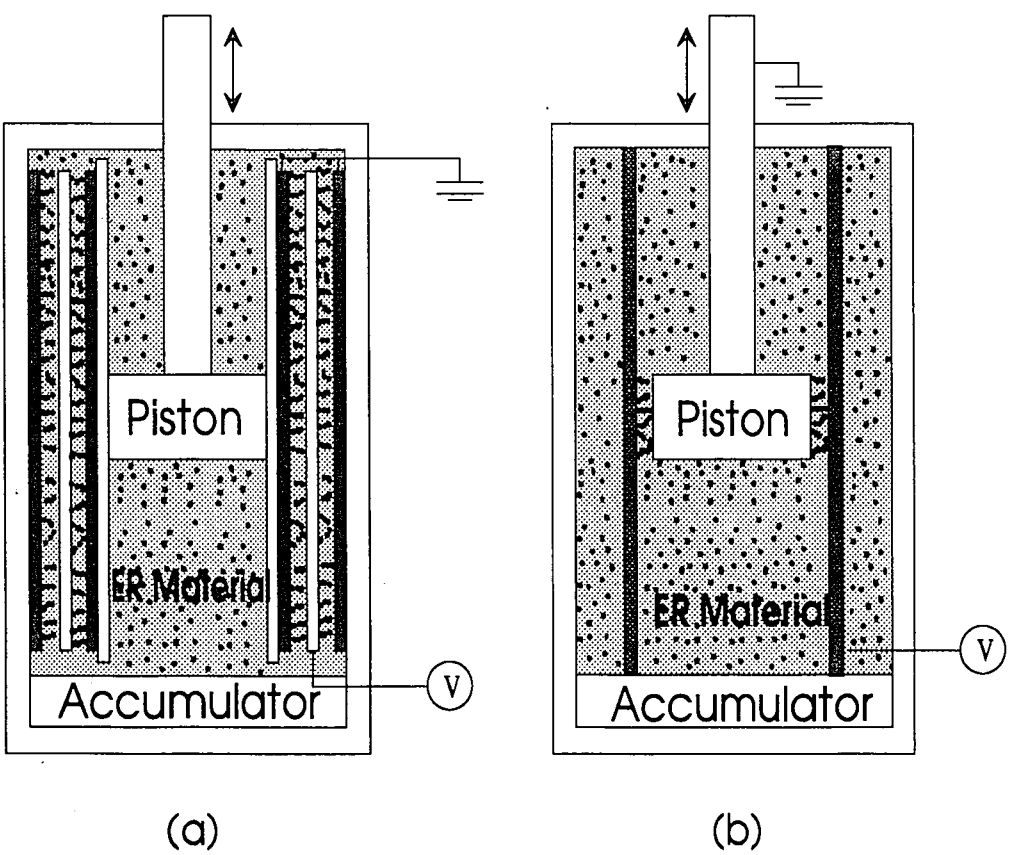

Figure 1.2.3 ER Controllable Damper
(a) Fixed Plate Damper (b) Sliding Plate Damper

of a passive structure must be predetermined to known operating conditions. There are two fundamental ways to incorporate variability in a mechanical system. One involves the addition of mechanical energy to the system (active control), while the other involves the modification of the mechanical properties of the system (semi-active control). Active and semi-active sytems comprise the realm of adaptive structures. Piezoelectric, electrostrictive, magnetostrictive, and shape memory materials are all capable of adding external mechanical energy to systems, and are useful within the active domain. Structures comprised of ER material elements have the capability to control their stiffness and damping; hence are classified as semi-active. A conceptualization of an ER based adaptive structural system is shown in Figure 1.2.4. Semi-active systems are advantageous to passive and active structures in many ways.

ER adaptive structures will potentially be able to replace present methods of structural damping in which passive polymer damping systems are presently being employed. In many applications engineers seek to reduce the resonance phenomenon. Resonance is the most efficient condition for energy transfer and occurs when the forcing frequency approaches the natural frequency of the structure. To passively dampen the resonant response, thin layers of polymer material are sandwiched between the structure and a constraining layer. This arrangement produces shearing strains within the polymer layer. When sheared, the polymer material absorbs some of the energy and transforms it into heat; thereby reducing some of the response. By replacing this polymer layer with ER material, as shown in Figure 1.2.4, the structure would be able to alter its natural frequency; avoiding resonance altogether. The result is a much larger reduction in response versus a totally passive polymer damping system.

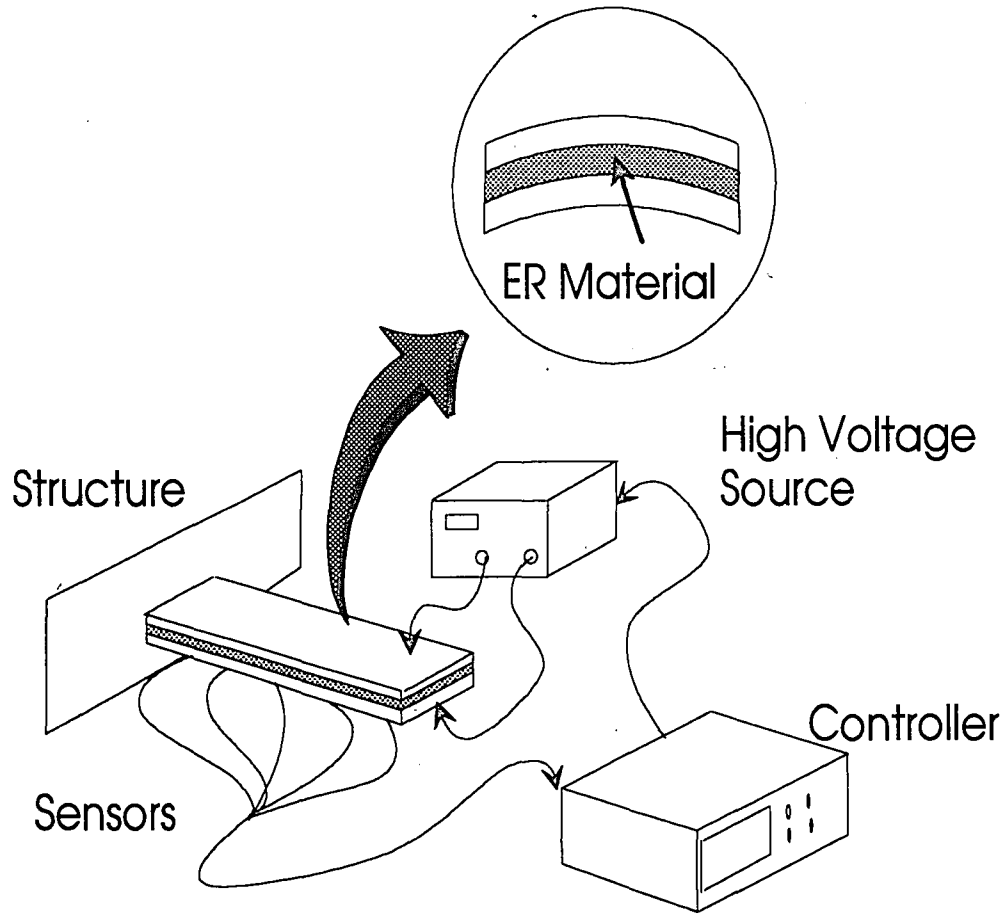

Figure 1.2.4 A Conceptualization of an ER Adaptive Structural System

Another advantage ER based structures have over passive polymer systems is the frequency and temperature dependence of the polymer material. Systems utilizing polymers have a optimal effectiveness at only one temperature and frequency. By using ER systems, again with the ability to alter their damping properties, the goal would be to develop some type of control system where damping would always be optimal.

ER adaptive structures may also be advantageous when compared with active structures. Two types of active structures are shape memory and piezoelectric structures. Shape memory adaptive structures apply very strong forces, but are only responsive in low frequency range(< 5 Hz). Piezoelectric structures are much more responsive but are very hard to fabricate, too brittle, and weigh too much to be used in some applications. Newer piezoelectric polymers which solve the problem of manufacturing, brittleness, and weight do not have enough force to be effective in some applications. The use of ER materials in adaptive structures may be able to solve some of these problems in a semi-active fashion [29].

Several examples of ER adaptive structure configurations that have been suggested are shown in Figure 1.2.5. A simple constrained layer design similar to that which was described above was patented by Carlson et. al [29]. This is shown in Figure 1.2.5a. Suggested along the same lines was the use of stacked constrained layers as shown in Figure 1.2.5b. This would allow the ER elements to contribute more in the structural dynamics by increasing the area of the ER layer. A design which compartmentalizes the ER elements allows the structure to utilize the ER extensional properties, rather than the shear properties as in a constrained layer approach is shown in Figure 1.2.5c. Multi-electrode configurations within the structure, such as in Figure 1.2.5d, allow the possibility for the structure to change or enhance it's modal shapes. In many circumstances, most possible shapes of the structure can be approximated by a

weighted summation of the mode shapes. These mode shapes are based upon the stiffness of the structure. If a structure is fabricated with different regions of stiffness these modes could be altered. ER adaptive structures would be able to achieve different areas of stiffness and therefore have different mode shapes. The significance of the application has yet to be examined. Possible real world applications for these designs include helicopter rotor blades, space platforms, airplane skins, robotics, complex manufacturing, etc [30-34].

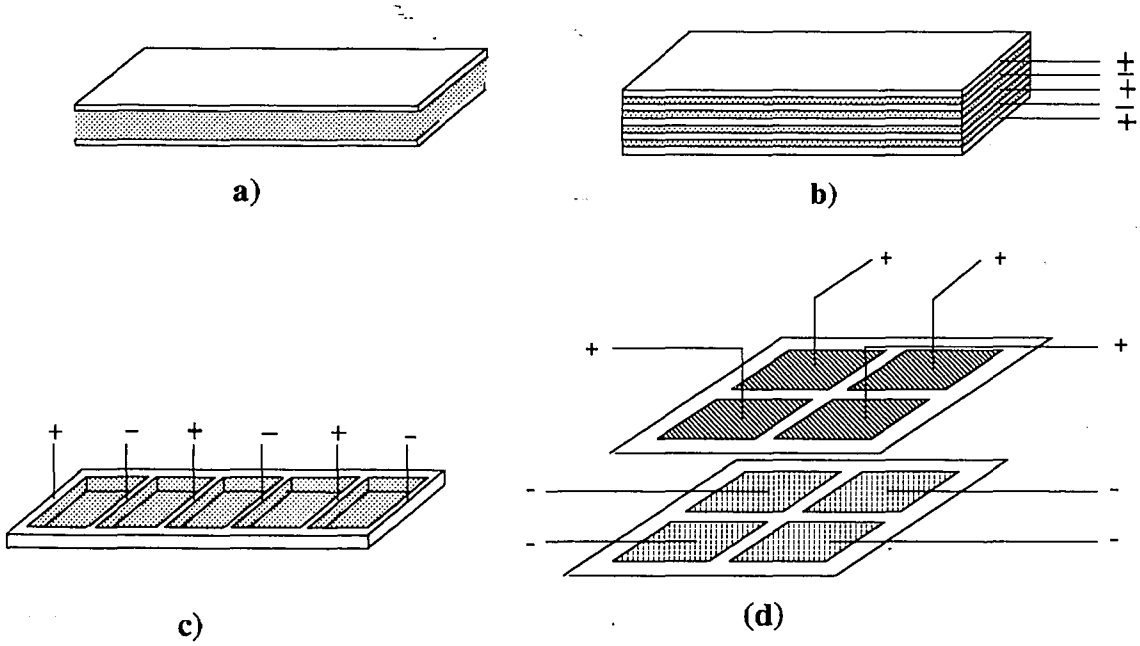

Figure 1.2.5 ER Adaptive Structure Designs
a) Single Constrained Layers b) Multiple Stacked Constrained Layers c) Extensional Structure
d) Multi-Electrode Structure

1.3 Purpose of this investigation

The purpose of this investigation is to examine some of the problems concerning the eventual physical realization of **ER adaptive structures** - this includes addressing some of the rheological, modeling, and feasibility problems. The directions for the investigation are shown in Figure 1.3.1.

Specifically, an in-depth rheological characterization was performed to increase the scope of the understanding of the dynamic behavior of ER materials at small strains characteristic of structural applications. Many of the previous investigations use the quantity known as the complex modulus G*, where G' is the real part and G'' is the imaginary part, to describe a materials viscoelastic behavior without adequately commenting on the linearity. This quantity is a measurement of a materials *linear* viscoelastic behavior and is virtually meaningless outside the linear range. The present study provided a quantified definition of linear viscoelastic behavior in terms of yield strain. The investigation experimentally examined the effects of electric field and frequency on the transition from linearity. In hopes of developing a model to predict the materials rheological response, the behavior of the complex modulus of the material was also observed with respect to frequency and electric field. The repeatability of the material over an expanded time frame was noted.

Utilizing the experimentally determined ER material properties, the behavior of some simple ER structures were modeled using both Ross, Kerwin, and Ungar and Mead and Markus theories. These pre-existent theories model the dynamic behavior of three-layer sandwiched composite structures. Experimental ER Structures were built and tested to compare theory and experiment. In addition, a more complex plate structure was experimentally tested to verify a possible application in mode shape control.

In summary:

- An in-depth rheological characterization of an electrorheological material was performed.
- The results of the rheological investigation were substituted into the Ross, Kerwin, and Ungar model and Mead and Markus model to predict dynamic structural response.
- Experimental adaptive structures were fabricated and tested to verify these models.
- A experimental investigation was performed on a multi-electrode structure to examine the feasibility of mode shape based adaptive structure control.

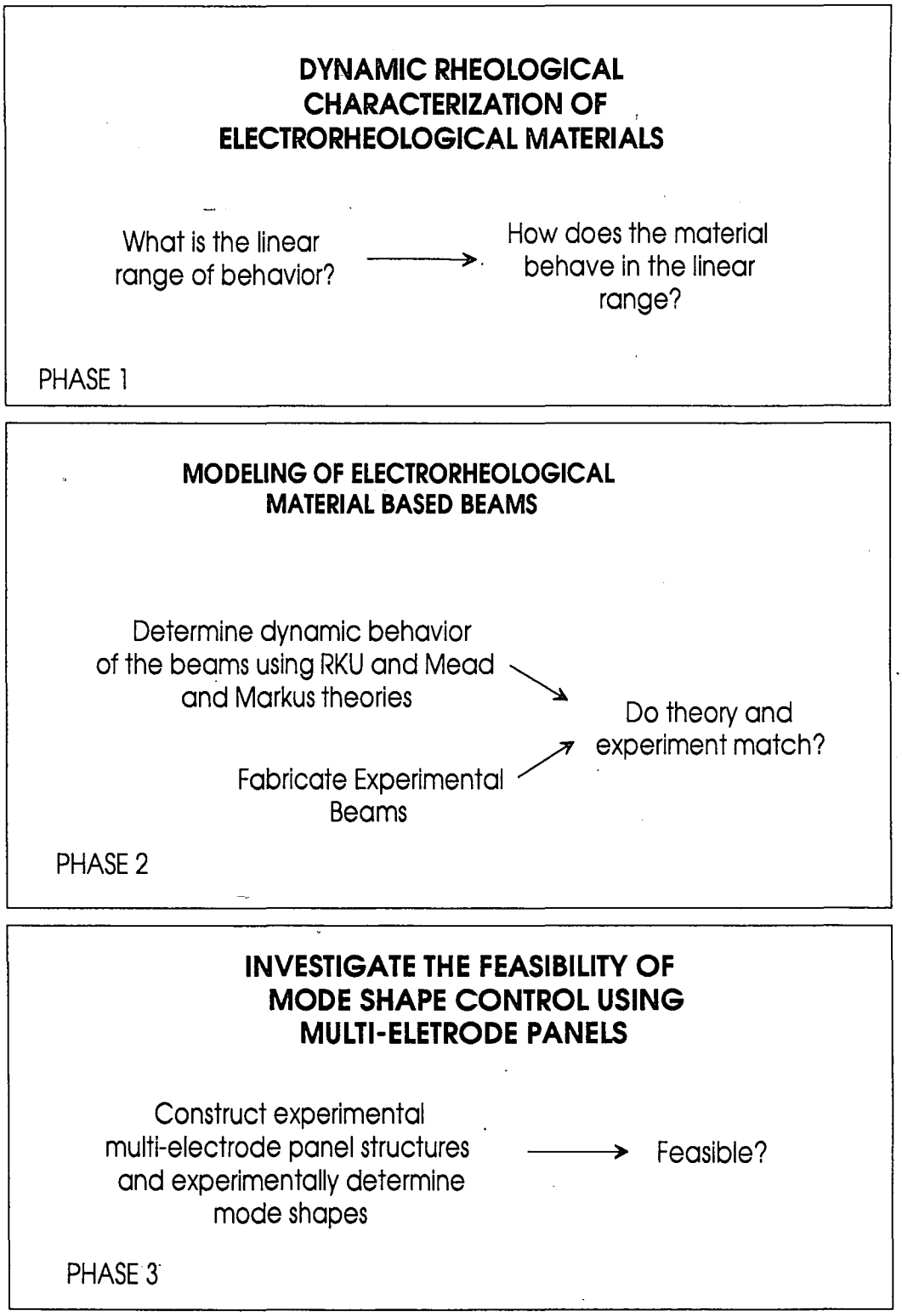

Figure 1.3.1 Summary of Investigation

CHAPTER 2: BACKGROUND ON STATE OF THE ART ENGINEERING OF ER ADAPTIVE STRUCTURES

2.1 Effectiveness of ER Adaptive Structures

Several studies investigated the effectiveness of a ER based constrained layer structures. Coulter et al. [30, 35] examined ER material sandwiched between constraining layers of aluminum. Latex material, attached along the sides, sealed in the ER material. At ends and the middle of the beam, silicon rubber completed the seal and acted as a spacer to keep the electrodes apart. The investigation determined the resonance and damping of simply supported structures. The investigators characterized these properties over a frequency range from 0-200 Hz for electric fields up to 2.5 kV/mm. Structural resonant frequency increased linearly with respect to changes in electric field. The slope of this increase for modes 1, 2, and 3 was 12.1, 13.0, and 18.6 (Hz·mm)/kV, respectively. Structural loss factors ranging from 0.03 to 0.11 also increased with electric field, but decreased with mode number. There was no clearly observable relationship between increases in loss factor and electric field.

Choi et al. [36, 37] investigated beams comprised of polystyrene, aluminum, and 70/30 brass constraining layers. Silicon rubber, attached around the entire outside edge of the beam, sealed in the ER material. The investigation calculated the effective bending modulus and the effective loss factor per equations provided in ASTM standard G756-83 [45] for cantilevered beams. The effective bending modulus increased 25-100% and the effective loss factor increased 42-133% with an electric field of 2 kV/mm. The magnitude of increase depended upon the material used as constraining layers.

Thompson and Gandhi [31-34, 37-39] investigated ER beams with aluminum constraining layers. Again, silicon rubber, around the entire outside edge, sealed the ER

material in. Both resonant frequency and damping increased with increases in electric field. The investigation also examined the effects of temperature on these properties. Changes in resonant frequencies and damping with respect to increases in electric field, decreased at higher temperatures.

Though these studies have shown the potential applications and effectiveness of ER structures, some problems need to be addressed before the systems are physically realizable.

2.2 Rheological Problems

One fundamental problem is the rheological understanding of ER material behavior. Most rheological investigations performed to date utilized constant shear rate tests. There is a need to do more dynamic type testing at shear strain amplitudes that are characteristic of structural damping applications. More specifically, there is a need to model the behavior, standardize the testing, and expand the operational testing parameters of the materials. Several studies have partially address these rheological issues.

Jordan et al. [9] tested a suspension of a mineral in oil, supplied by Lord Corporation, using both parallel plate and Couette rheometry. The instruments used were a Rheometrics Mechanical Spectrometer model 7200 and a Rheometrics System IV. The investigation presented a model based on the assembly of particle strings between two plates. For small strains, they approximated the elastic storage modulus to be

$$G' = \frac{3\varepsilon_0\varepsilon_1\beta^2 E^2\phi}{4(1+2\gamma)}\left[4-3\gamma^2\right] \tag{2.2.1}$$

where

$$\beta = \frac{\varepsilon_2 - \varepsilon_1}{\varepsilon_2 + 2\varepsilon_1} \tag{2.2.2}$$

and ε_0 is the permittivity in a vacuum, ε_1 is the permittivity of dispersing medium, ε_2 is the permittivity of a particulate phase, E is the electric field, ϕ is the volume fraction of particulate phase, and γ is the shear strain. A point dipole model under predicted the elastic modulus of their materials. A multipolar approximation used for highly

polarizable particles more accurately predicted the modulus. In addition, they microscopically observed the fracture of particle chains and reformation within the material. When the thin fibrils break off, they reformed and joined onto other chains forming thick columns.

Gamota and Filisko [25, 26] studied ER materials composed of alumina-silicate particles in paraffin oil. The materials were tested using rotational rheometry at moderate frequencies; 10-50 Hz, and at high frequencies; 300-400 Hz. The investigation identified three regions of behavior: pre-yield, yield, and post-yield. Each region had its own deformation characteristics; linear viscoelastic in the pre-yield, viscoelastic plastic in the yield, and plastic in the post-yield. The yield strain was defined as a sharp deviation of the first derivative of the stress function with respect to time. Yield strain decreased with increases in electric field, while yield strain increased with increases in frequency. A Zener element modeled the pre-yield behavior.

Yen and Achorn [23] experimented with hydrated particulates of lithium salt of poly(methacrylate) dispersed in chlorinated paraffin oil. The materials were tested with a Rheometrics RMS-605 parallel plate rheometer. They observed linear elastic behavior at small strains and plastic behavior at high strains. Yield stress, defined as the stress transition point from elastic to plastic behavior, increased with increases in particle concentration and electric field.

Spurk and Huang [40] tested dispersions of silica particles in silicone oil using a non-conventional low inertia rheometer system. The investigation observed a deterioration of the electroviscosity under the application of a d.c. electric field over a period of time, while a.c. fields were found to be more stable.

Thurston and Gaertner [41] tested corn starch in mineral oil fluid using a rectangular channel. They observed a rapid change in viscoelastic response with the

initial application of electric field and a slower change in viscoelasticity with the continued application. Their conclusions conjectured that though the initial response is very fast, the formation of a complete and final microstructure was a very slow process.

Coulter et al. [35] tested ER materials using an axial rheometer attached to an MTS testing system. The investigation found that G' increased with increases in electric field while the loss factor decreased. Storage modulli as high as 70 kPa were seen. Loss factors generally remained within the range 0 to 4.

Shulman et al. [18, 42] and Vinagradov et al. [17] tested diatomite particles in transformer oil using a Couette type rheometer. At high electric fields G' and G" increased dramatically with increases of particle concentration until about 30%. With further increased particle concentration G' still increased, though less dramatically, while G" remained constant. They attribute this phenomenon to the increase in defects in the skeleton of the structure and the enhancement of the elastic interactions between the particles. They also observed a frequency dependence of G' and G" related to what they called the natural frequency of the micro structures. G' and G" were constant at frequencies below the natural frequency, as the frequency approached the natural frequency there were abrupt changes in the moduli.

Brooks et al. [43] did investigations using lithium poly methacrylate dispersed in cholorinated hydrocarbon oil. The materials were tested using shear wave propagation with the Rank Pulse Shearometer at a frequency of 191 Hz. The storage and loss moduli increased with applied field to a maximum then decreased. At lower fields, the storage modulus was higher than the loss modulus, but at higher fields, the moduli are found to be similar.

2.3 Modeling of the Dynamic Behavior of ER Based Beam Structures

Another problem that needs to be addressed, is the "intelligence" that will control the structure. By themselves these ER structures are not different from passive polymer systems. The "adaptiveness" arises when a control system is added. Some suggested control systems are classical feedback, state-space, or neural network based methodologies. One of the first steps in selecting an appropriate control system is to develop a mathematical model of the system response. The development of a model will significantly aid in the selection and creation of a control scheme.

Much work has been done in modeling the vibration of composite beams. These models are based on constrained layer polymer damping systems, whose shear behavior of the sandwiched layer accounts for the damping. It is generally accepted that ER materials will shear before elongating in a bending arrangement as suggested in Figure 1.2.4. Some of these theories may be applicable. Two generally accepted theories in the vibration community are the Ross, Kerwin, and Ungar (RKU) model [44, 45] and the Mead and Markus model [46]. The RKU model is based on the classical fourth order Bernoulli-Euler beam, while the Mead and Markus model is based on a sixth order equation. Section 4.2 examines these theories in detail. Several previous investigations have attempted to model ER based beams using these theories.

Coulter et al. [30, 35] investigated the applicability of the RKU model in its original form using a simply supported boundary condition. The study substituted material property data obtained from a rheological investigation into the RKU model. The theory under predicted both the modal frequencies and the damping of the structure. The author's attribute this to uncertainty in the rheology and the experimental deviation from the theories original assumptions. The deviation of the original assumptions in the

theories were mainly attributed to the use of the silicon rubber to seal and separate the electrodes surrounding the ER material.

Choi et al. [36] theoretically modeled the behavior of ER material beams using the ASTM standard number G756-83. The ASTM standard measures damping properties of polymers utilizing a cantilevered beam based on the RKU model. The methodology is to measure material properties of the sandwiched layer by calculating the resonance and damping of a constrained layer structure containing that material. In this investigation, ER material replaced the polymer layer. The study compared rheological data in the form of G' and G" obtained from a previous investigation to the rheological data obtained from the ASTM standard. The results showed that the ASTM standard did not adequately predict the results obtained from rheological testing. The change in the stiffness of the ER layer obtained from results on a rheometer was on the order of 10^5 Pa while change in effective stiffness of the structure based on the ASTM standard was on the order of 10^9 Pa.

Mahjoob et al. [47] investigated both the RKU and the Mead and Markus models. The investigation determined rheological data from the results of a structural investigation examining the resonance and damping of ER based beams. Mead and Markus models better predicted the properties. A linear extrapolation of the behavior of a beam with no interference from sealant was performed based on the results obtained for experimental tests using varying amounts of the sealant. The conclusions of the investigation seem to find that both of these models could be used to predict the response of structures. The results of this investigation were dubious since G' was observed to be around 300 kPa; three to four times as strong as any other material available.

None of these investigations has definitively concluded that the prior theories were applicable or inapplicable to ER adaptive structures. There are three plausible explanations why previous investigations faltered.

One, the rheology data was not accurate. Many of the investigations reported rheology data while none adequately comment on the linearity of the materials, repeatability of the testing, or the uncertainty of the properties.

Two, the experimental structures did not meet the theoretical models specified criteria. The theories assumed pure sinusoidal mode shapes and unconstrained shear strain within the sandwiched layer. Some of the experimental investigations used cantilevered boundary conditions and completely sealed the edges of their structures with silicon. A cantilevered beam at the first modal frequency does not have a sinusoidal modal shape. The use of silicon sealant constrained the shear within the sandwiched layer.

Three, the past theories may not have been applicable due to some of the approximations used in the theories. Use of these theories may not have been sensitive enough for materials in the range of hundreds of kPa.

It would seem practical, before concluding that these theories were completely inapplicable, to investigate the rheology more thoroughly and modify the experimental procedure to simulate the theoretical models more accurately.

2.4 Feasibility of Mode Shape Control

Many investigations describe the use of a multi-paneled electrode design. The advantages of using multi paneled electrodes are two fold. These configurations are used to stiffen or weaken different areas of the structure. By changing the stiffness in different areas, one, the resonance frequency and damping have more variability, and two, the modal shapes of the structure can be altered. The advantages of varying the resonance and damping of the structure are discussed in the preceding sections. The use of mode shape control is a more innovative application. The concept would be for the structure to be able to choose what shape it vibrates in. For example, if a simply supported beam is forced at a frequency that excites the second mode there is no vibration in the center. This point of zero displacement is known as a node. If the designer wanted to put a piece of equipment, sensitive to motion, onto the structure the best place would be to put it in the center. The advantage ER materials have over a passive system methodology is increased *robustness*. A passive system could use this application for only one pre-determined forcing frequency and at only one location. ER materials make it possible to excite different modes and place nodal points onto different areas of the structure. The feasibility and effectiveness of this innovative application has not been researched significantly.

CHAPTER 3: RHEOLOGICAL INVESTIGATION

3.1 Introduction

The motivation for this phase of the research was to increase the scope and understanding of ER material dynamic behavior at small strains. The investigation proposed to define a linear range of behavior for ER materials and quantify this region in terms of a yield strain. The yield strain's dependence on frequency and electric field was observed. The investigation then examined the rheological property known as the complex shear modulus within this linear region.

A annular pumping mechanism described in Section 3.3, was used to measure the properties. The methodology was to induce a shear strain and measure the transmitted stress across the material. By comparing the induced shear strain and transmitted stress, the rheological properties were determined. The following section describes the usage of the complex shear modulus in characterizing linear viscoelastic shear behavior.

3.2 Rheology Theory

A quantity known as the complex shear modulus describes a materials linear viscoelastic shear behavior. More specifically, the complex shear modulus quantifies the steady-state dynamic behavior using models based on discrete springs and dampers as shown in Figure 3.2.1. The definition is presupposed upon the materials time dependent behavior being modeled according to a ***linear*** ordinary differential equation. If the material does not behave in a linear fashion, the complex modulus is virtually meaningless. The linear dependence can be expressed in the condition that the transmitted stress must be proportional to the induced strain within the Laplace domain,

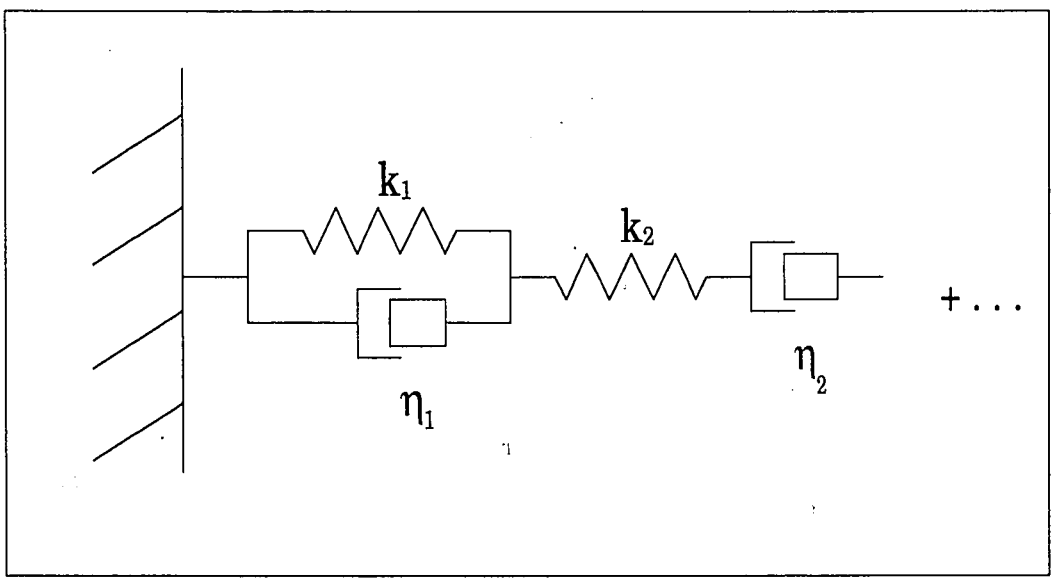

Figure 3.2.1 Modeling of a Linear Viscoelastic Material with Discrete Springs and Dampers

$$\tau(s) = G(s)\,\gamma(s) \tag{3.2.1}$$

where τ is the transmitted stress, γ is the induced strain, and G is the shear modulus defined as some ratio of two polynomials in s.

The complex shear modulus is a steady state property that describes the materials behavior when exposed to a sinusoidal strain input,

$$\tau(s) = G(s)\frac{\gamma\ \omega}{s^2+\omega^2} \tag{3.2.2}$$

By performing a partial fraction expansion of equation 3.2.2,

$$\tau(s) = \frac{a}{s+j\omega} + \frac{\bar{a}}{s-j\omega} + \frac{b_1}{s+s_1} + \frac{b_2}{s+s_2} + \frac{b_3}{s+s_3} + \ldots \tag{3.2.3}$$

where a, and $\bar{a}$ are complex conjugates, and s_1, s_2, and s_3 are the poles of G(s). If the inverse Laplace transform is performed on equation 3.2.3,

$$\tau(t) = ae^{-j\omega t} + \bar{a}e^{j\omega t} + b_1e^{-s_1 t} + b_2e^{-s_2 t} + b_3e^{-s_3 t} + \ldots \tag{3.2.4}$$

The exponential terms drop out as time goes to infinity, and are left with,

$$\tau_{ss}(t) = ae^{-j\omega t} + \bar{a}e^{j\omega t} \tag{3.2.5}$$

which is defined as steady state stress response. The constants a and $\bar{a}$ can be evaluated from equation 3.2.2 where,

$$a = G(s)\frac{\gamma\omega}{s^2+\omega^2}(s+j\omega)\ \Big|_{s=-j\omega} \tag{3.2.6a}$$

and

$$\bar{a} = G(s)\frac{\gamma\omega}{s^2+\omega^2}(s-j\omega)\ \Big|_{s=+j\omega} \tag{3.2.6b}$$

By performing the substitutions for s, we realize that G($j\omega$) is now a complex quantity, or what we have been describing as the complex shear modulus. The complex function can be written in phasor notation,

$$G(j\omega) = |G(j\omega)|e^{j\phi} \tag{3.2.7a}$$

and

$$G(-j\omega) = |G(-j\omega)|e^{-j\phi} \tag{3.2.7b}$$

where ϕ is the phase angle of the material. Note that

$$|G(j\omega)| = |G(-j\omega)| \tag{3.2.8}$$

and the Laplace transform of the steady state stress is,

$$\tau_{ss}(s) = \frac{a}{s+j\omega} + \frac{\bar{a}}{s-j\omega} \tag{3.2.9}$$

Substituting equations 3.2.6a, 3.2.6b, 3.2.7a, 3.2.7b, and 3.2.8 into equation 3.2.9, and taking the inverse transform,

$$\sigma_{ss}(t) = |G(j\omega)||\gamma| \frac{e^{j\omega t+\phi} - e^{-j\omega t-\phi}}{2j} \tag{3.2.10}$$

This reduces to

$$\tau_{ss}(t) = |G(j\omega)||\gamma| \sin(\omega t + \phi) \tag{3.2.11}$$

In response to a sinusoidal shearing input, a material that behaves linear viscoelastically has a stress output with the same frequency, proportional amplitude, and a phase shift. Typical linear viscoelastic behavior can be seen in Figure 3.2.2.

A definition of linear behavior can now be proposed. There are two simultaneous criteria for yield. One, the stress amplitude must be proportional to the strain amplitude,

$$|\tau| = |G(j\omega)||\gamma| \tag{3.2.12}$$

Two, the phase angle must only be a function of frequency and not strain. This is proposed because of phasor notation in equations 3.2.7a and 3.2.7b. The property $G(j\omega)$ is *only* dependent on frequency.

To completely characterize the material's linear viscoelastic behavior, the magnitude of $G(j\omega)$ and phase must be measured over a desired frequency range. A

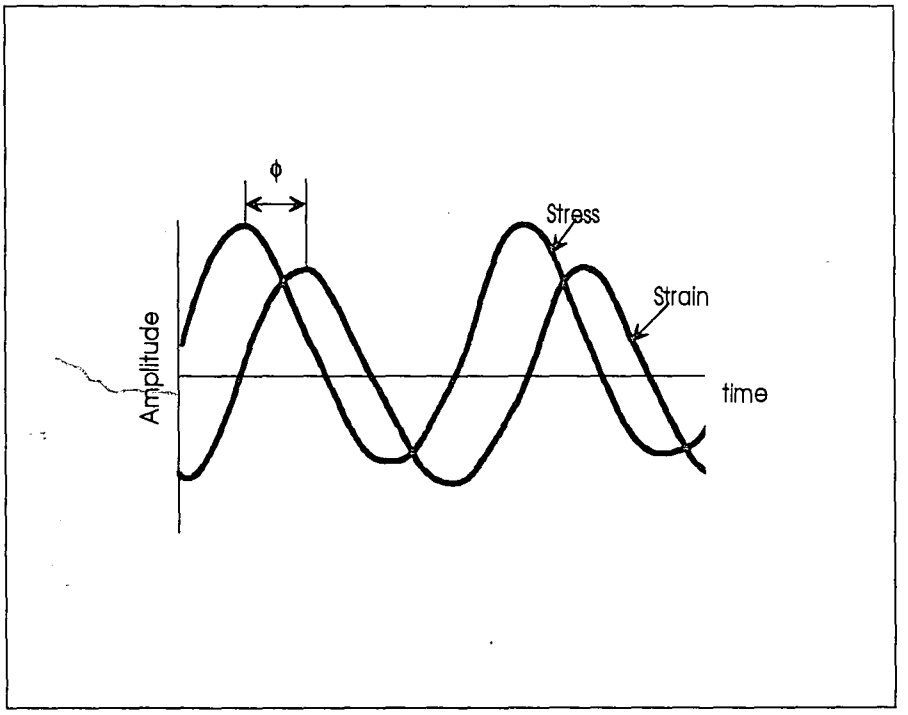

Figure 3.2.2 Response of a Linear Viscoelastic Material to a Sinusoidal Strain Input

perfectly elastic material will have no phase angle, while a perfectly viscous material will have a phase angle of 90°. All materials do not act perfectly and have in phase and out of phase portion. We can express the complex modulus by

$$G' = |G(j\omega)|\cos\phi \tag{3.2.13}$$

and

$$G'' = |G(j\omega)|\sin\phi \tag{3.2.14}$$

where G' represents the in phase portion and G" represents the out of phase portion. In rheology terminology these are known as the storage and loss modulus respectively.

An experiment was designed to quantify the region of linear behavior in terms of yield strain, and examine the effects of electric field and frequency on the complex shear modulus. A description of the experimental apparatus utilized follows.

3.3 Experimental Set up

3.3.1 Experimental Apparatus

An axial rheometric device, as shown in Figure 3.3.1.1, measured the rheological properties of the ER material. The cup had an inner radius of 22.96 mm and the bob had an outer radius of 21.96 mm resulting in a 1 mm gap between the two. The material was placed in a gap between the cup and the bob. An electric field was applied across this gap. Displacement of the cup induced a strain on the material. By comparing the transmitted stress across the material and induced strain, the $|G(j\omega)|$ and the phase between the two were obtained.

MTS machine model number 305-02, controlled by an MTS 442 feedback controller, provided the strain on the material. The feedback sensor was a Lucas Schaevitz 1" LVDT. An Onosokki CF920 Dynamic Analyzer provided the sinusoidal signal to the MTS machine. An Interface SM-250 load cell with a stiffness of 7300 kN/m and a corresponding natural frequency of approximately 1000 Hz, measured the load and/or stress transmitted across the material. A Series 230 Bertan High Voltage Power Supply applied the electric fields. In addition, for more accurate strain signals, a Bentley-Nevada Series 7200 proximity sensor measured the actual strain. The transmitted stress from the load cell and the induced strain from the proximity probe were compared using the Onosokki Dynamic Analyzer. The analyzers FFT hardware calculated amplitude and phase of the complex modulus. A diagram of the instrumentation is shown in Figure 3.3.1.2.

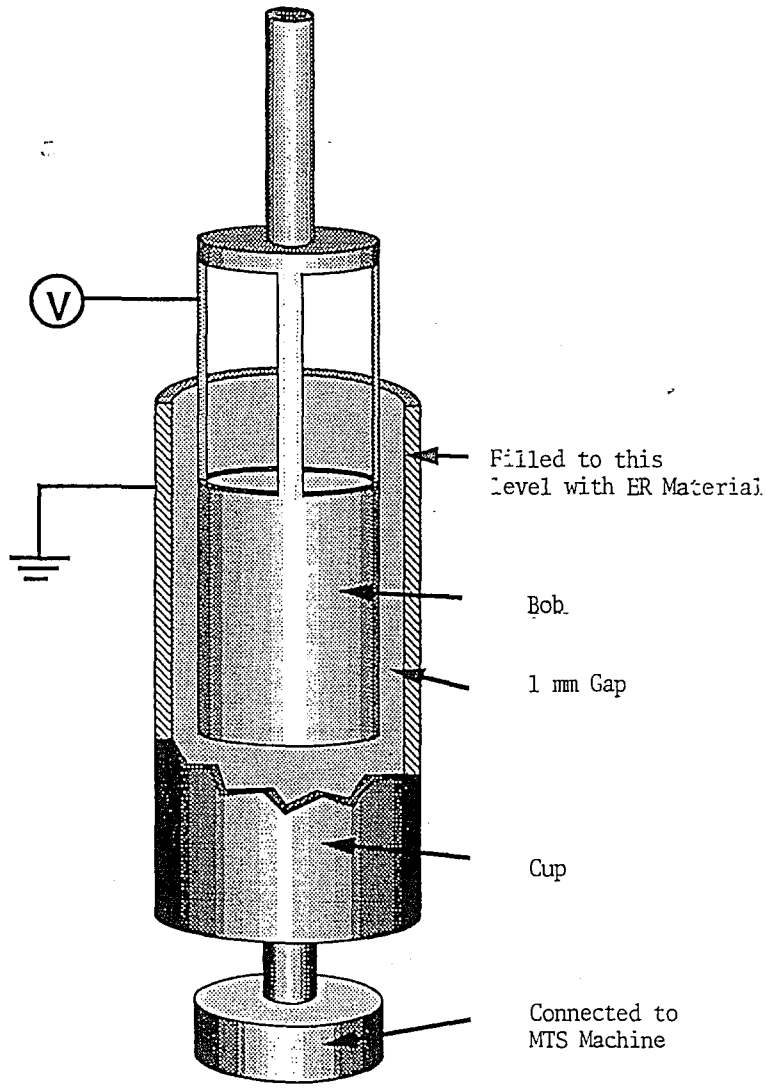

Figure 3.3.1.1 Concentric cylinder rheometer used in the investigation.

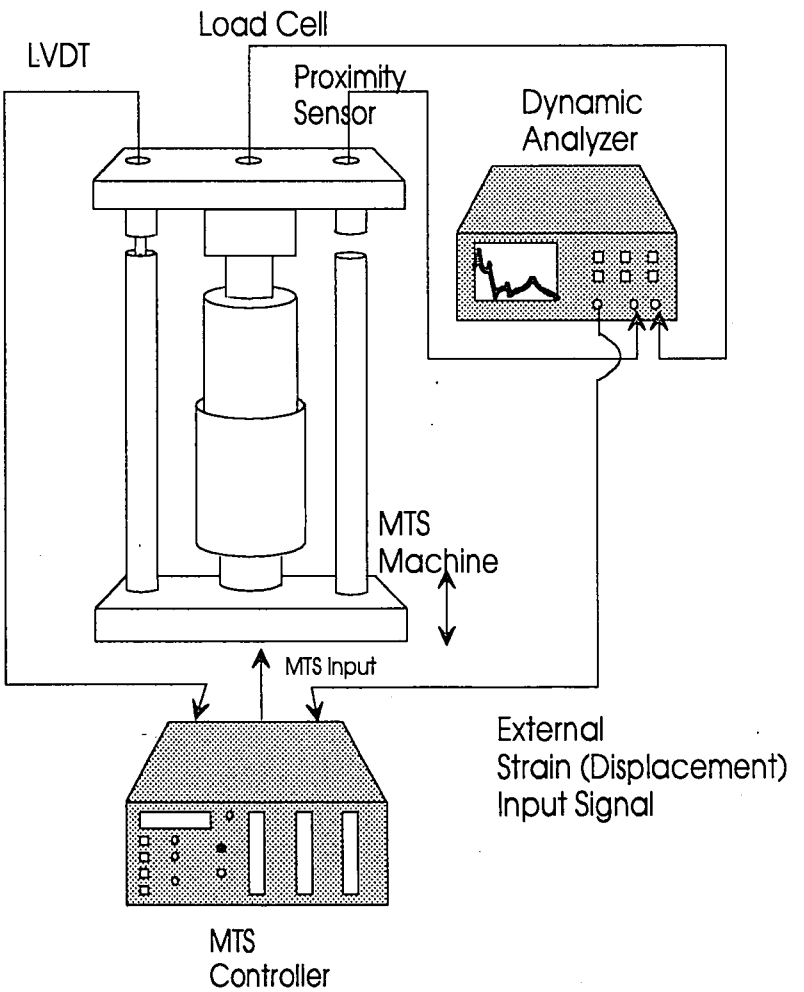

Figure 3.3.1.2 Instrumentation of Rheometer

3.3.2 Instrument Calibration

Testing of an S-8000 standard viscosity fluid verified the calibration of the load cell and proximity sensor. The standard kinematic viscosity for this material as reported by National Bureau of Standards was 41.92 Pa·s at 68 F. Two experimental tests using the described apparatus yielded 40.27 $\pm$ 2.96 Pa·s and 46.91 $\pm$ 6.31 Pa·s at room temperature. The estimated uncertainty of the experimental data was estimated to be 10-20% error.

3.3.3 Material Preparation

The investigation used ER material number 6533-30B obtained from Lord Corporation. Prior to actual testing of the material, preparation included placing the test sample on rollers for at least 24 hours, and afterwards, ultrasonically mixing it for 16 seconds. Ultrasonic mixing removed any residual particle flocculation. The ER material was then poured into the cup and evacuated by exposure to a vacuum for 30 minutes before testing. Vacuum desiccation removed air pockets. Testing began immediately after desiccation.

3.3.4 Experimental Procedure

The first purpose of the rheological investigation was to determine the range of linear behavior in terms of yield strain and its dependence on electric field and frequency. This rheological study exposed the ER material sample to strains from 0.001 to 0.1 at frequencies of 10, 30 and 50 Hz. Testing was performed with applied electric fields of 1.5, 2, 2.5, and 3 kV/mm.

The material was first tested at 10 Hz and 3.0 kV/mm. Strain was swept from 0.001 to 0.01 in increments of 0.001, then from 0.01 to 0.1 in increments of 0.01. The

experiment measured the stress amplitude and phase angle at each respective strain amplitude. The applied field was reduced to 2.5 kV/mm, and the procedure was repeated. At each successive electric field this procedure was performed.

After all the electric fields were tested the frequency was increased to 30 Hz. The strain at all the electric fields was repeated at this new frequency. After which, the frequency was increased to 50 Hz and the strain sweep repeated. The entire procedure was repeated two more times for each frequency.

The experiment produced three strain sweeps at each given electric field and frequency. Stress amplitude and phase angle data were measured for each electric field and frequency.

The second purpose of the investigation was to gain a more in depth understanding of the behavior within this defined linear region. The stress and strain amplitudes were measured within the frequency range from 0 to 50 Hz at electric fields of 1.5, 2, 2.5, and 3 kV/mm. The complex shear modulus was calculated.

3.3 Results and Discussion

The first objective was to define the strain amplitudes in which the material behaved linearly with respect to stress. The material behavior was considered linear only if the shear stress was a linear function of strain per equation 3.2.12, and the phase angle was independent with respect to strain by the definition of the complex modulus, equation 3.2.7a and 3.2.7b. Both of these conditions were met simultaneously.

Figure 3.3.1 shows a typical dynamic stress-strain relationship. An ideal linear relationship between stress and strain existed at small strain amplitudes. It must be noted that the strain axis was plotted on the log scale to clarify observation of the stress-strain relationship. When a certain strain was reached, there was a dramatic decrease in the transmitted stress that signifies a yielding of this linear behavior. As strain increased further, pseudo linear relationship as described in equation 1.1.1, between stress and strain appeared signifying typical Bingham plastic behavior. This behavior was similar to that seen in Yen and Achorn [23].

The investigation observed significant changes in the stress-strain relationship when electric field was increased as seen in Figure 3.3.2. The slope of the curve within the linear region, $|G(j\omega)|$, increased, and the yield stress increased with increases in electric field. This behavior was seen by Yen and Achorn [23] and Chrzan and Coulter [48]. The increase in slope and the yield stress when the field was applied was likely due to the increase in dipole moment of the particles as discussed in Jordan et al. [9]. The increased moment increased the strength of the particle chains formed between the electrodes.

The stress-strain behavior dependence on frequency was not as clearly observable as was seen in Figure 3.3.3. There was little change in the slope of the curve, the yield stress or the yield strain. Jordan et al. [9] and Shulman et al.

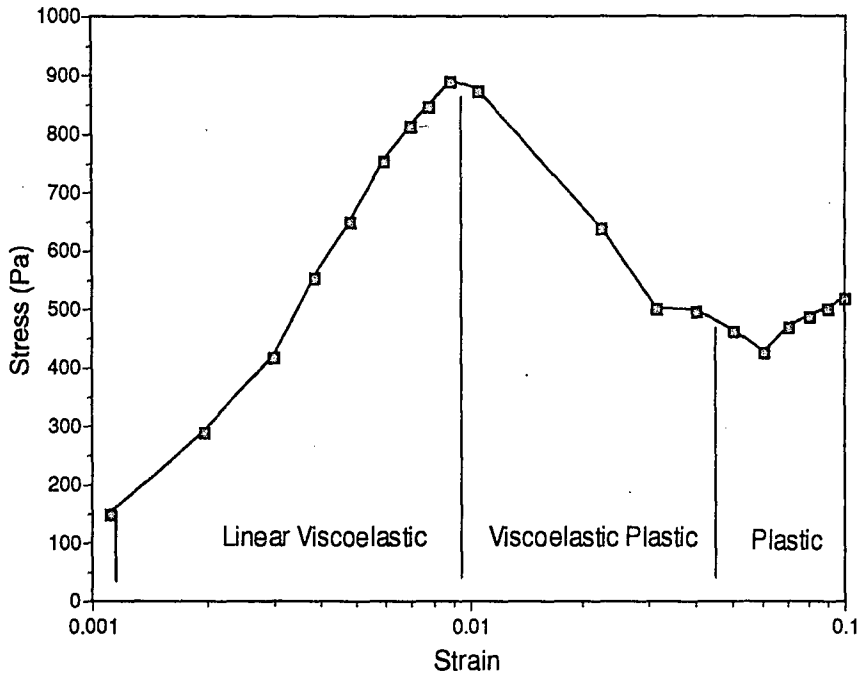

Figure 3.3.1 Magnitude of Stress versus Strain at 3 kV/mm at 30 Hz

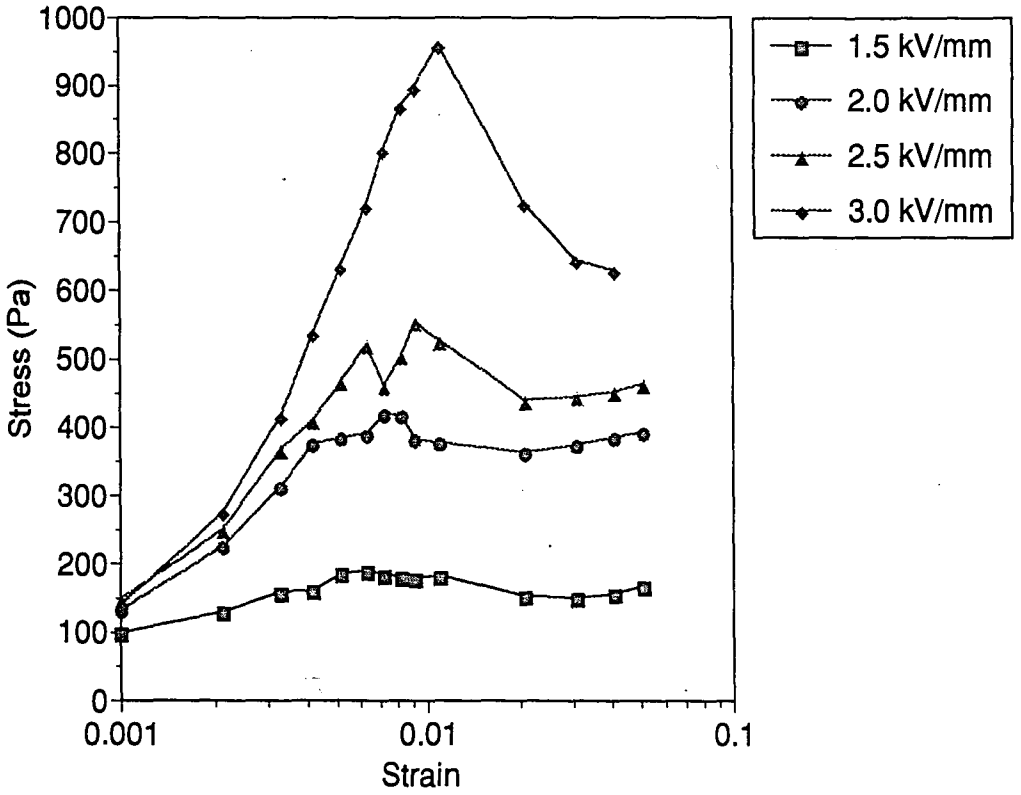

Figure 3.3.2 Magnitude of Stress versus Strain at Electric Fields of 1.5, 2.0, 2.5, and 3.0 kV/mm

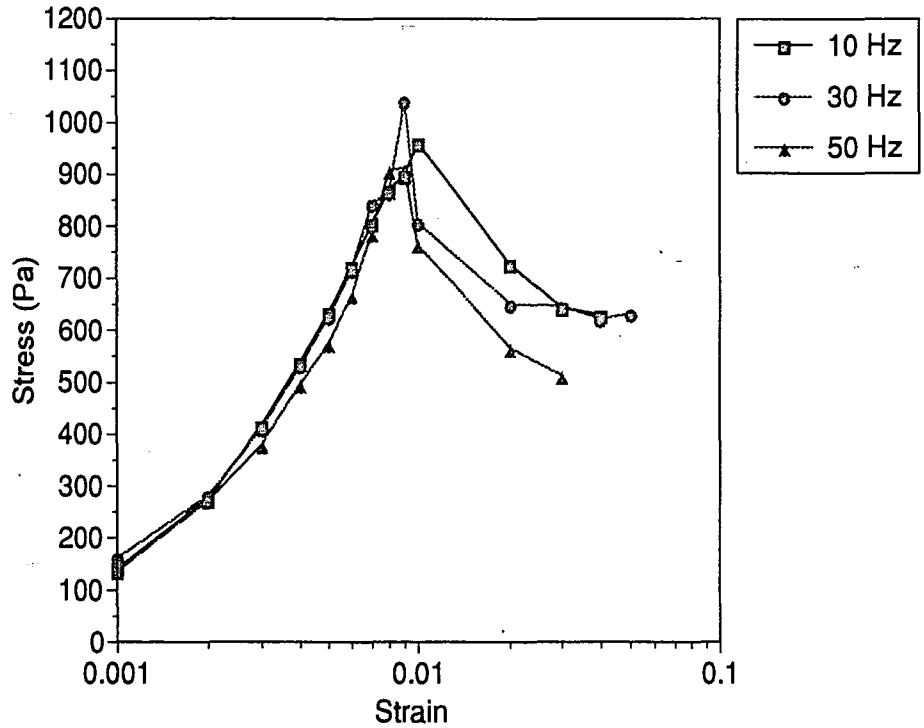

Figure 3.3.3 Magnitude of Stress vs. Strain at Frequencies of 10, 30, and 50 Hz at 3 kV/mm

[42] also reported a relatively flat G' with respect to frequency at low frequencies.

A typical phase-strain relationship is shown in Figure 3.3.4. The phase angle had two asymptotic regions. The first region exhibited mostly elastic behavior; phase angles near zero degrees, while the second region exhibited mostly viscous behavior; phase angles approaching ninety degrees. The region between the two is defined as a transition region where there is a dramatic change in the slope of the phase-strain curve. This dramatic change in the phase from a constant near the end of the first asymptotic region signified a yielding of linear behavior - as phase should have been independent of strain amplitude. Gamota and Filisko [25] also observed this type of behavior. At small strains they observed a linear viscoelastic region, followed by a viscoelastic plastic in the transition region, and then finally a totally plastic deformation region.

This investigation also observed a dependence of electric field on the phase-strain relationship as seen in Figure 3.3.5. The linear viscoelastic region defined by the phase-strain curves, elongated with increases in electric field. Again, this was most likely due to the increase in the dipole moment of the particles. The transition from linearity due to breaking of these particle chains was conjectured.

There were also slight increases in the linear viscoelastic region with decreases in the frequency as was seen in Figure 3.3.6. As frequency was increased the yield strain decreased. This supports the notion that the material became non-linear "easier" at higher frequencies. The non-linear behavior could be due to a natural frequency within the material or some type of non-linear hydrodynamic phenomenon with the liquid matrix.

In terms of defining a region of linear viscoelastic behavior, both the stress-strain and phase-strain relationship criteria must be satisfied. It was clearly seen that there was

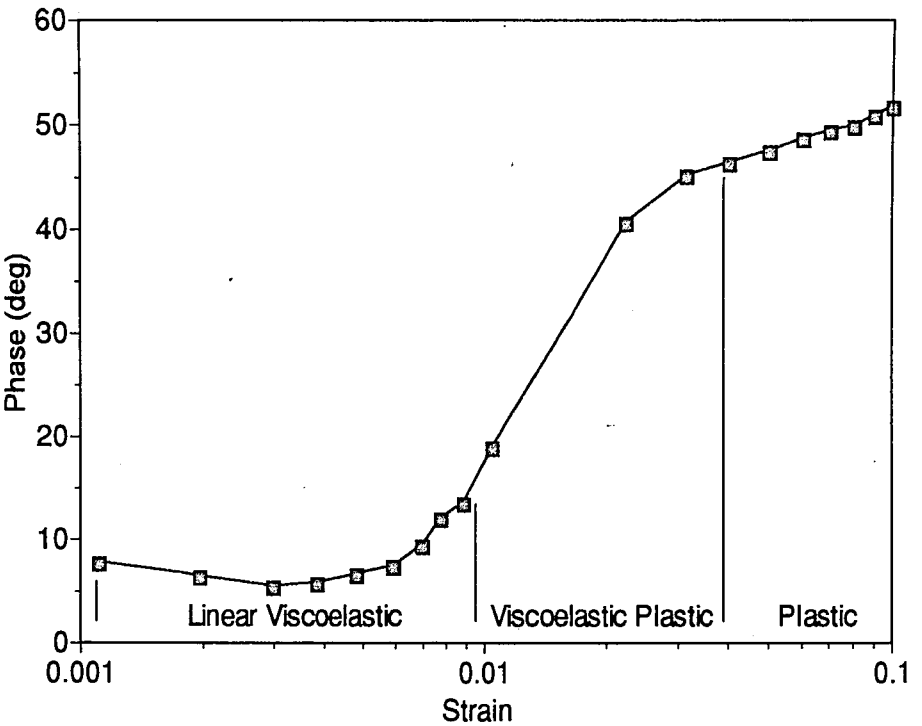

Figure 3.3.4 Phase Angle versus Strain at an Electric Field of 3 kV/mm and 10 Hz

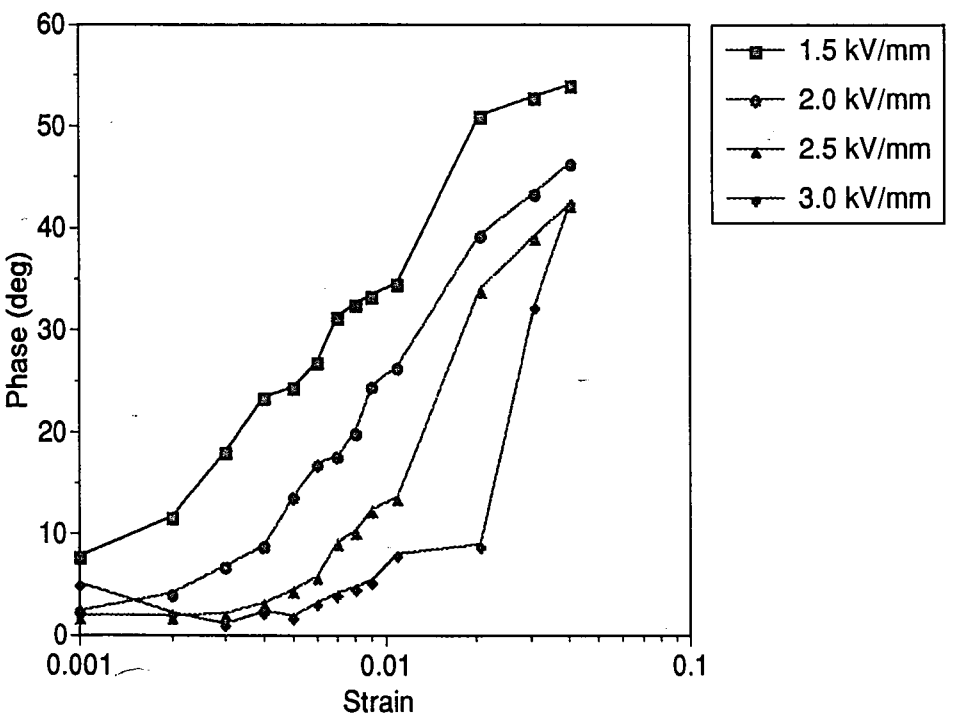

Figure 3.3.5 Phase Angle versus Strain at 10 Hz and Electric Fields of 1.5, 2.0, 2.5, and 3.0 kV/mm

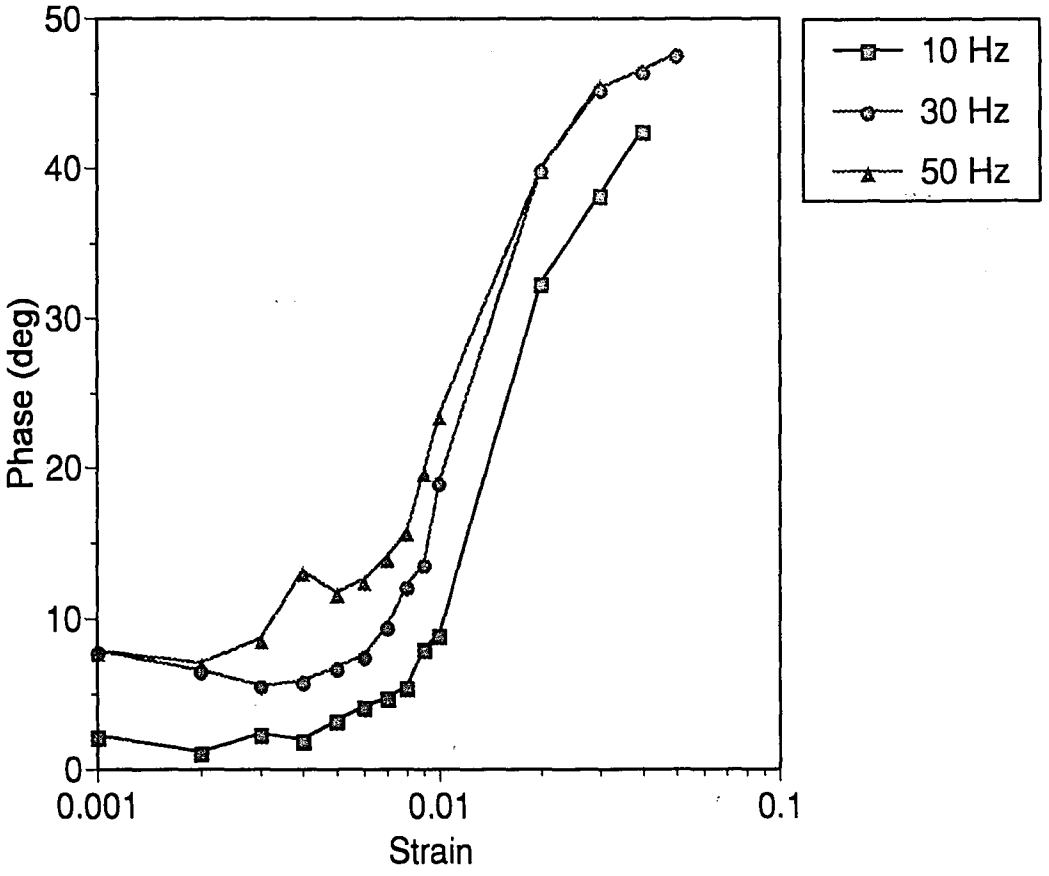

Figure 3.3.6 Phase Angle versus Strain at an Electric field of 3.0 kV/mm at 10, 30 and 50 Hz

a linear stress-strain relationship. The material was not as "linear" considering the second criteria - independent phase with respect to strain. Experimental trends for these yields with respect to electric field and frequency existed.

The stress yield was defined as the yield strain where there was a dramatic decrease in the transmitted stress. The phase yield limit was quantified to the yield strain where there was a deviation of five degrees from the asymptotic constant. The observed relationship between the stress-strain yield, and electric field and frequency is presented in Figure 3.3.7a. The observed relationship between phase-strain yield and electric field and frequency is shown in Figure 3.3.7b. Generally, for both cases, the yield strain increased with increases in electric field and decreases in frequency. This was contradictory to what was found in Gamota and Filisko[25].

Though the apparatus was able to observe these experimental trends in transition from linearity, it is not believed that the instrumentation was sensitive enough to quantify these small phase angles. As was observed, in many of the instances the phase angle approached an asymptotic constant, generally less than 5 degrees, around .1% strain. The question then became how to define the phase angle, and more specifically what were G' and G".

Phase yield was defined at the point where the phase strain relationship approached an asymptotic constant. The instrumentation of this investigation was not sensitive enough to measure such small phase angles, and apply such small strains accurately. The investigation *was* able to safely conclude that at 1.5 kV/mm or greater, G' was usually greater than 90% of $|G(j\omega)|$ due to the small phase angles.

With the present instrumentation, the quantification of material behavior within the linear viscoelastic region was limited to observation of $|G(j\omega)|$ or in this case G'. This is seen in Figure 3.3.8. As electric field was increased, there was significant

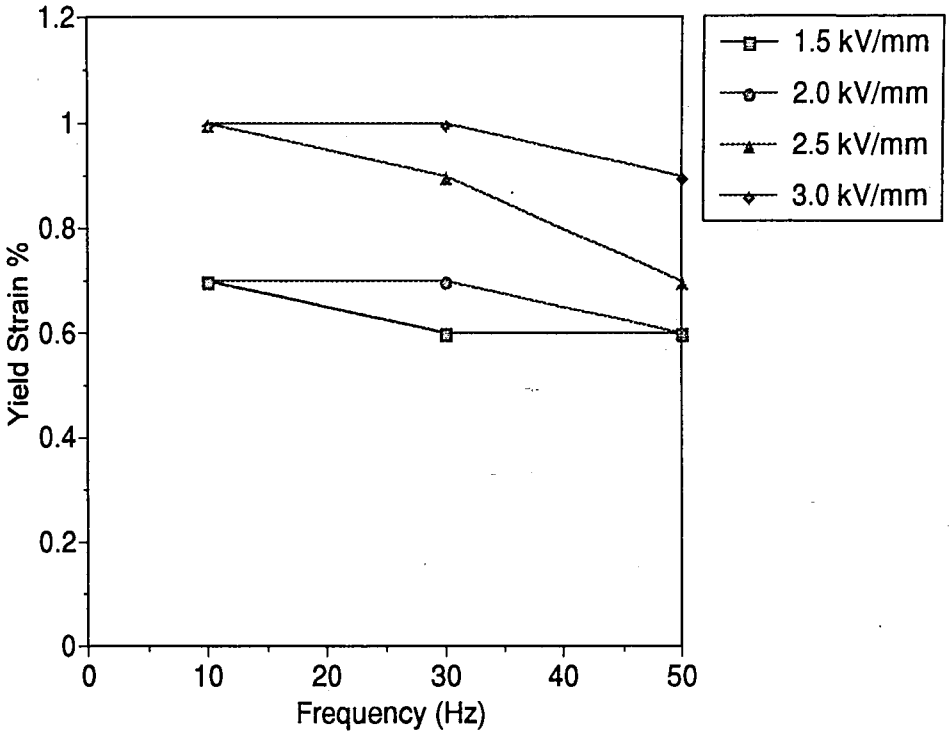

Figure 3.3.7a Yield Strain as Defined by the Stress Criteria versus Frequency at Electric Fields of 1.5, 2.0, 2.5, and 3.0 kV/mm

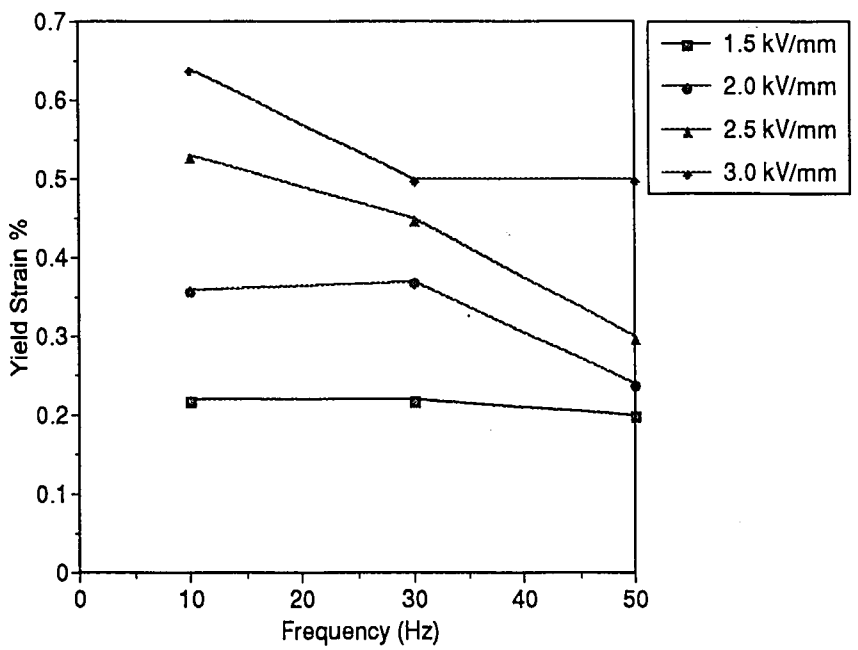

Figure 3.3.7b Yield Strain as Defined by the Phase Criteria versus Frequency at Electric Fields of 1.5, 2.0, 2.5, 3.0 kV/mm.

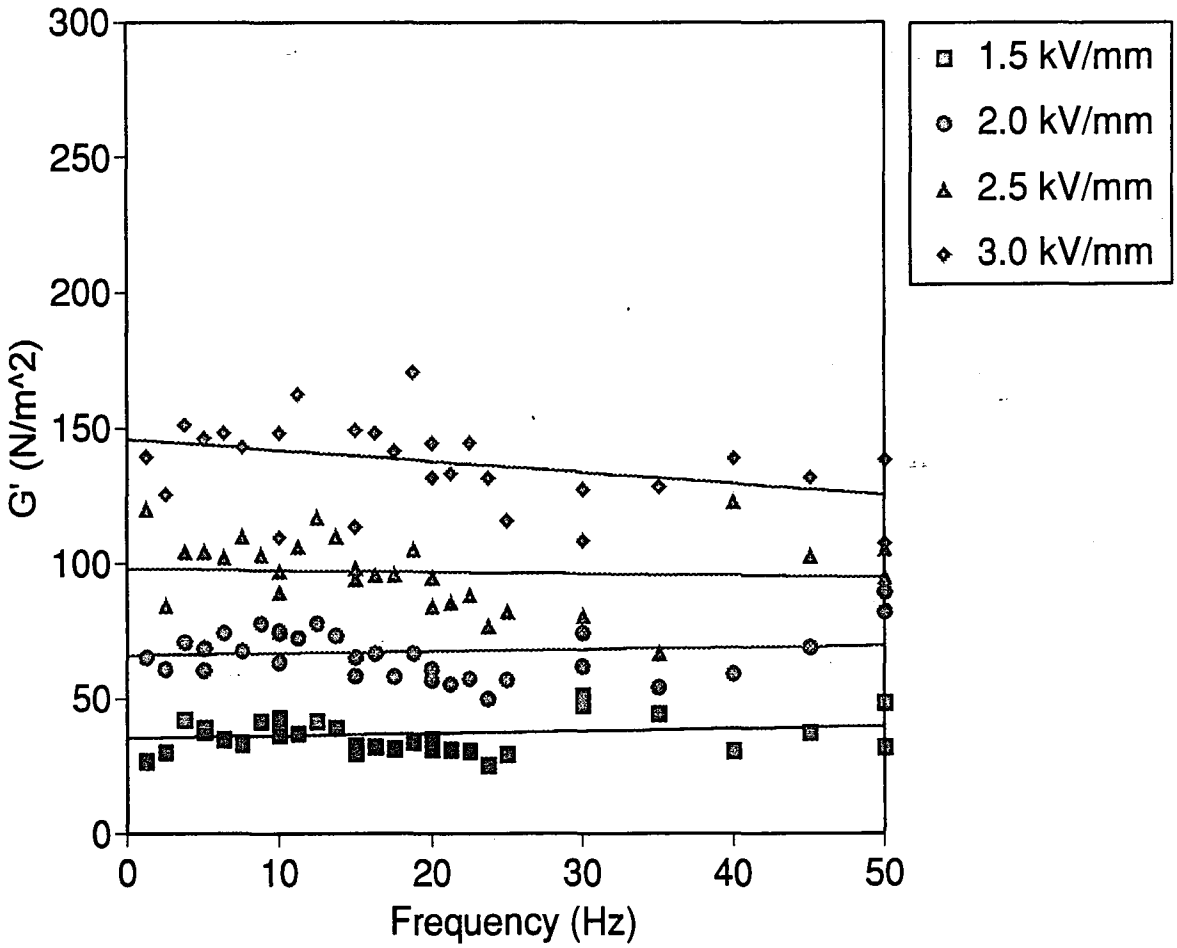

Figure 3.3.8 Magnitude of G versus Frequency at Electric Fields of 1.5, 2.0, 2.5, and 3.0 kV/mm

increase in G', while the dependence on frequency was less notable. Since the elastic portion of the complex modulus dominated the behavior, an approximation based on the relationship,

$$G'(j\omega) = kE^2 \qquad (3.3.1)$$

where k was a constant and E represents the applied field was adopted as seen in Figure 3.3.9. This squared dependence was also observed by Gamota and Filisko [25] and Jordan et al. [9]. The dependence on frequency was less notable as was again seen in Figure 3.3.8. Since G' dominated the behavior of $|G(j\omega)|$, this was not unexpected. Vinogradov [17] and Jordan et al. [9] also observed constant G' with respect to frequency.

The material utilized during the present study was found to be rather reliable, as $|G(j\omega)|$ was observed to be repeatable during three tests performed at different times. $|G(j\omega)|$ was found to be 36.9 $\pm$ 6.4 kPa, 67.3 $\pm$ 9.0 kPa, 96.9 $\pm$ 14.2 kPa, and 137.5 $\pm$ 15.9 kPa for electric fields of 1.5, 2.0, 2.5, and 3.0 kV/mm respectively. These results confirm that the material behavior did not change dramatically over the extended experimental testing time period. The error was estimated to be about 15%.

There were also other notable characteristics of the material which should be reported. First, there was significant flocculation of the particles after an electric field was applied and then removed. After removing the electric field it took time for the material to return to it's original state. This cause of this delay could have been the flocculation of the particles. The material's behavior was not completely reversible in that it took longer for it to return to it's original state then it did to react to an electric field. Second, the material was not able to hold a high electric field for a period of time

at strains within the linear viscoelastic region. After yield was reached, high electric fields were able to be maintained signifying the fracturing of some type of physical conductive bridge between the electrodes. Third, the magnitude of the complex shear modulus kept slightly increasing as the electric field was left on for long periods of time. Thurston and Gaenter [41] also describe a slow response to the formation of final microstructure.

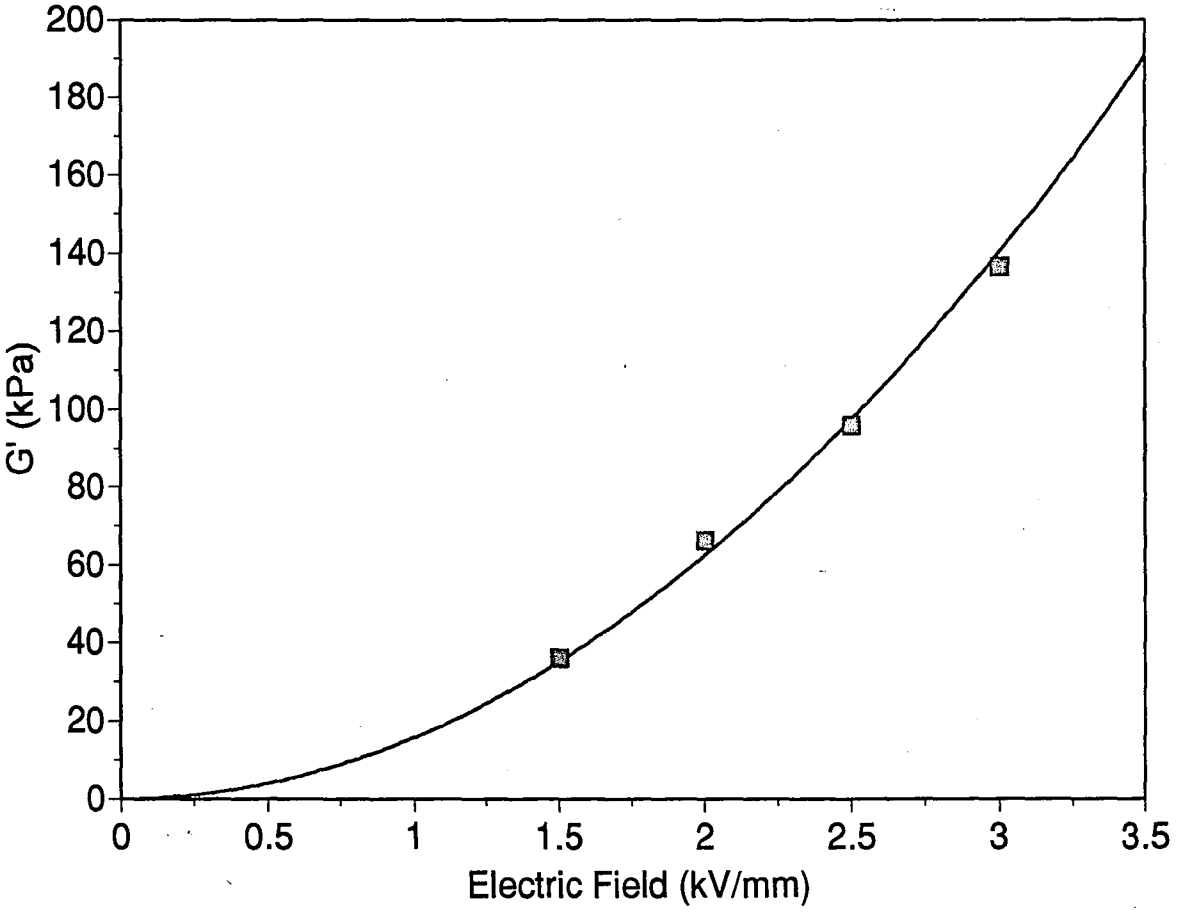

Figure 3.3.9 Magnitude of G' versus Electric Field

CHAPTER 4: INVESTIGATION ON THE MODELING OF ER BASED STRUCTURAL BEAMS

4.1 Introduction

None of the previous investigations has definitively concluded whether or not the Ross, Kerwin, and Ungar (RKU) and Mead and Markus structural theories are applicable to ER material based adaptive structures. There were three plausible explanations. One, their rheology data was not accurate. Two, their experimental beams did not meet the theoretical models specified geometric criteria. Three, the theories are not applicable.

The modeling phase of the present investigation tested the applicability of the RKU and Mead and Markus theories to ER based beam structures. Theoretical structural resonance and damping predictions were derived. The investigation then compared these theoretical results to experimental data from actual ER beam structures.

4.2 Structural Theory

The purpose of this section is to familiarize the reader with the RKU and Mead and Markus theories. It will be useful for the reader to know that both theories assume simply supported boundary conditions and sinusoidal mode shapes.

An energy method approach, described more thoroughly in Meirovitch's ***Analytical Methods in Vibrations*** [49], provides a methodical and tractable method of deriving the equations of motion and boundary conditions for systems with more than one-degree of freedom. The equations of motion and boundary conditions for a simply supported Bernoulli-Euler beam are derived as an example of this methodology.

4.2.1 Derivation of a Bernoulli-Euler Beam

The Lagrangian (L) is the basis for the energy approach. The variational equality

$$\int_{t_1}^{t_2} \delta L dt = \int_{t_1}^{t_2} (\delta T - \delta V) dt = 0 \tag{4.2.1.1}$$

where δL is the variation of the Lagrangian, δT is variation of the kinetic energy, and δV is the variation of the potential energy, is the governing equation for the derivation. This equality is based on variational principles more adequately described in Meirovitch [49]. The Lagrangian for a Bernoulli-Euler beam is,

$$\int_{t_1}^{t_2} \delta L dt = \int_{t}^{t_2} \frac{1}{2} \int_0^L m(x) \delta \left(\frac{\partial w}{\partial t} \right)^2 dx dt - \int_{t}^{t_2} \frac{1}{2} \int_o^L EI \delta \left(\frac{\partial^2 w}{\partial t^2} \right)^2 dx dt \tag{4.2.1.2}$$

where the first term represents the kinetic energy, and the second term represents the potential energy caused by bending of the beam. The rotary inertia and shear deformation are ignored. A schematic of the motion is shown in Figure 4.2.1.1.

The relationships,

$$\frac{1}{2} \delta \left(\frac{\partial w}{\partial t} \right)^2 = \frac{\partial w}{\partial t} \left(\frac{\partial (\delta w)}{\partial t} \right) \tag{4.2.1.3}$$

and

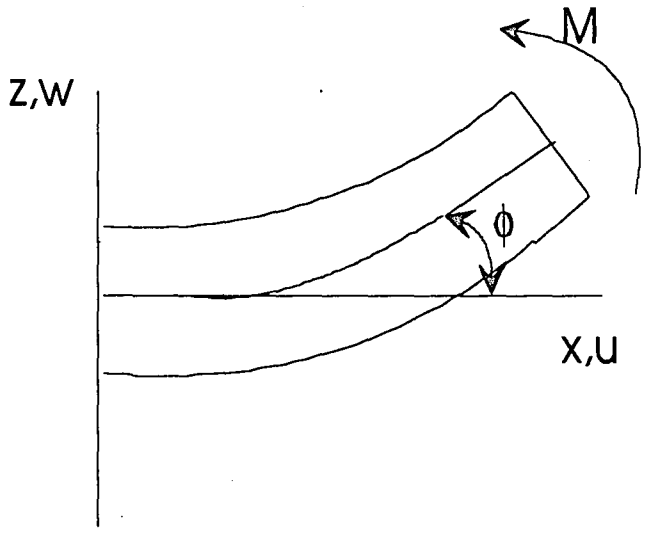

Figure 4.2.1.1 Schematic of a Bernoulli-Euler Beam

$$\frac{1}{2}\delta\left(\frac{\partial^2 w}{\partial x^2}\right)^2 = \frac{\partial^2 w}{\partial x^2}\left(\frac{\partial^2(\delta w)}{\partial x^2}\right) \tag{4.2.1.4}$$

can be substituted into the Lagrangian equation 4.2.1.2 yielding,

$$\int_t^{t_2}\frac{1}{2}\int_0^L m(x)\frac{\partial w}{\partial t}\left(\frac{\partial(\delta w)}{\partial t}\right)dxdt - \int_t^{t_2}\frac{1}{2}\int_o^L EI\frac{\partial^2 w}{\partial x^2}\left(\frac{\partial^2(\delta w)}{\partial x^2}\right)dxdt = 0 \tag{4.2.1.5}$$

Integrating by parts, equation 4.2.1.5 becomes,

$$m(x)\frac{\partial w}{\partial t}\delta w\Big|_{t_1}^{t_2} - \int_0^L\int_{t_1}^{t_2} m(x)\frac{\partial^2 w}{\partial t^2}\delta w dt dx \; - EI\frac{\partial^2 w}{\partial x^2}\delta\left(\frac{\partial w}{\partial x}\right)\Big|_0^L + \frac{\partial}{\partial x}\left(EI\frac{\partial^2 w}{\partial x^2}\right)\delta w\Big|_0^L$$
$$-\int_{t_1}^{t_2}\int_0^L \frac{\partial^2}{\partial x^2}\left(EI\frac{\partial^2 w}{\partial x^2}\right)\delta w dx dt = 0 \tag{4.2.1.6}$$

The first term in equation 4.2.1.6 goes to 0 by definition of the variance; the change in w from some initial time to some final time is 0. By collecting terms on the expression we find that

$$-\int_0^L\int_{t_1}^{t_2}\left[m(x)\frac{\partial^2 w}{\partial t^2} + \frac{\partial^2}{\partial x^2}\left(EI\frac{\partial^2 w}{\partial x^2}\right)\right]\delta w dt dx - EI\frac{\partial^2 w}{\partial x^2}\delta\left(\frac{\partial w}{\partial x}\right)\Big|_0^L$$
$$+\frac{\partial}{\partial x}\left(EI\frac{\partial^2 w}{\partial x^2}\right)(\delta w)\Big|_o^L = 0 \tag{4.2.1.7}$$

Each of the terms in equation 4.2.1.7 is independent and must go to 0 independently. For the first term in equation 4.2.1.7, $\delta w=0$ is a trivial solution, hence, the term in parenthesis must go to zero for a non-trivial solution,

$$m(x)\frac{\partial^2 w}{\partial t^2}+\frac{\partial^2}{\partial x^2}\left(EI\frac{\partial^2 w}{\partial x^2}\right)=0 \qquad (4.2.1.8)$$

Equation 4.2.1.8 represents the equation of motion for the beam. The last two terms in equation 4.2.1.7 represent the boundary conditions,

$$EI\frac{\partial^2 w}{\partial x^2}\delta\left(\frac{\partial w}{\partial x}\right)\Big|_0^L=0 \qquad (4.2.1.9)$$

$$\frac{\partial}{\partial x}\left(EI\frac{\partial^2 w}{\partial x^2}\right)\delta w\Big|_0^L=0 \qquad (4.2.1.10)$$

where equation 4.2.1.9 represents the moment and slope at 0 and L, and equation 4.2.1.10 represents the shear and deflection at 0 and L. The variational terms in equations 4.2.1.9 and 4.2.1.10 represent the geometric constraints while the derivative terms are the moment and shear constraints. For example in the simply supported case, the slopes at locations 0 and L are arbitrary, therefore

$$EI\frac{\partial^2 w}{\partial x^2}\Big|_0^L=0 \qquad (4.2.1.11)$$

Since the displacement w at locations 0 and L is 0, the variation is also 0. This a geometric constraint. These four constraints make up the boundary conditions for the problem.

Using separation of variables a solution to the problem is

$$w = w(x)T(t) \tag{4.2.1.12}$$

Substituting equation 4.2.1.12 into the equation of motion equation 4.2.1.8, two independent ordinary differential equations can be derived,

$$\ddot{T}(t) + \omega^2 T(t) = 0 \tag{4.2.1.13}$$

$$\frac{\partial^4 w(x)}{\partial x^4} - \frac{m(x)}{EI}\omega^2 w(x) = 0 \tag{4.2.1.14}$$

where ω is the radial natural frequency of the structure. The solution to equation 4.2.1.14 is of the form,

$$w = A\sin(\lambda x) + B\cos(\lambda x) + C\sinh(\lambda x) + D\cosh(\lambda x) \tag{4.2.1.15}$$

where λ is the root of equation 4.2.1.14,

$$\lambda^4 = \frac{m(x)}{EI}\omega^2 \tag{4.2.1.16}$$

By substituting this into the boundary conditions, three of the coefficients in equation 4.2.1.15 can be eliminated for the simply supported case leaving,

$$w = A\sin(\lambda x) \tag{4.2.1.17}$$

and

$$\lambda = \frac{n\pi}{L} \tag{4.2.1.18}$$

where n is the mode number, and L is the length of the beam. From this the natural frequency of the structure can be solved,

$$\omega = (\lambda)^2 \sqrt{\left(\frac{EI}{m(x)}\right)} \tag{4.2.1.19}$$

4.2.2 Derivation of the Ross, Kerwin, Ungar (RKU) Model

The RKU theory is based on this classical Bernoulli-Euler beam. Their modification of this theory centers around deriving a new, complex flexural rigidity.

Consider Figure 4.2.2.1. Assume that layers 1 and 3 experience a flexural motion ϕ , while the middle layer assumes the same flexural motion plus a superimposed shear strain γ. The total bending moment about the neutral plane can be expressed as,

$$M = B\frac{\partial \phi}{\partial x} = \sum_{1}^{3} M_{ii} + \sum_{1}^{3} F_i H_{i0} \qquad (4.2.2.1)$$

where B is the effective flexural rigidity, $\frac{\partial \phi}{\partial x}$ is the slope of the flexural angle, M_{ii} is the moment of the *i*th layer about it's own neutral plane, F_i is the net extensional force on the *i*th layer, and H_{i0} is the distance from the mid plane of the *i*th layer to a new neutral plane created by the addition layers 2 and 3. The old neutral plane, defined as the neutral plane without any additional layers, is the mid plane of the first layer. Therefore,

$$H_{i0} = H_{i1} - D \qquad (4.2.2.2)$$

where H_{i1} is the distance between the mid-plane of the ith layer and the mid-plane of layer 1, and D is the displacement of the old neutral plane.

The moments about each layer can be expressed in terms of the curvature,

$$M_{11} = E_1 I_1 \frac{\partial \phi}{\partial x} \qquad (4.2.2.3)$$

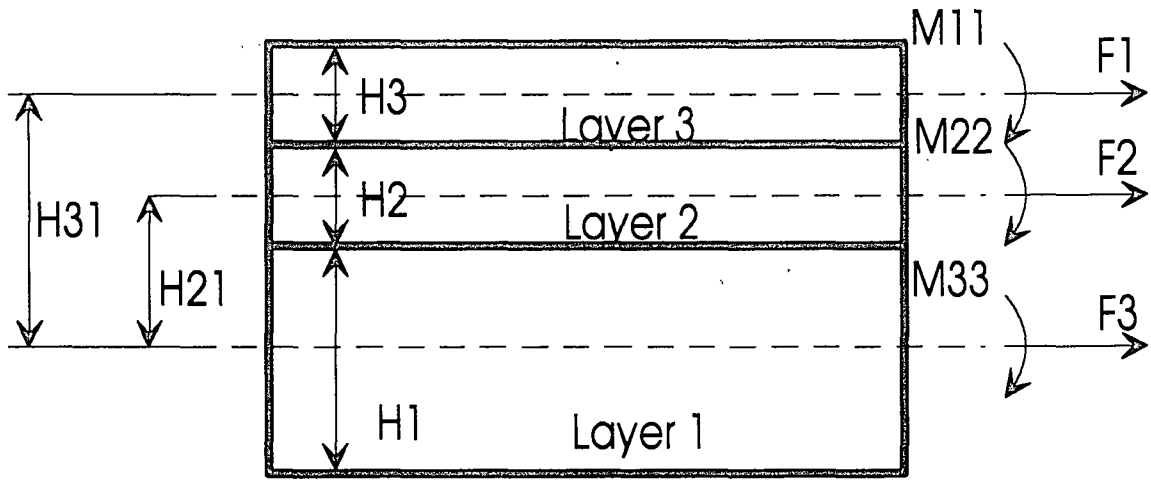

Figure 4.2.2.1 RKU Free-Body Diagram

$$M_{22} = E_2 I_2 (\frac{\partial \phi}{\partial x} - \frac{\partial \gamma}{\partial x}) \tag{4.2.2.4}$$

$$M_{33} = E_3 I_3 \frac{\partial \phi}{\partial x} \tag{4.2.2.5}$$

where I is the moment of inertia per unit depth, E is the elastic modulus of each layer, ϕ is the flexural angle, and γ is the shear strain.

The net extensional force can be assumed to be the extensional force exerted at the mid plane of each layer. The force is the product of the extensional stiffness and the strain of the mid-plane which can be derived by geometry. For small strains the force can be expressed as,

$$F_1 = E_1 H_1 H_{10} (\frac{\partial \phi}{\partial x}) \tag{4.2.2.6}$$

$$F_2 = E_2 H_2 (H_{20} \frac{\partial \phi}{\partial x} - \frac{H_2}{2} \frac{\partial \gamma}{\partial x}) \tag{4.2.2.7}$$

$$F_3 = E_3 H_3 (H_{30} \frac{\partial \phi}{\partial x} - H_2 \frac{\partial \gamma}{\partial x}) \tag{4.2.2.8}$$

The effective flexural rigidity can be solved using these relations. First assume the following relation,

$$\frac{\partial \gamma}{\partial \phi} = \frac{(\frac{\partial^n \gamma}{\partial x^n})}{(\frac{\partial^n \phi}{\partial x^n})} \tag{4.2.2.9}$$

Equation 4.2.2.9 represents the ratio of shear strain to flexural angle. Substituting equations 4.2.2.3-4.2.2.9 into equation 4.2.2.1, and solving for the effective flexural rigidity,

$$B = E_1 I_1 + E_2 I_2 + E_3 I_3 + E_1 H_{10}^2 + E_2 H_{20}^2 + E_3 H_{30}^2 - E_2 I_2 \frac{\partial \gamma}{\partial \phi} - \left[\frac{E_2}{2} H_{20} + E_3 H_{30} \right] H_2 \frac{\partial \gamma}{\partial \phi} \quad (4.2.2.10)$$

There are two unknown variables: the displacement of the neutral plane D as described in equation 4.2.2.2, and $\frac{\partial \gamma}{\partial \phi}$.

The displacement of the neutral plane can be solved by assuming that the motion is in pure flexure. In pure flexure the sum of the extensional forces of all three layers must be equal to zero;

$$(E_1 + E_2 + E_3) D \frac{\partial \phi}{\partial x} + (E_2 H_{21} + E_3 H_{31}) \frac{\partial \phi}{\partial x} - (\frac{E_2}{2} + E_3) H_2 \frac{\partial \gamma}{\partial x} = 0 \quad (4.2.2.11)$$

solving for D,

$$D = \frac{E_2 H_2 H_{21} + E_3 H_3 H_{31} - (\frac{E_2 H_2}{2} + E_3 H_3) H_2 \frac{\partial \gamma}{\partial \phi}}{E_1 H_1 + E_2 H_2 + E_3 H_3} \quad (4.2.2.12)$$

The second variable we must solve for is $\frac{\partial \gamma}{\partial \phi}$. This is where the RKU theory includes the shear modulus of the middle layer. The effective shear stress is equal to the net force on the top and bottom layer. The shear force is assumed to be small and approximately corresponds to the net force on layer 3. The stress-strain relationship can be expressed as,

$$\gamma = -\frac{1}{G_2}\frac{\partial F_3}{\partial x} \tag{4.2.2.13}$$

where G_2 is the shear modulus of the second layer. Substituting equation 4.2.2.8 into equation 4.2.2.13,

$$\gamma = -\frac{1}{G_2} E_3 H_3 \left(H_{30}\frac{\partial^2 \phi}{\partial x^2} - H_2 \frac{\partial^2 \gamma}{\partial x^2}\right) \tag{4.2.2.14}$$

If the all the layers experience the same flexure then the shear strain must be proportional flexural angle. Since we assume simply supported boundary conditions the flexural angle and the shear strain are both sinusoidal; therefore, the shear strain is proportionally to it's second derivative,

$$\gamma(x) = -\frac{1}{\lambda^2}\frac{\partial^2 \gamma(x)}{\partial x^2} \tag{4.2.2.15}$$

where λ is the wave number. For the simply supported case, λ is $n\pi/L$.

Using equations 4.2.2.14 and 4.2.2.15 the second variable $\frac{\partial\gamma}{\partial\phi}$ is obtained,

$$H_2 \frac{\partial\gamma}{\partial\phi} = \frac{H_{31} - D}{1+g} \tag{4.2.2.16}$$

where

$$g = \frac{G_2}{E_3 H_3 H_2 \lambda^2} \tag{4.2.2.17}$$

By substituting equation 4.2.2.16 into equation 4.2.2.10, we now have an effective flexural rigidity,

$$\begin{aligned} B = {} & E_1 I_1 + E_2 I_2 + E_3 I_3 + E_1 H_1 H_{10}^2 + E_2 H_2 H_{20}^2 + E_3 H_3 H_{30}^2 \\ & - \frac{E_2 I_2}{H_2} \frac{H_{31} - D}{1+g} - \left[\frac{E_2 H_2}{2} H_{20} + E_3 H_3 H_{30} \right] \frac{H_{31} - D}{1+g} \end{aligned} \tag{4.2.2.18}$$

where

$$D = \frac{E_2 H_2 (H_{21} - H_{31}/2) + g(E_2 H_2 H_{21} + E_3 H_3 H_{31})}{E_1 H_1 + E_2 H_2 / 2 + g(E_1 H_1 + E_2 H_2 + E_3 H_3)} \tag{4.2.2.19}$$

The model includes the affects of damping by using complex notation. The separated equations of motion for the beam become,

$$\ddot{T}(t) + \omega^2 (1 + i\eta) T(t) = 0 \tag{4.2.2.20}$$

$$\frac{\partial^4 w(x)}{\partial x^4} - \frac{m(x)}{B' + iB''} \omega^2 (1 + i\eta) w(x) = 0 \tag{4.2.2.21}$$

where η is the effective structural damping, B' is the real part of the flexural rigidity, B" is the imaginary part of the flexural rigidity. The flexural rigidity becomes complex due to the incorporation of the damping in the second layer. This damping is represented by the complex shear modulus,

$$G_2 = G_2' + iG_2'' \tag{4.2.2.22}$$

If equation 4.2.2.21 is separated into it's real and imaginary parts the following equations are obtained,

$$\frac{\partial^4 w(x)}{\partial x^4} - \frac{m(x)}{EI'^2 + EI''^2}\omega^2 (B' + \eta B'')w(x) = 0 \tag{4.2.2.23}$$

$$-\frac{m(x)}{EI'^2 + EI''^2}\omega^2 (\eta B' - B'')w(x) = 0 \tag{4.2.2.24}$$

From equation 4.2.2.24 the effective structural damping η can be solved,

$$\eta = \frac{B''}{B'} \tag{4.2.2.25}$$

If we assume simply supported boundary conditions, the damped natural frequency of the structure can be derived from equation 4.2.2.23,

$$\omega = \lambda^2 \sqrt{\frac{B'^2 + B''^2}{m(x)(B' + \eta B'')}} \tag{4.2.2.26}$$

where $\lambda = \frac{n\pi}{L}$.

4.2.3 Derivation of the Mead and Markus Model

The derivation of the Mead and Markus model is examined using the methodology in Section 4.2.1; an energy approach. The kinetic energy of the beam is considered only in the w direction as seen in Figure 4.2.3.1,

$$\delta T = \int_{t}^{t_2} \frac{1}{2} \int_0^L m(x) \delta \left(\frac{\partial w}{\partial t} \right)^2 dx dt \qquad (4.2.3.1)$$

The potential energy of the beam is a summation of the energy stored due to bending, energy stored due to elongation of the constraining layers, and the energy stored within the shear layer. The deformation can be seen in the free body diagram in Figure 4.2.3.1.

The variation in potential energy can be represented by,

$$\delta V = \frac{1}{2} \delta \int_0^L (E_1 I_1 + E_2 I_2 + E_3 I_3) \left(\frac{\partial^2 w}{\partial x^2} \right)^2 dx + \frac{1}{2} \delta \int_0^L E_1 A_1 \left(\frac{\partial u_1}{\partial x} \right)^2 dx + \frac{1}{2} \delta \int_0^L E_3 A_3 \left(\frac{\partial u_3}{\partial x} \right)^2 dx$$
$$+ \frac{1}{2} \delta \int_0^L G_2 A_2 (\gamma)^2 dx + + \delta \int_0^L q(x,t) w dx \qquad (4.2.3.2)$$

where the first term represents the contribution due to bending, the second and third term represent the contribution due to elongation of the constraining layers, the fourth term represents the contribution due to the shear layer, and the last term represents the potential due to loading.

The shear within the middle layer is coupled to the elongation of the constraining layers and the flexural angle due to bending geometrically. The shear strain of an element is defined as

$$\gamma = \frac{\partial w}{\partial x} + \frac{\partial u}{\partial z} \tag{4.2.3.3}$$

which can be seen geometrically in Figure 4.2.3.2. $\frac{\partial u}{\partial z}$ in equation 4.2.3.3 can be represented as a summation of the shear due to rotation and elongation,

$$\frac{\partial u}{\partial z} = \frac{\Delta u_{rotation}}{H_2} + \frac{\Delta u_{elongation}}{H_2} \tag{4.2.3.4}$$

This can be observed geometrically from Figure 4.2.3.1. From this geometry,

$$\frac{\partial u}{\partial z} = \frac{1}{H_2}\left(\frac{H_1}{2} + \frac{H_3}{2}\right)\frac{\partial w}{\partial x} + \frac{u_1 - u_3}{H_2} \tag{4.2.3.5}$$

The shear strain can now be calculated from equations 4.2.3.3 and 4.2.3.5 to be related to the elongation of the first and third layers, and the rotation of the entire beam,

$$\gamma = \left(\frac{\partial w}{\partial x}\frac{d}{H_2} + \frac{u_1 - u_3}{h_2}\right) \tag{4.2.3.6}$$

where

$$d = H_2 + \frac{1}{2}(H_1 + H_3)$$

The problem now has 3 degrees of freedom - w, u_1, and u_3. Substituting equation 4.2.3.6 back into equation 4.2.3.2 the variation in the potential becomes,

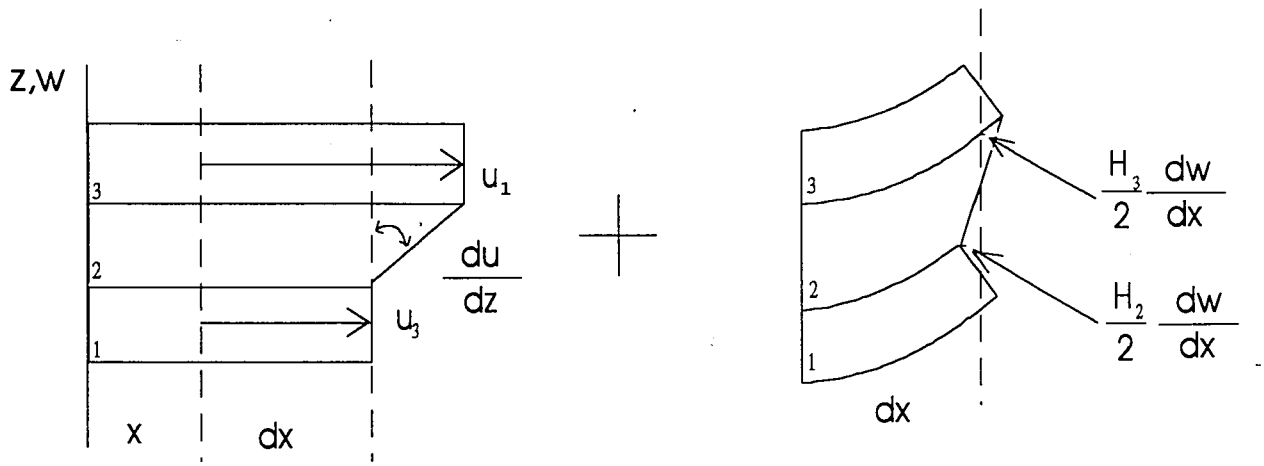

Figure 4.2.3.1 Schematic of the Strain due to Elongation and Bending

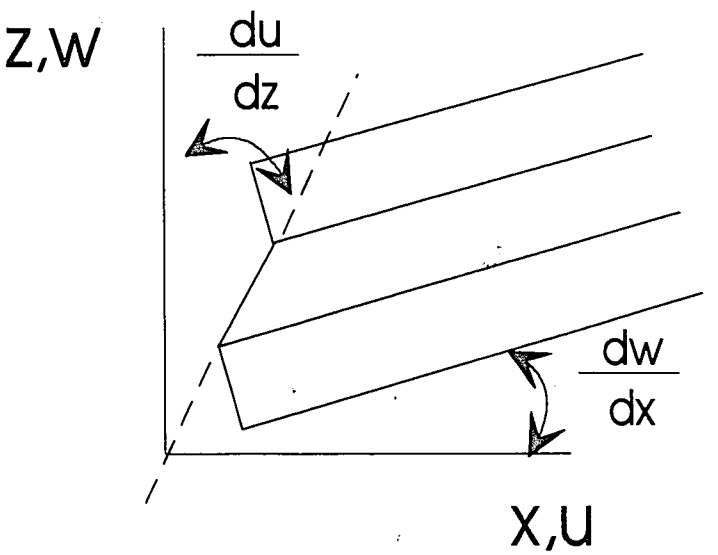

Figure 4.2.3.2 Strain in the Second Layer

$$\delta V = \frac{1}{2}\delta\int_0^L(\overline{EI})\left(\frac{\partial^2 w}{\partial x^2}\right)^2 dx + \frac{1}{2}\delta\int_0^L E_1 A_1\left(\frac{\partial u_1}{\partial x}\right)^2 dx + \frac{1}{2}\delta\int_0^L E_3 A_3\left(\frac{\partial u_3}{\partial x}\right)^2 dx$$
$$+\frac{1}{2}\delta\int_0^L G_2 A_2\left(\frac{\partial w}{\partial x}\frac{d}{h_2} + \frac{u_1 - u_3}{h_2}\right)^2 \qquad (4.2.3.7)$$

where $\overline{EI} = E_1 I_1 + E_2 I_2 + E_3 I_3$. Using the same methods in Section 4.2.1 the equations of motion are derived.

The first equation of motion represents the motion in the w direction,

$$m(x)\frac{\partial^2 w}{\partial t^2} + \overline{EI}\frac{\partial^4 w}{\partial x^4} - GA\frac{d}{H_2}\frac{\partial}{\partial x}\left(\frac{\partial w}{\partial x}\frac{d}{H_2} + \frac{u_1 - u_3}{H_2}\right) = q(x,t) \qquad (4.2.3.8)$$

where q(x,t) is a forcing function.

The second two equations of motion represent the elongational forces of the second and third layers,

$$E_1 A_1\frac{\partial^2 u_1}{\partial x^2} - \frac{G}{H_2}\left(\frac{\partial w}{\partial x}\frac{d}{H_2} + \frac{u_1 - u_3}{H_2}\right) = 0 \qquad (4.2.3.9)$$

$$E_3 A_3\frac{\partial^2 u_3}{\partial x^2} + \frac{G}{H_2}\left(\frac{\partial w}{\partial x}\frac{d}{H_2} + \frac{u_1 - u_3}{H_2}\right) = 0 \qquad (4.2.3.10)$$

Notice there are no inertial terms in equations 4.2.3.9 and 4.2.3.10. By combining equations 4.2.3.9 and 4.2.3.10 we see that the net longitudinal force on the first and third layers is zero,

$$E_1 A_1 \frac{\partial u_1}{\partial x} = -E_3 A_3 \frac{\partial u_3}{\partial x} \tag{4.2.3.11}$$

and similarly,

$$E_1 A_1 u_1 = -E_3 A_3 u_3 \tag{4.2.3.12}$$

Substituting equation 4.2.3.12 back into equation 4.2.3.8,

$$\frac{m(x)}{\overline{EI}} \frac{\partial^2 w}{\partial t^2} + \frac{\partial^4 w}{\partial x^4} - gY \frac{\partial^2 w}{\partial x^2} + g \frac{E_3 H_3 d}{\overline{EI}} \frac{\partial u_3}{\partial x} = \frac{q(x,t)}{\overline{EI}} \tag{4.2.3.13}$$

where

$$g = \frac{G}{H_2} \left(\frac{1}{E_1 H_1} + \frac{1}{E_3 H_3} \right)$$

$$Y = \frac{d^2}{\overline{EI}} \left(\frac{E_1 H_1 E_3 H_3}{E_1 H_1 + E_3 H_3} \right)$$

It would be desirable for the equation of motion to only be in terms of the w-direction which means finding $\frac{\partial u_3}{\partial x}$ in terms of w or its derivatives. Equations 4.2.3.9 and 4.2.3.10 can be combined to solve for $\frac{\partial u_3}{\partial x}$.

$$\frac{\partial^2 u_3}{\partial x^2} - g u_3 = -gY \frac{\overline{EI}}{E_3 H_3} \frac{\partial w}{\partial x} \tag{4.2.3.14}$$

By differentiating equation 4.2.3.14, and solving equation 4.4.3.13 for $\frac{\partial u_3}{\partial x}$ and $\frac{\partial^2 u_3}{\partial x^2}$, a single equation of motion for forced vibratory motion in the w direction is derived,

$$\frac{\partial^6 w}{\partial x^6} - g(1+Y)\frac{\partial^4 w}{\partial x^4} + \frac{m(x)}{\overline{EI}}\left(\frac{\partial^4 w}{\partial x^2 \partial t^2} - g\frac{\partial^2 w}{\partial t^2}\right) = \frac{1}{\overline{EI}}\left(\frac{\partial^2 q(x,t}{\partial x^2} - gq(x,t)\right) \quad (4.2.3.15)$$

This equation can be solved using separation of variables methodology per equation 4.2.1.12. In addition, the model assumes a harmonic loading proportional to the displacement and the mass per unit length,

$$q(x,t) = Pmw(x)e^{i\omega t} \quad (4.2.3.16)$$

Substituting equations 4.2.3.12 and 4.2.3.16 into equation 4.2.3.15 we find that the equation of motion can be written in a familiar, separable form,

$$\ddot{T}(t) + \omega^2(1+i\eta)T(t) = Pe^{i\omega t} \quad (4.2.3.17)$$

$$\frac{\partial^6 w(x)}{\partial x^6} - g(1+Y)\frac{\partial^4 w(x)}{\partial x^4} - \omega^2(1+i\eta)\left(\frac{m(x)}{\overline{EI}}\right)\left(\frac{\partial^2 w(x)}{\partial x^2} - gw(x)\right) = 0 \quad (4.2.3.18)$$

The quantity g is a complex quantity by virtue of the complex shear modulus,

$$g'(1+i\beta) = \frac{1}{H_2}\left(\frac{1}{E_1 H_1} + \frac{1}{E_3 H_3}\right)G'(1+i\beta) \quad (4.2.3.19)$$

where β is the loss factor of the ER material and defined as,

$$\beta = \frac{G''}{G'}$$

Since this is the case, equation 4.2.3.18 can be separated into its real and imaginary parts respectively,

$$\frac{\partial^6 w(x)}{\partial x^6} - g'(1+Y)\frac{\partial^4 w(x)}{\partial x^4} - \omega^2\left(\frac{m(x)}{\overline{EI}}\right)\left(\frac{\partial^2 w(x)}{\partial x^2} - g'(\eta\beta - 1)w(x)\right) = 0 \quad (4.2.3.20)$$

$$-g'\beta(1+Y)\frac{\partial^4 w(x)}{\partial x^4} - \omega^2\left(\frac{m(x)}{\overline{EI}}\right)\left(\eta\frac{\partial^2 w(x)}{\partial x^2} - g'(\eta+\beta)w(x)\right) = 0 \quad (4.2.3.21)$$

A solution for w must satisfy both of the real and imaginary equations of motion. For equation 4.2.3.20 there are six possible solutions, but four of these solutions must also satisfy equation 4.2.3.21. In that case a possible solution for w is of the form,

$$w = A\sin(\lambda x) + B\cos(\lambda x) + C\sinh(\lambda x) + D\cosh(\lambda x) \quad (4.2.3.22)$$

There are only four possible solutions to the equation of motion but there are six boundary conditions. Those six boundary conditions are,

$$\overline{EI}\frac{\partial^2 w}{\partial x^2}\delta\left(\frac{\partial w}{\partial x}\right)\Big|_0^L = 0 \quad (4.2.3.23)$$

$$\overline{EI}\frac{\partial^3 w}{\partial x^3} - G\frac{d}{H_2}\left(\frac{d}{H_2}\frac{\partial w}{\partial x} + \frac{u_1 - u_3}{H_2}\right)\delta(\partial w)\Big|_0^L = 0 \quad (4.2.3.24)$$

$$E_1 H_1 \frac{\partial u_1}{\partial x}(\delta u_1) + E_3 H_3 \frac{\partial u_3}{\partial x}(\delta u_3)\Big|_0^L = 0 \quad (4.2.3.25)$$

The **only** possible ***real*** solution is that

$$w = A\sin(\lambda x) \tag{4.2.3.26}$$

where $\lambda = \frac{n\pi}{L}$.

The forced natural frequency and damping for the structure can now be determined. By substituting equation 4.2.3.26 into equations 4.2.3.20 and 4.2.3.21 we see that there are two unknowns, ω and η , and two equations. We find that,

$$\omega = \lambda^2\sqrt{\frac{EI}{m}\frac{g^2\beta^2+\lambda^4+2\lambda^2 g+\lambda^2 gY+g^2+g^2Y}{\lambda^4+2\lambda^2 g+g^2\beta^2+g^2}} \tag{4.2.3.27}$$

and

$$\eta = g^2 Y\frac{\beta}{g^2\beta^2+\lambda^4+2\lambda^2 g+\lambda^2 gY+g^2+g^2Y} \tag{4.2.3.28}$$

These represent the natural frequency and the damping of the structure respectively.

4.3 Experimental Set up

4.3.1 Fabrication of ER Adaptive Beam Structures

The ER beam structures built utilized a constrained layer design: ER material sandwiched between two elastic constraining layers. There were three concerns that were addressed in designing these structures,

1. What type of constraining layer and electrodes to use.
2. How to keep a constant gap between the electrodes without restricting the shear.
3. How to seal in the ER material without restricting the shear.

Figure 4.3.1.1 shows the general procedure utilized during structure fabrication.

The first design concern was the selection of the constraining structure and the electrodes. Aluminum was chosen due to it's low damping properties which reduced the complexity of the theoretical modeling (No damping in either of the constraining layers was assumed). Wire leads were spot welded onto the aluminum layers. These spot welds proved to be weak; sometimes breaking due to constant handling of the structure. The preferred method which was later utilized was to attach a copper terminal to the aluminum electrode and paint, with a conductive coating, a connection between the terminal and the structure.

The second concern was to keep a uniform gap distribution without restricting the shear of the sandwiched layer. Previous investigations used a restrictive layer of silicon to separate the electrodes. Instead of silicone rubber, this investigation tried a polyester fabric mesh. The mesh was attached to only one of the electrodes keeping the electrode gap constant and reducing the restriction to the sandwiched layer. The problem with this design was that it was hard to remove the air from within the mesh. These structures

tended to arc at electric fields close to where air would begin to arc. The preferred design utilized polycarbonate spacers. The spacers were 5mm x 5mm and attached only to one of the constraining layers. The polycarbonate spacers kept a uniform gap while the reducing the restrictions placed on the middle layer and did not create electric problems. The polycarbonate was also more elastic and had less damping than silicon sealant.

The third design concern was to seal the ER material into the structure. The first ER structures had silicone sealant around outside edges of the beams. These structures were not responsive to changes in ER material behavior and their behavior deviated significantly from theoretical models. The silicon impaired the shear strain within the sandwiched layer reducing net effect of the ER phenomenon. The structural dynamic models did not include the addition of the restraining silicone.

One purpose of this phase of the investigation was to fabricate structures that were consistent with the geometric assumptions made in the theories. Coulter et al. [30, 35] attempted to minimize the use of silicone sealant by attaching a thin latex material loosely around the edge of the structure. This investigation used the same concept. Two different wraps were investigated, a plastic film and rubber latex. The plastic film was found to be too conductive at higher electric fields. The tested structures had the loosely wrapped latex seal.

The latex wrap, .5mm thick, was attached using two materials; a rubber based 3M tape, and epoxy. ER material tended to leak through the tape seal so a small amount of acrylic sealant was used to completely seal the material in around the edges of the wrap. The leakage was caused by degradation of the rubber based tape in the presence of ER material. The additional sealant changed the structural stiffness. The use a epoxy not affected by petroleum based products solved the problem. Finally, in both the tape and

epoxy sealed beams, a liquid sealant was put around the corners due to the gaps between the latex wrap. Care was taken to avoid placing this final sealant onto the structure but to adhere it only to the wrap, so as to reduce interference of the shear. It was noted that the corners still leaked. A nitrile sheet was wrapped around both corners of the beam and the leakage stopped. A summary of the different procedures and materials investigated in fabrication of the ER material structure beams was shown in Table 4.3.1.1.

Once the beam was sealed a small hole at one end of the beam was made with a hypodermic needle. Another hypodermic needle injected ER material into the structure.

ELECTRODES	PURPOSE
Aluminum	Investigation of theoretical structural dynamics models
Polycarbonate	Investigation of controlling fluid dynamics in a water channel
Etched Kapton	Investigation of mode shape control using mult-electrode panels

SEALANT	PERFORMANCE
Latex	Held high electric fields but was degraded when exposed to ER material
Window insulation film	Sealed well but the electrical properties were not sufficient to hold high electric fields

ADHESIVE	PERFORMANCE
3M Tape (Rubber base	Easy to handle but did effectively seal in the ER material
Epoxy (Seal-All)	Sealed in ER material effectively

LIQUAD SEALANT	PERFORMANCE
Acrylic Caulking	Sealed the best but was brittle and sometimes cracked
RTV Silicon Gel	Over an extended time ER material leaked through

Table 4.3.1.1 Summary of materials to make ER structures

The beams that were constructed for this investigation were classified S5, S8 and S9. The dimensions, as shown in Figure 4.3.1.2, for the beams were the same.

S5 - Aluminum beam electrodes and constraining layers. Separated by polycarbonate spacers. Latex was used around the edges to seal the ER material in. 3M double sided microscopy (#17840) tape was used attach the latex sealant. Acrylic caulking was used near the edges and the corners to complete the seal. Significant leaking over the entire beam was observed.

S8 - Aluminum beam electrodes and constraining layers. Separated by polycarbonate spacers (The spacing was doubled for this structure). Latex was used around the edges to seal the ER material in. Epoxy was used to adhere the latex to the structure. Silicone was used near the edges and the corners to complete the seal. The seal around the edges held, but leakage near the corners was observed.

S9 - Aluminum beam electrodes and constraining layers. Separated by polycarbonate spacers. Latex was used around the edges to seal the ER material in. Epoxy was used to adhere the latex to the structure. This structure used nitrile wraps at the ends of the beam to prevent leakage.

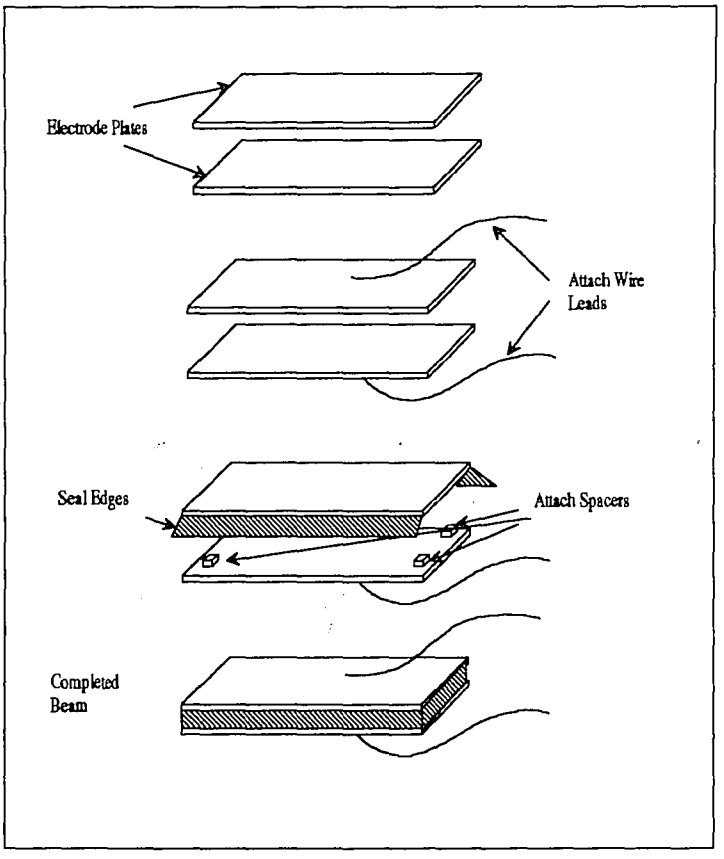

Figure 4.3.1.1 Basic Preparation of an ER Structure

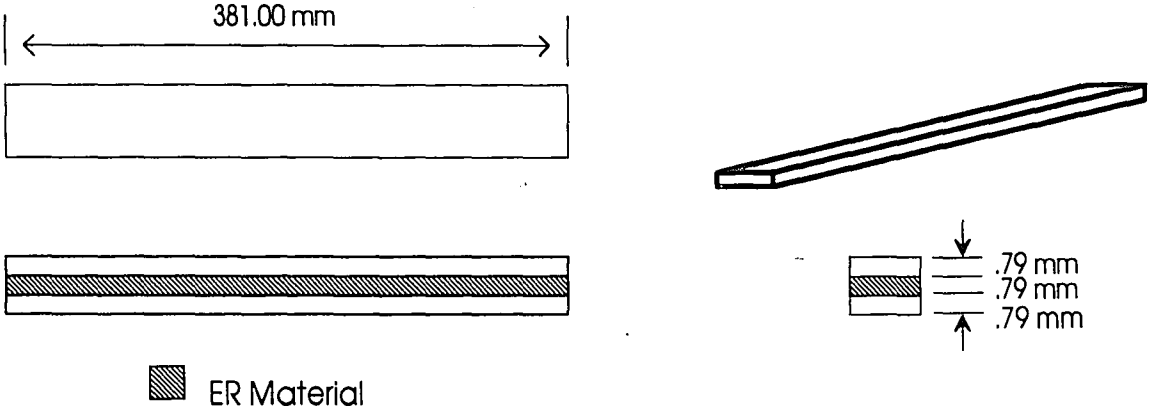

Figure 4.3.1.2 Structures S5 and S8: Composite beams

4.3.2 Instrumentation

The purpose of experimentation was to measure dynamic characteristics of ER based beam structures at different electric fields. Specifically, the investigation accomplished this by measuring the frequency response at various applied electric fields.

The actuating force on the beam was a swept sine wave. This excitation consisted of a constant amplitude force with an incrementing frequency as shown in Figure 4.3.2.1. For example, the input force first actuated the beam at some amplitude at 1 Hz, then would increase the frequency to 2 Hz, 3 Hz, 4 Hz, and so on while still keeping the amplitude of this force constant. A proximity sensor measured the displacement at one location on the beam. FFT (Fast Fourier Transform) algorithms analyzed this response.

A Bently Nevada 3040 HTB electromagnetic probe provided the actuating force. A Bently Nevada 7200 Probe measured the vertical response, in terms of displacement, of a point on the beam. The Onosokki Dynamic analyzer created the swept sine signal which was fed to the actuating probe. The Onosokki analyzer, utilizing it's FFT Hardware, analyzed the response of the displacement probe. A Bertan High Voltage power supply applied the electric fields. The experimental set up is shown in Figure 4.3.2.2.

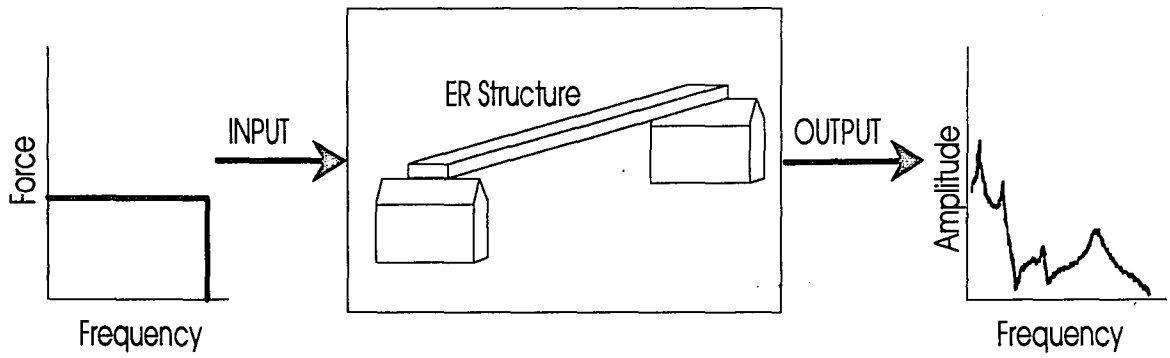

Figure 4.3.2.1 Experimental Input and Output

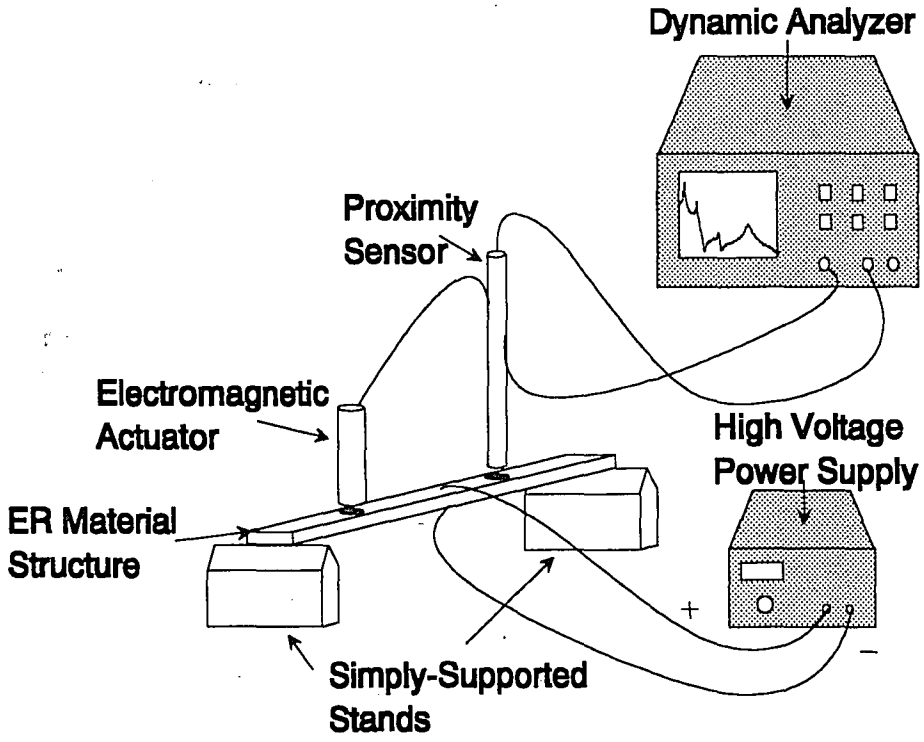

Figure 4.3.2.2 Experimental Setup for Testing Composite Beams

4.3.3 Experimental Procedure

Three beams were fabricated as described in Section 4.3.1. The beams were tested with simply supported boundary conditions as shown in Figure 4.3.2.2. Swept sine waves ranging from 0-250 Hz at 1.25 Hz increments were the forcing functions. The resonant frequencies of the structures were found by determining the corresponding frequencies of the peaks of the frequency response curves shown in Figure 4.4.1. Damping was measured using the 3dB power loss approximation. The approximation is taken by determining the location of the frequencies corresoponding to a 3db reduction in response in front of and behind the natural frequency,

$$\eta = \frac{\omega_+ - \omega_-}{\omega_n} \qquad (4.3.3.1)$$

where ω_+ and ω_- are the frequencies corresoponding to the 3db losses, and ω_n is the natural frequency. The experiment determined resonance and damping for electric fields varied from 0-4.41 kV/mm in .631 kV/mm increments.

During testing flexural vibration was induced by sweeping the 0-250 Hz force excitation range while the displacement at a single location was simaltaneously measured. The electric field was increased in .631 kV/mm intervals and the sweep repeated until the field reached 4.41 kV/mm. Each structure was tested three times. In between each of the tests, the beam was moved and stretched. The purpose for this was to determine a range of deviation caused by the boundary conditions and remove any possible agglomerations within the ER material layer.

4.4 Results and Discussion

The previous rheological investigation, discussed in Chapter 3, measured the complex modulus of ER material number 6533-30B obtained from Lord Corporation at various electric fields and frequencies. This structural investigation substituted these rheological results into two models that predict the dynamic response of three-layer composite structures - the RKU and Mead and Markus theories. A procedure described in Section 4.3.3 examined the experimental frequency response of three structures: S5, S8, and S9. The experimental and theoretical results were then compared.

The experimentally observed frequency responses, as seen in Figure 4.4.1, display the dependence of the ER structural system on electric field. The peaks of the curves represent the resonant frequencies. As electric field increased, the curves shifted to the right while the amplitudes simultaneously reduced.

The experiment examined the frequency response of three different structures at various electric fields. Figures 4.4.2-4.4.5 show the resonance relationship between electric field for structures S5, S8, S9, and the theoretical predictions for modes 1 through 4. The experimental resonant frequencies obtained for structures S5 and S8 were similar. This was expected since the only difference between the two structures was the adhesive used to attach the latex sealant. Structure S9, on the other hand, was found to be different than the other structures. This was reasonable since the construction of the structure was considerably different resulting in different dynamic properties.

It was found that the theoretical models generally under predicted the observed natural frequencies for modes 1 through 3 and over predicted the results at the fourth mode. The theoretical predictions were quantitatively in the area of the experimental results, but the qualitative behavior with respect to electric field was visibly different.

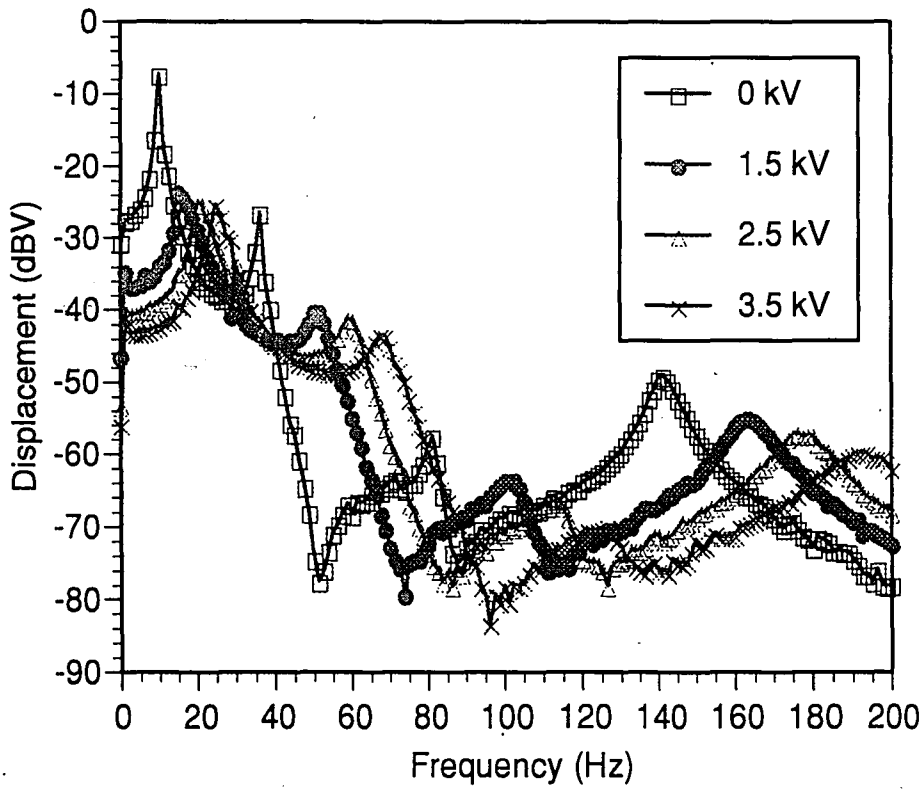

Figure 4.4.1 Frequency Response for Structure S5 at Electric Fields of 0, 1.5, 2.5, and 3.5 kV/mm

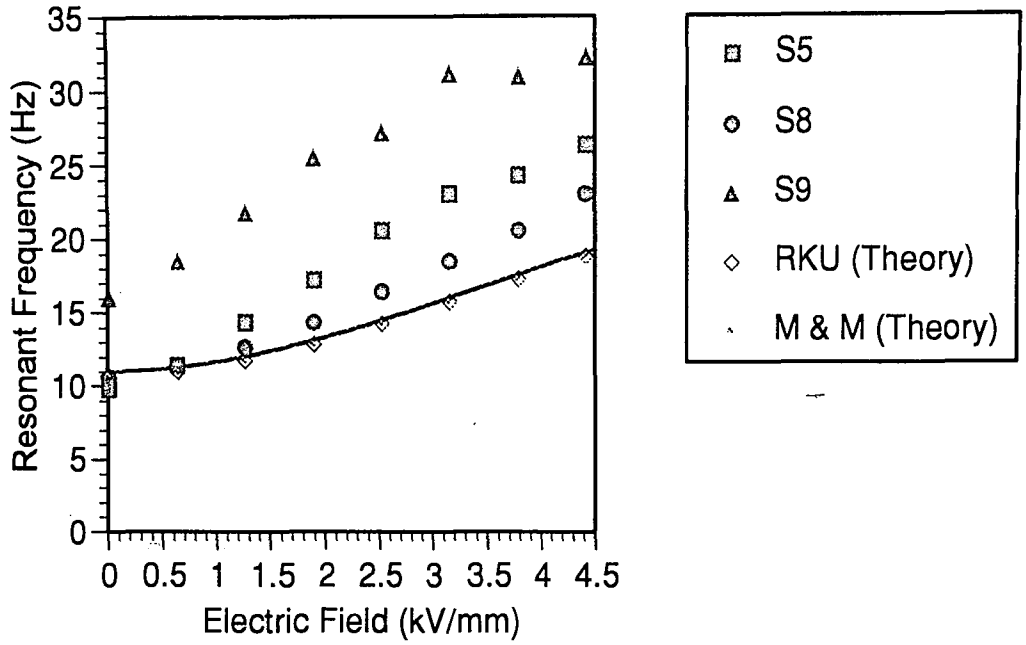

Figure 4.4.2 Resonance frequency dependence on electric field for mode 1

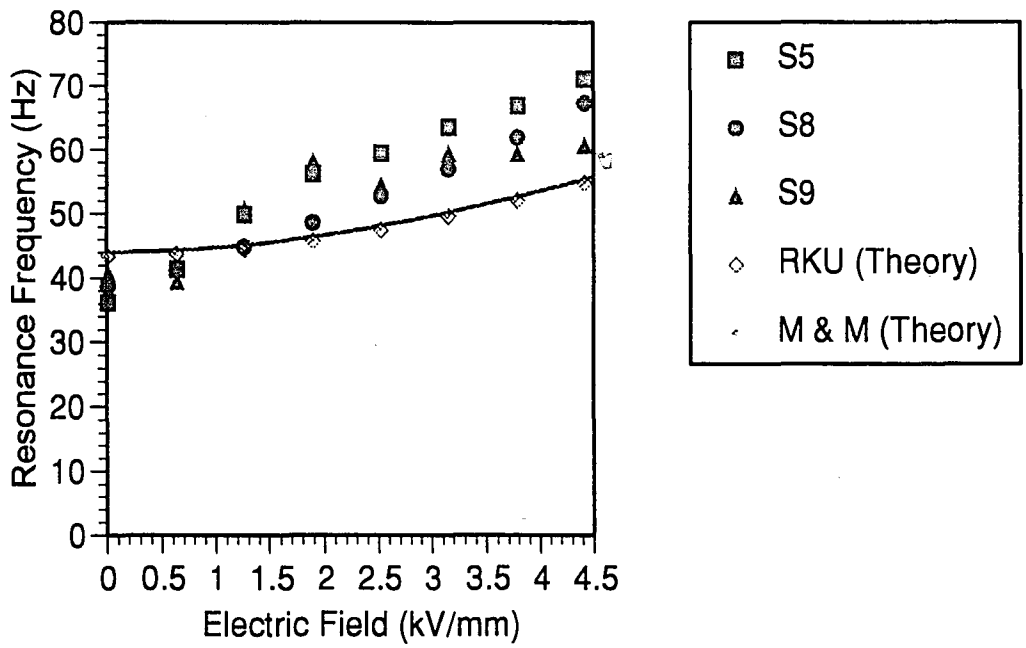

Figure 4.4.3 Resonance frequency dependence on electric field for mode 2

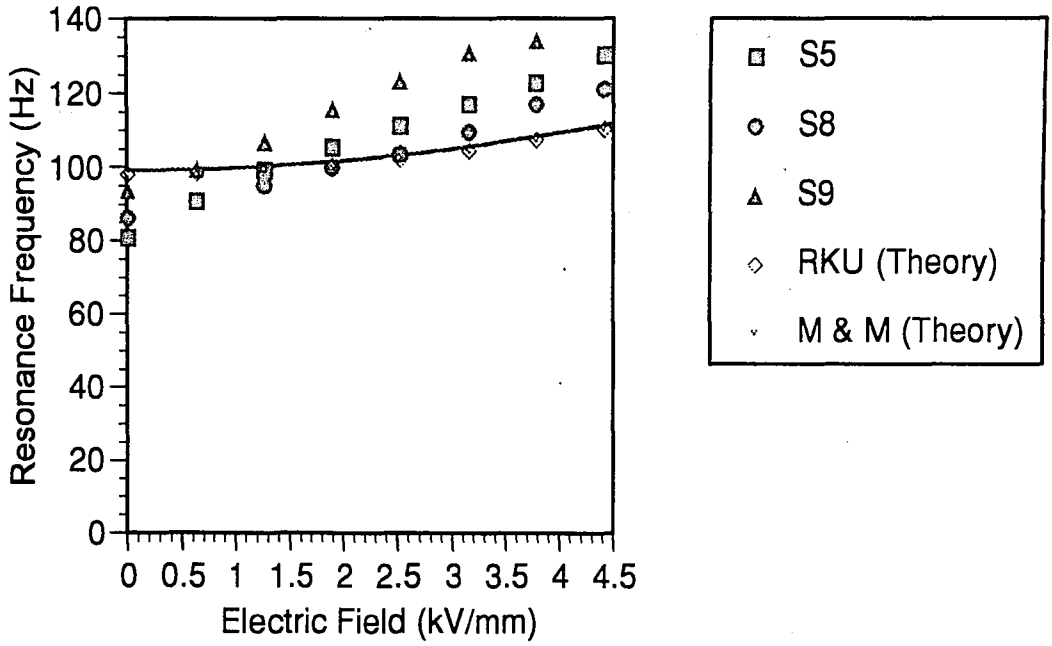

Figure 4.4.4 Resonance frequency dependence on electric field for mode 3

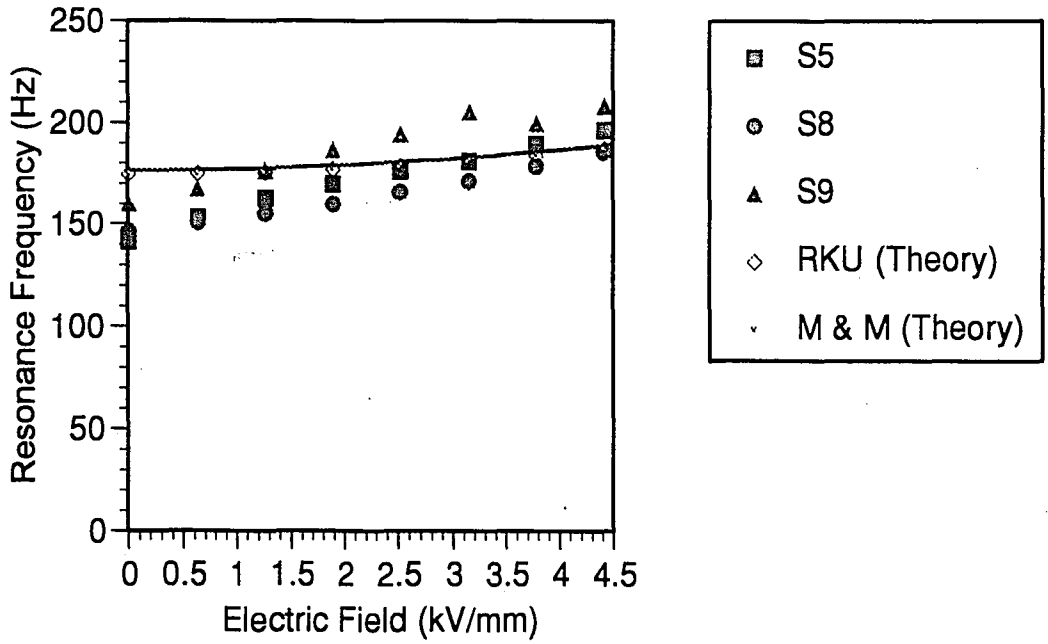

Figure 4.4.5 Resonance frequency dependence on electric field for mode

The experimental results showed a linear increase in resonance frequency of the structure with respect to increases in the electric field. This was also seen in Coulter et al. [35]. The theoretical results displayed a more parabolic relationship.

The average damping of all three structures is shown in Figures 4.4.6-4.4.9 using the 3dB approximation for linearly damped systems. Figures 4.4.6-4.4.9 show the relationship between damping of the structures and electric field for the four different modes. As was seen the damping of the structure was much less predictable than natural frequency. This was understandable since the damping of the experimental structures was more sensitive to experimental deviations. This included the damping of the seal technique and constraining layers. The frequency resolution of the experimentation was 1.25 Hz. The actual resonance was accurate, but the measurement of the frequencies corresponding to a -3dB change were less predictable due to the resolution. Therefore, the determination of experimental damping was generally less precise than the determination of the resonant frequencies.

It is believed that most of the differences between theory and experiment were associated with the fabrication of the experimental ER structures. First, the beams were overfilled with ER material. Overfilling the beam contributed to the deviation in the predicted behavior due to the increase in mass and decrease in effective electric field. The decrease in effective electric field was due to the increase in the spacing of the sandwiched layer.

Second, after the structure sat for some extended time period the liquid matrix of the ER material began to seep through the corners of the beam and in between the adhesive layer attaching the latex material. From previous rheological investigations the complex modulus was found to very dependent upon particle concentration. Losing the liquid matrix was the same as increasing the particle concentration and thereby changing

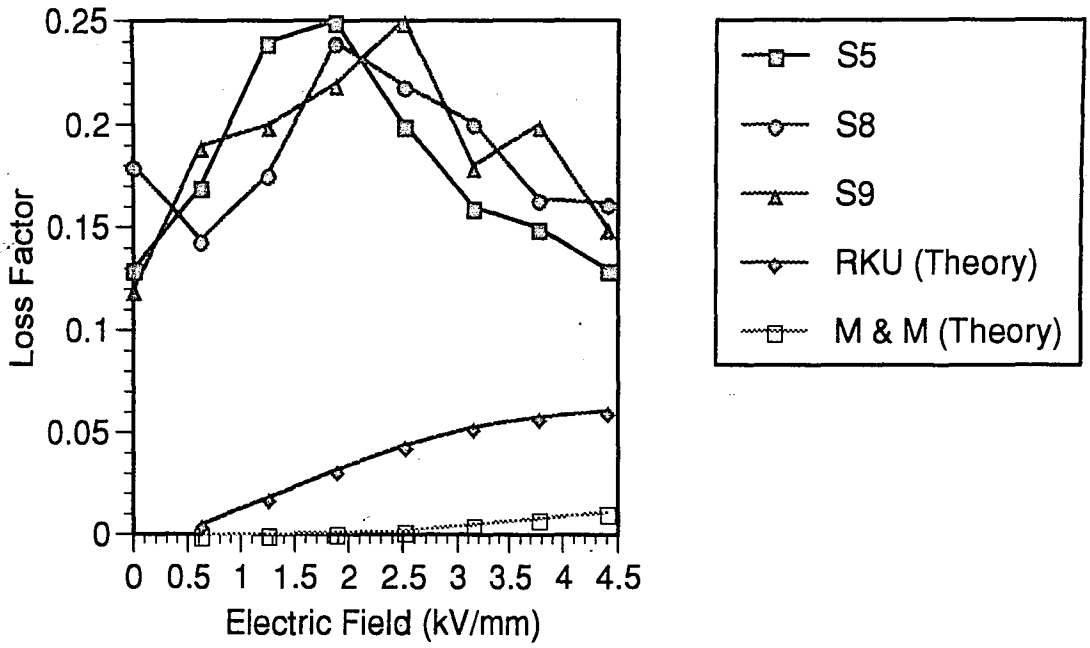

Figure 4.4.6 Structural Damping dependence on electric field for mode 1

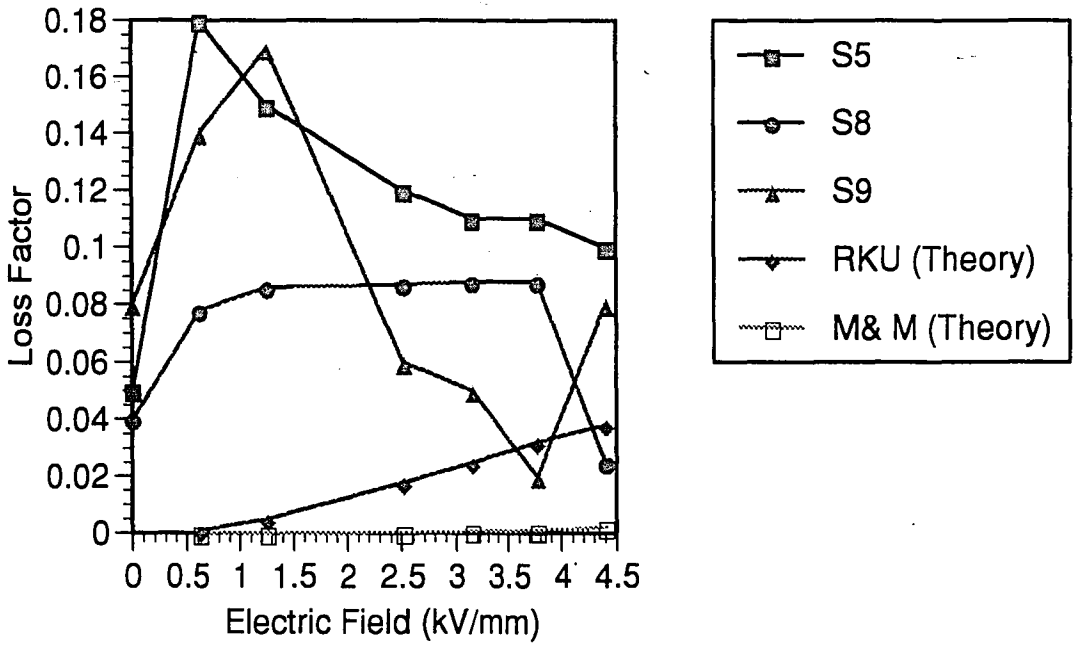

Figure 4.4.7 Structural Damping dependence on electric field for mode 2

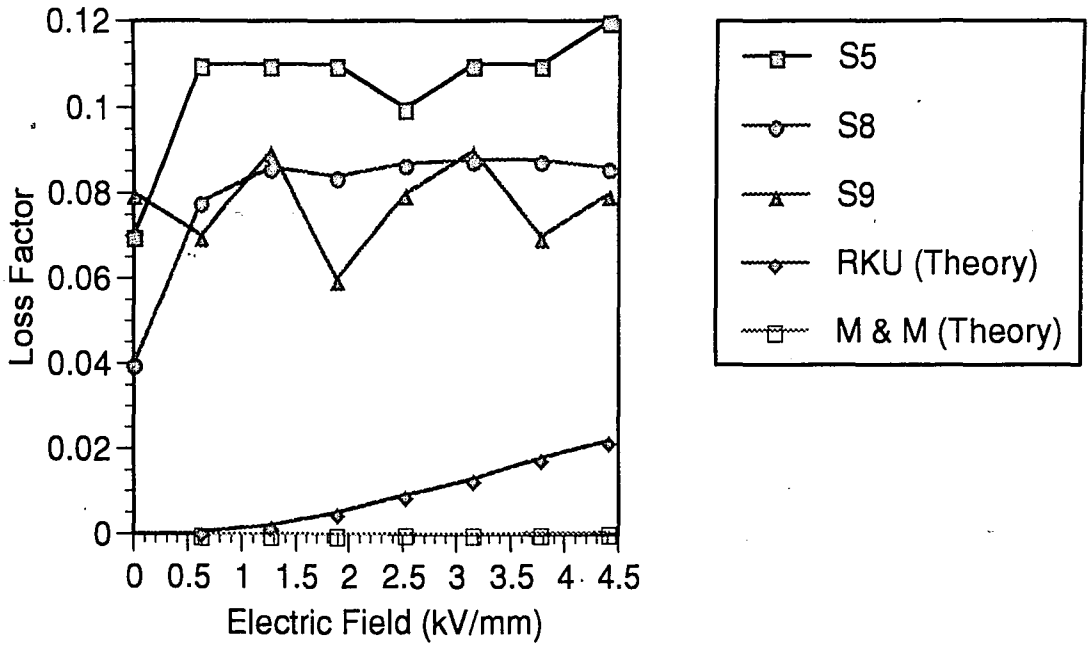

Figure 4.4.8 Structural Damping dependence on electric field for mode 3

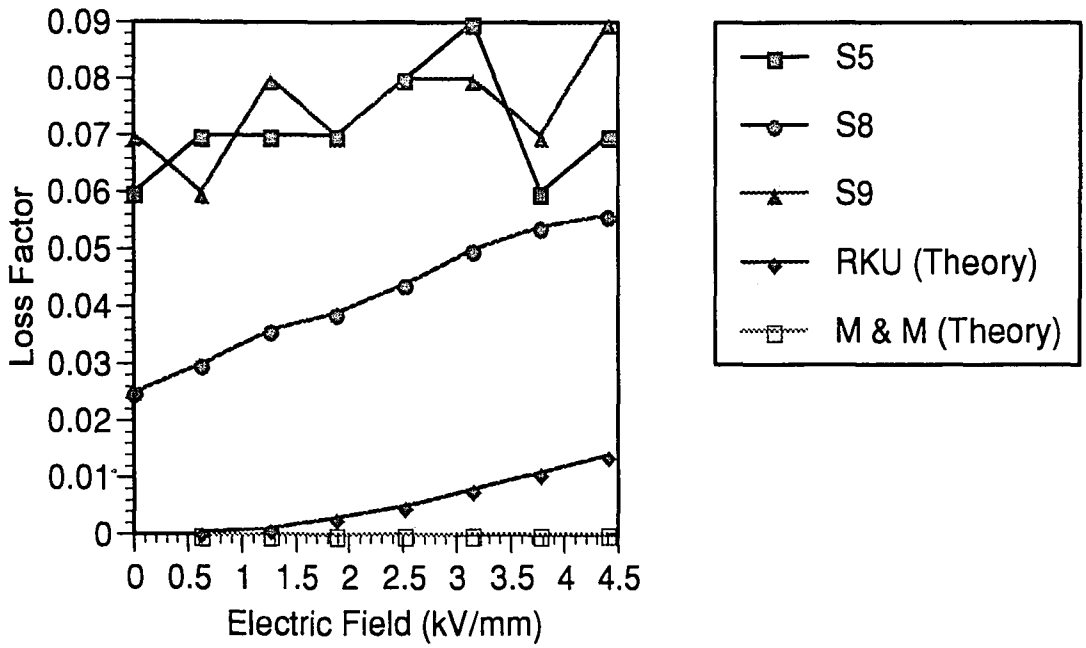

Figure 4.4.9 Structural Damping dependence on electric field for mode 4

the rheological behavior of the ER material used in the beam. This meant the properties measured in Chapter 3, substituted into the theoretical models, and the properties of the actual materials used in the beams were different.

Lastly, though the experimental structures design attempted to reduce the effects of the sealant on the dynamic behavior, its contribution was most likely included. This was due to the relatively low bending stiffness of the first and third layers and the low elastic shear modulus of the ER material compared to the material properties of the sealant materials.

The fabrication and filling of structure S9 reduced the overfilling and leakage problems. The amount of ER material placed in the structure was more closely monitored than in structures S5 and S8 to ensure an even distribution within the sandwiched layer. In addition, a leak-proof structure was fabricated by attaching the nitrile flaps on both ends of the beam. In the first test on structure S9, at electric fields greater than 2 kV/mm, the structures began to arc. A conductive pathway developed and more ER material was injected to destroy this path. This solved the arcing problem but created an overfilling of the structure. The results of the first test on S9 were interesting because they emphasize the effects of overfilling the structure.

These results before the arcing of structure S9 are shown in Figures 4.4.10-4.4.13. The theoretical models under predicted the results greater than in the previous structures. What was interesting was that the resonance-electric field relationship was *more* "parabolic" than the theoretical predictions. This was contrary to results reported earlier. By ensuring the uniformity of the ER layer, the theoretical predictions were more qualitatively similar to experiments. Structure S9 showed that resonance-electric field relationship was not linear but parabolic. The observed linear increase was related to the overfilling and construction of the ER beams.

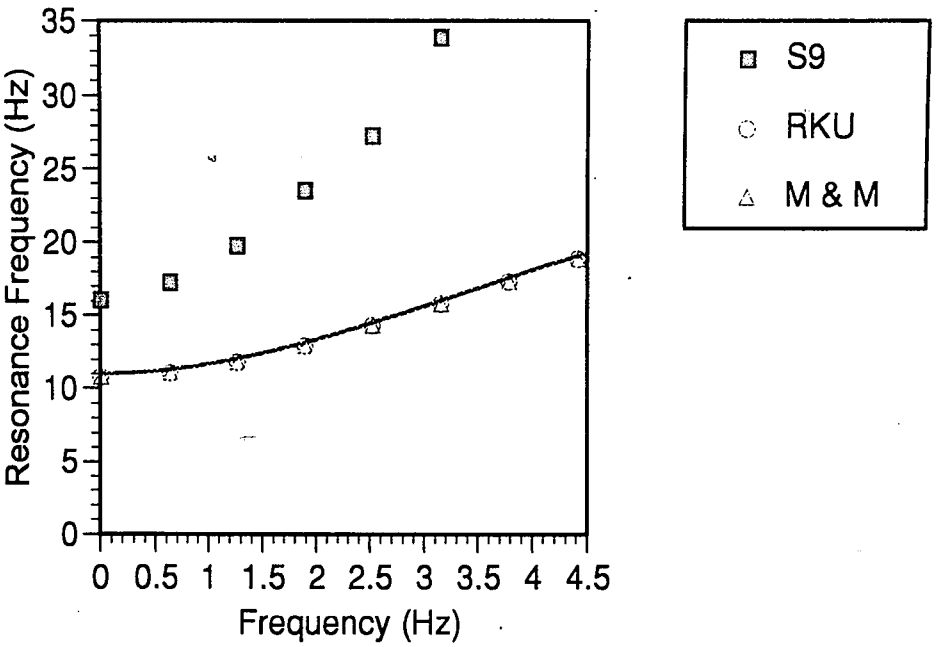

Figure 4.4.10 Resonance Frequency Dependence on Electric Field for Structure S9, Mode 1

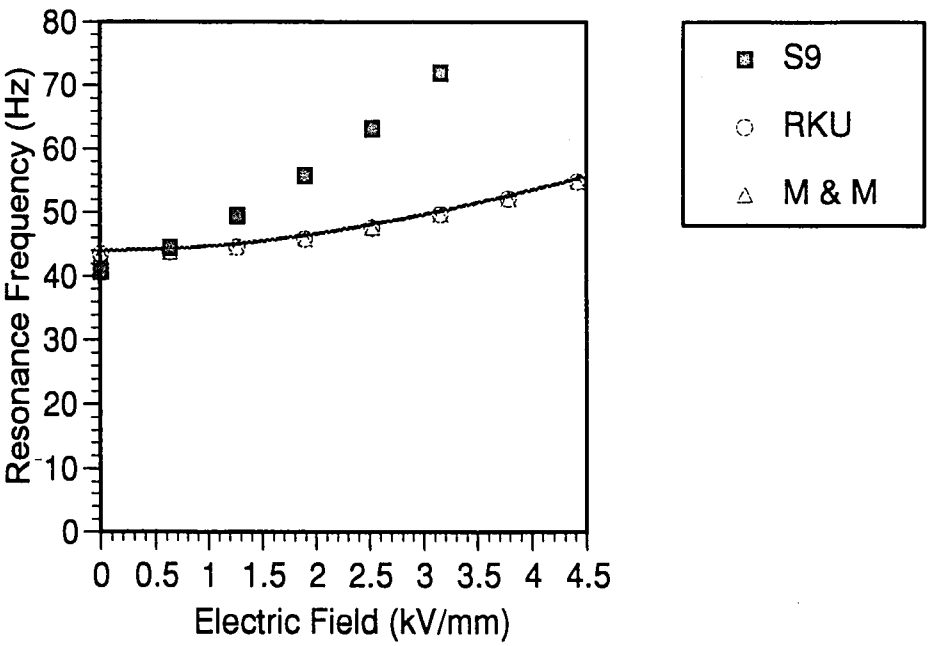

Figure 4.4.11 Resonance Frequency Dependence on Electric Field for Structure S9, Mode 2

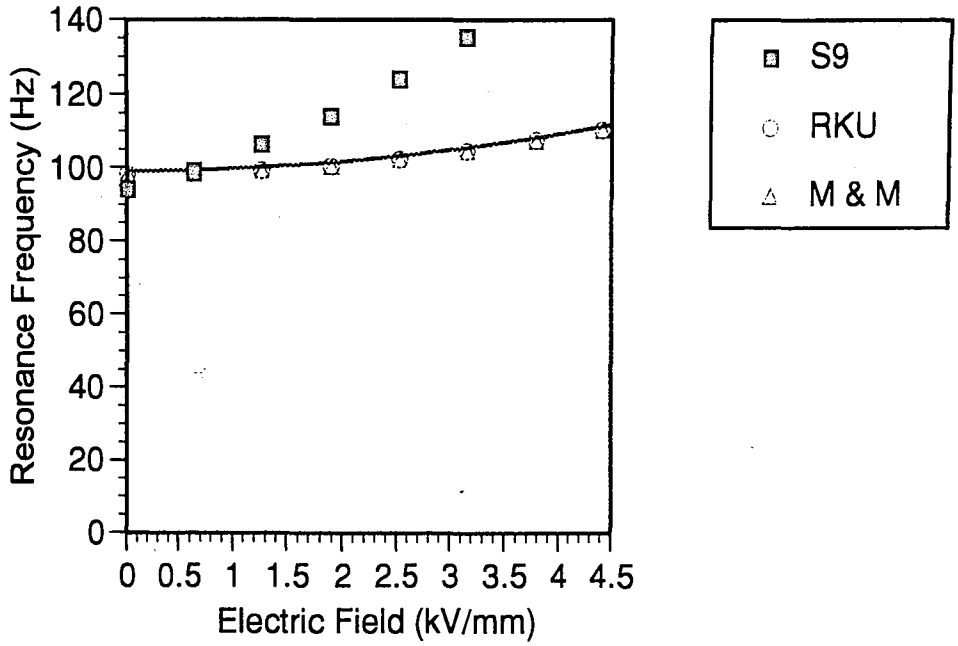

Figure 4.4.12 Resonance Frequency Dependence on Electric Field for Structure S9, Mode 3

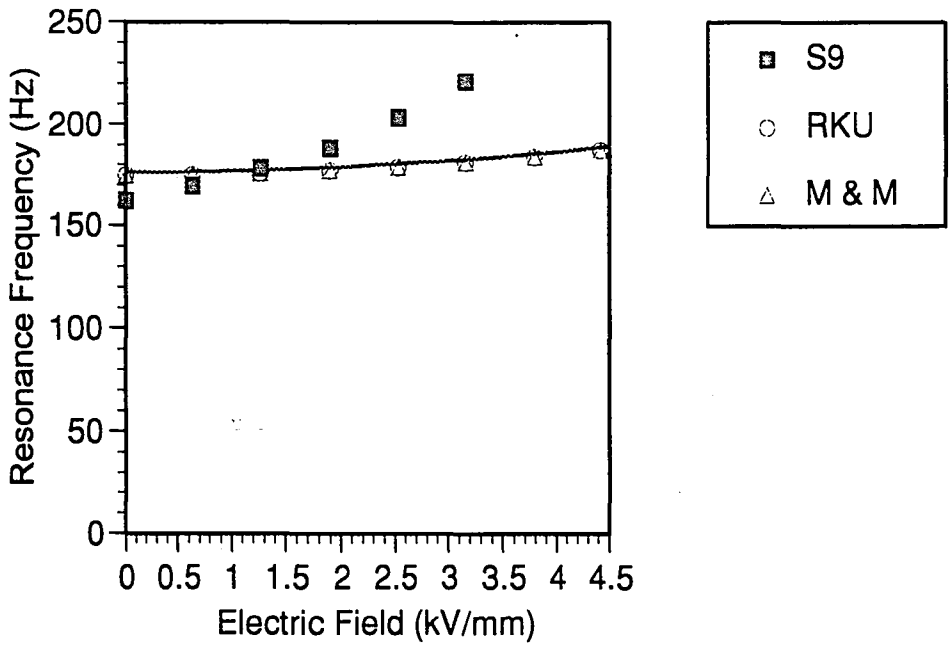

Figure 4.4.13 Resonance Frequency Dependence on Electric Field for Structure S9, Mode 4

CHAPTER 5: INVESTIGATION OF MODE SHAPE CONTROL USING A MULTI-ELECTRODE STRUCTURE

5.1 Introduction

The purpose of this phase of the study was to measure dynamic characteristics of an ER structure with multi-electrode panels. Specifically, the resonance characteristics and the mode shapes were determined with respect to each panel condition. By changing the stiffness in different areas the change in resonance frequency has potentially more variability. In addition, the modal shapes of the structure can be altered. The degree to which a multi-electrode ER based structure could accomplish these goals was evaluated.

5.2 Experimental Set up

5.2.1 Fabrication of a Multi-electrode Panel

Johns Hopkins Applied Physics laboratory fabricated the multi-electrode structure used in the experimentation. Copper film etched onto kapton, frequently used in building circuit boards, acted as the electrodes and constraining layers. The investigation chose etched kapton because it was easy to create multi-electrode panels. The structure had four independent electrodes. Holes drilled through the kapton attached the wire leads to the electrodes. Latex wrap adhered to the edges of the structure and acrylic caulking sealed the ER material in. The dimensions for the structure are shown in Figure 5.2.1.1.

5.2.2 Instrumentation

The actuating force on the beam was a swept sine wave. This excitation consisted of a constant amplitude force with an incrementing frequency. A reference proximity sensor measured the displacement at a fixed location, while another proximity sensor

measured the displacement at various locations on the plate as shown in Figure 5.2.2.1. FFT (Fast Fourier Transform) algorithms analyzed the responses.

A Bently Nevada 3040 HTB Probe provided the actuating force. Two Bently Nevada 7200 Probes measured the displacements. An Onosokki Dynamic analyzer created the swept sine signal which controlled the actuating probe. The Onosokki analyzer, utilizing it's FFT Hardware, analyzed the response of the displacement probes. The analysis produced phase differences between the two probes. A Bertan High Voltage power supply applied the electric fields

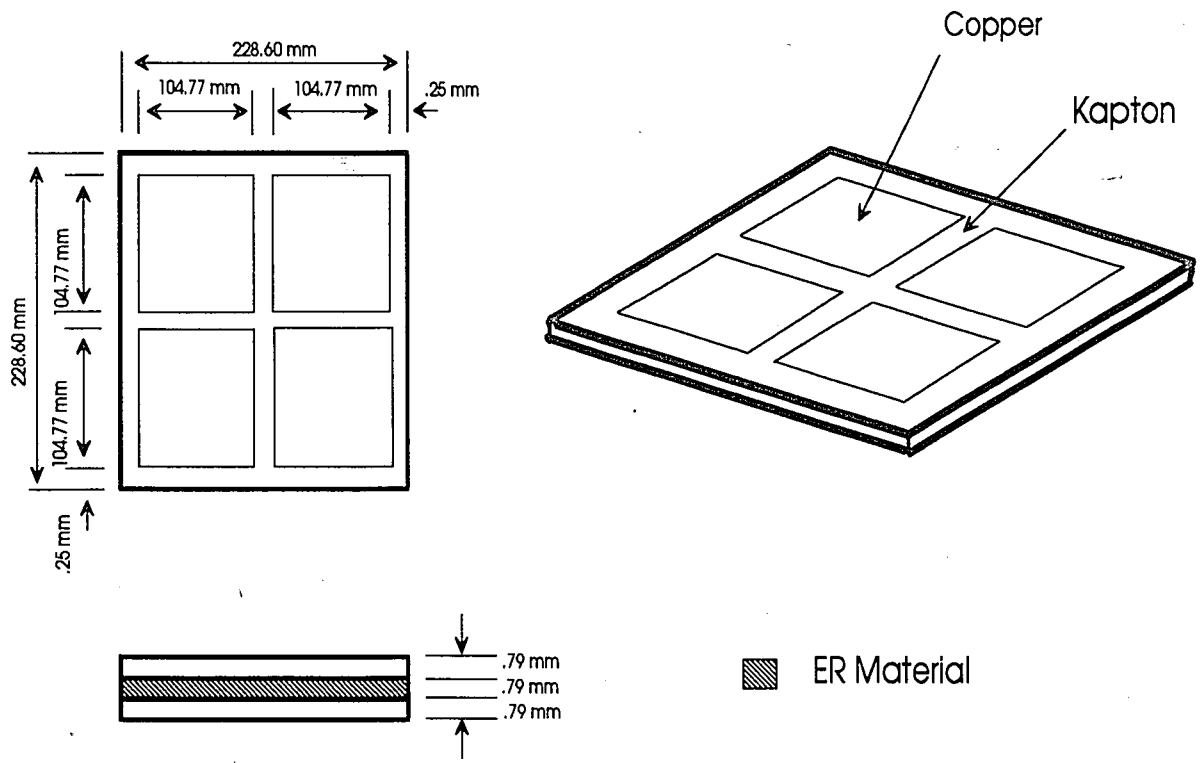

Figure 5.2.1.1 Structure S3: Multi-electrode Panel Structure

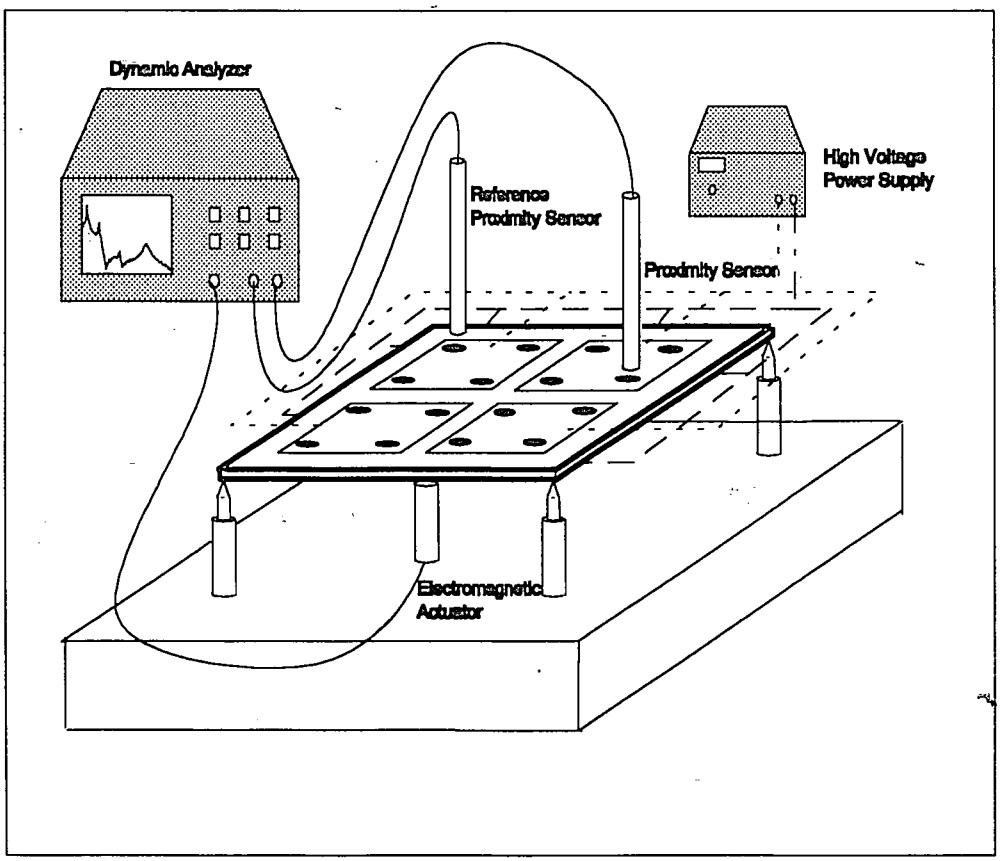

Figure 5.2.2.1 Experimental Setup for Plate Structure

5.2.3 Experimental Procedure

Resonance characteristics were determined using the same procedure as in Section 4. Mode shapes were determined by comparing the amplitude of vibration at a given modal frequency at 16 different locations on the structure as shown in Figure 5.2.2.1. The procedure was to excite the structure with a swept sine force. Simultaneously the displacement of 2 locations on the structure were measured using 2 proximity sensors. One sensor was used as a reference point, while the other measured the amplitude of displacement. By measuring the amplitude at which the system was in resonance, the shape of that mode was determined at that specific point.

Though the amplitude of the shape at a specific point can be measured, the direction each point is moving with respect to each other cannot - a reference must be used. The displacement of a location on the structure was either moving in the same direction as the reference or moving in the opposite direction from it. This was determined by comparing the phase between the two sensors. If it was moving with the reference then it was 0 degrees phase, while if it was moving against it was 180 degrees.

The amplitude and direction were determined at each of the 16 points by holding the reference sensor in one position and moving the other proximity sensor to the 16 different locations. Since there were only 2 sensors, the swept sine input had to be applied every time the sensor was moved. From this data the mode shapes were determined.

This procedure was repeated for each of the following panel conditions as shown in Figure 5.2.3.1.

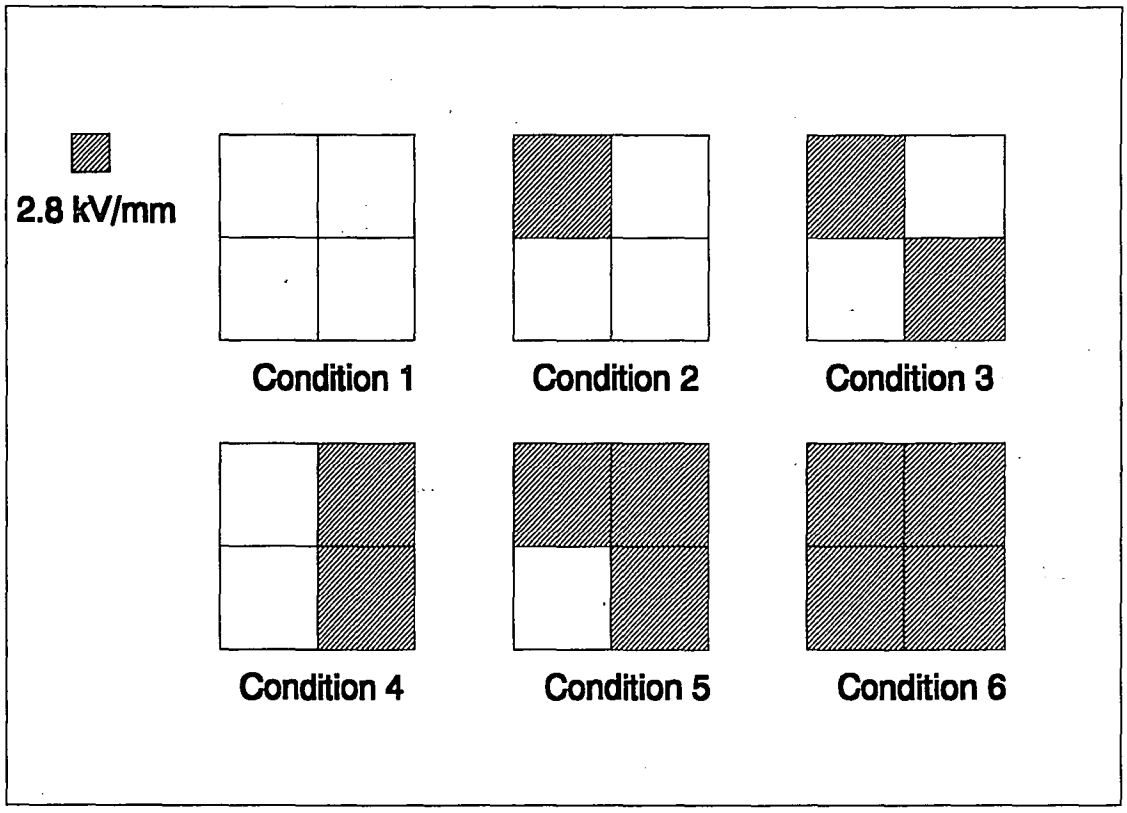

Figure 5.2.3.1 Different Electric Field Conditions of the Multi-electrode Plate

5.3 Results and Discussion

The observed variability of resonance frequency caused by the variation of stiffness in different areas of the structure is shown in Figure 5.3.1. The resonant frequency is found as a function of the different panel conditions. The resonant frequency clearly increased as the number of panels was turned on. For mode 11 the resonant frequency changed from 10 to 30 Hz. Mode 22 changed from 20 to 50 Hz.

The variation in modal shape was not as dramatic. Figures 5.3.2a-f show the relative magnitudes of displacement of the structure as it vibrates at the first modal frequency for the different panel conditions. There were not significant observable changes in mode shape 11. Throughout the experiment the structure maintained the modal shape of panel condition 1. The modal shapes of the separate panel conditions are presented in different scales, and should be only qualatatively compared. This was done to observe the possible changes in modal shape.

The second modal frequency, mode 22, observed more variation in mode shape as seen in Figures 5.3.3 a-f. Panel conditions 3 and 4, Figures 5.3.3c and 5.3.3d, observed the greatest changes. These panels activated two electrode panels diagonally across from each other, and next to each other, respectively. The relative displacement at the locations near the activated panels were reduced significantly resulting in a visible alteration of mode shape 2 without any panels activated.

The results of the experiment showed that the use of multi-paneled electrodes did change the resonant frequency significantly. The change in mode shape was less conclusive. One reason for this was the experimental error in the methodology used in measuring the mode shapes. The instrumentation did not adequately measure the relative displacements since the proximity sensor had to be moved during each of the tests.

Fabrication of the actual structure was another possible error. A larger, 2mm, gap may have caused decoupling of the two plates.

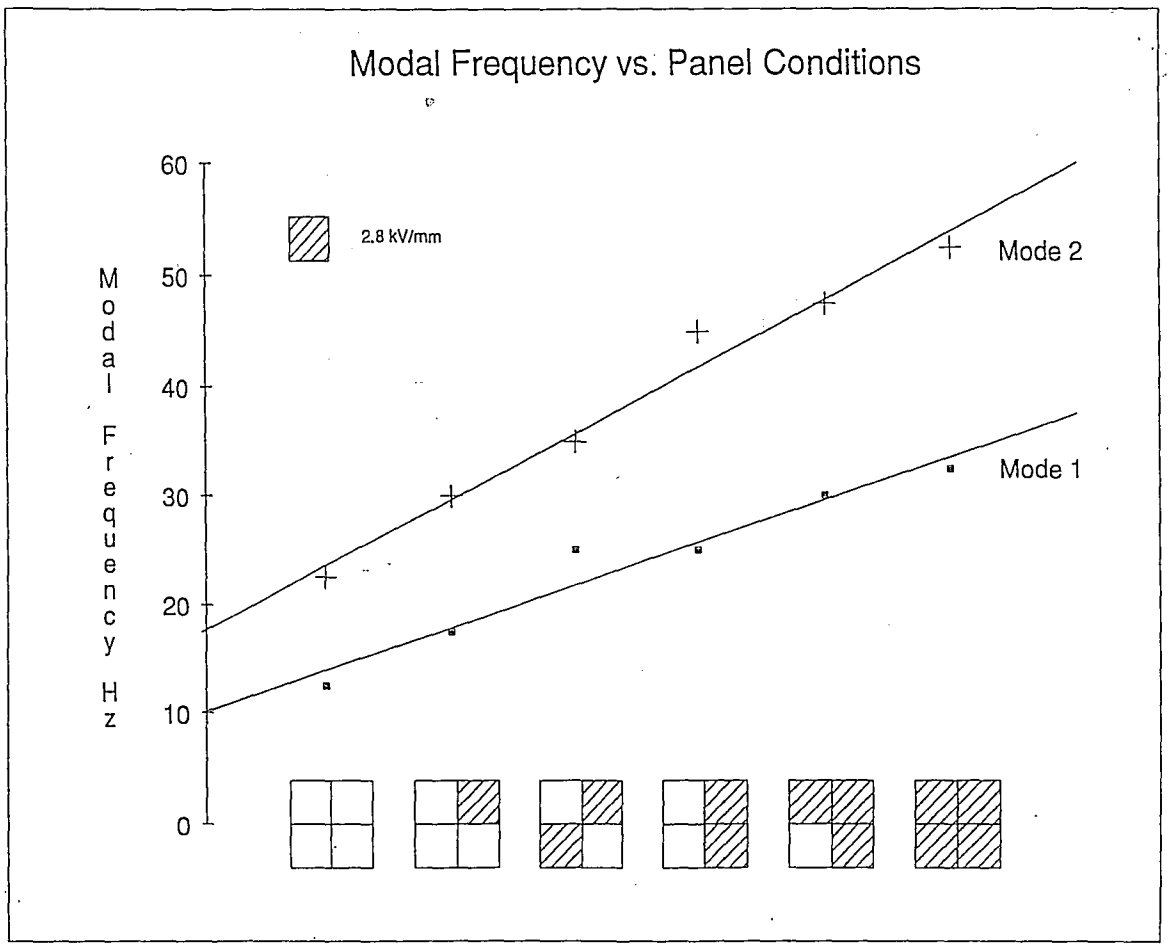

Figure 5.3.1 Resonance Frequency for Panel Conditions 1 through 6

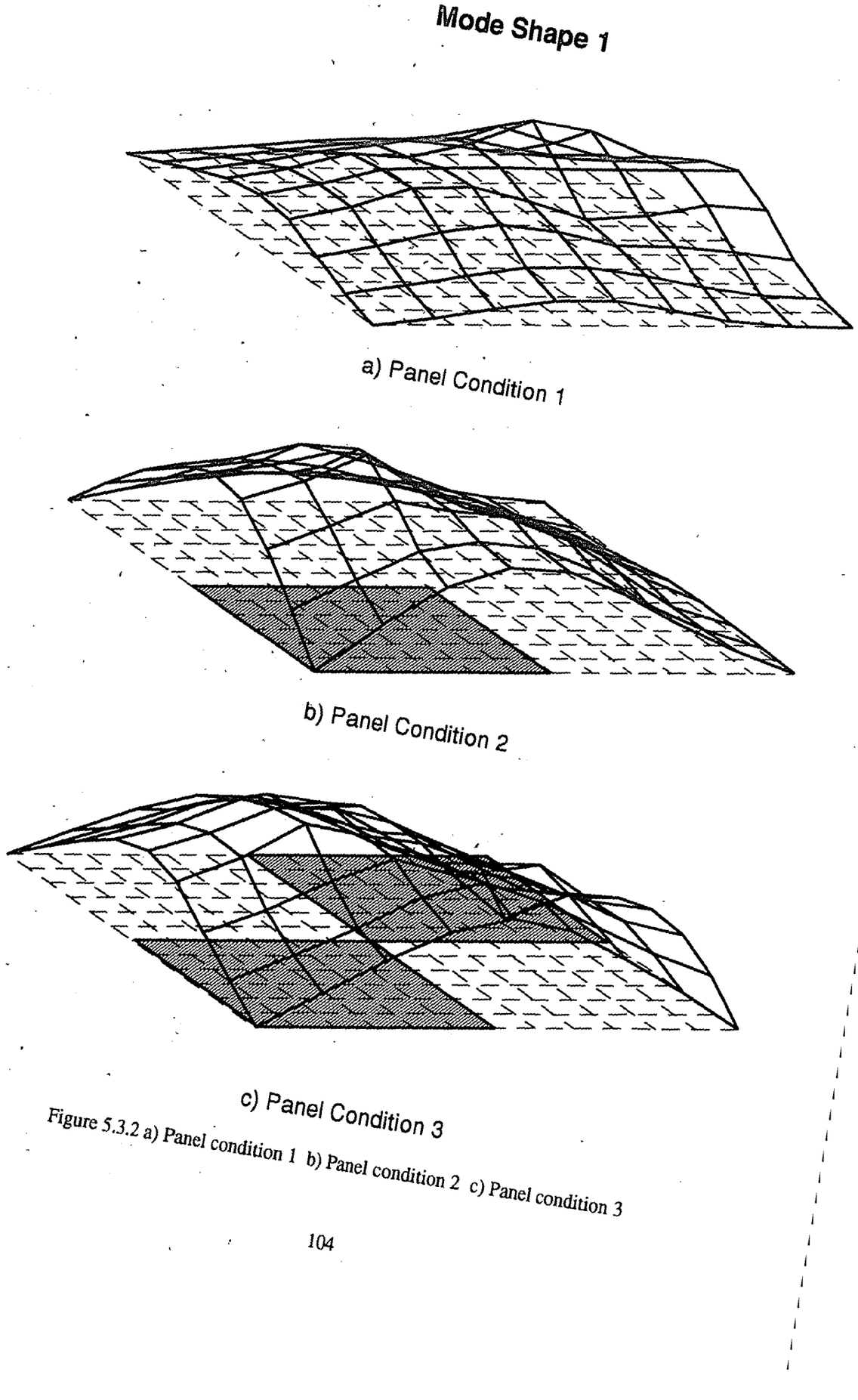

Figure 5.3.2 a) Panel condition 1 b) Panel condition 2 c) Panel condition 3

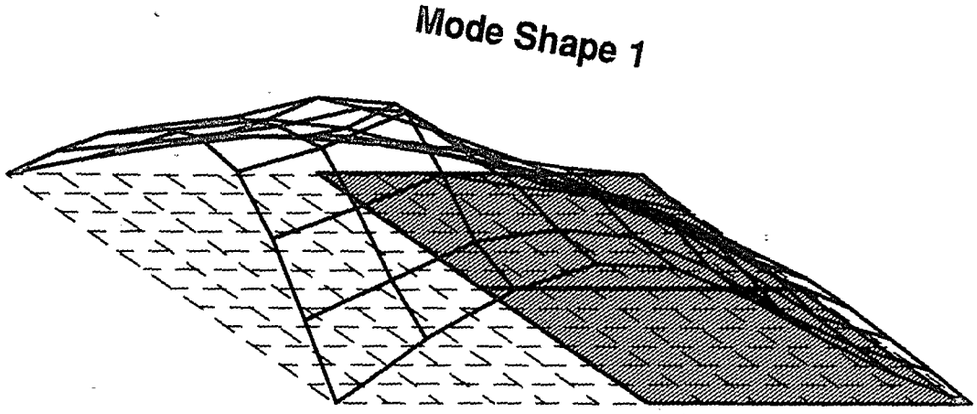

d) Panel Condition 4

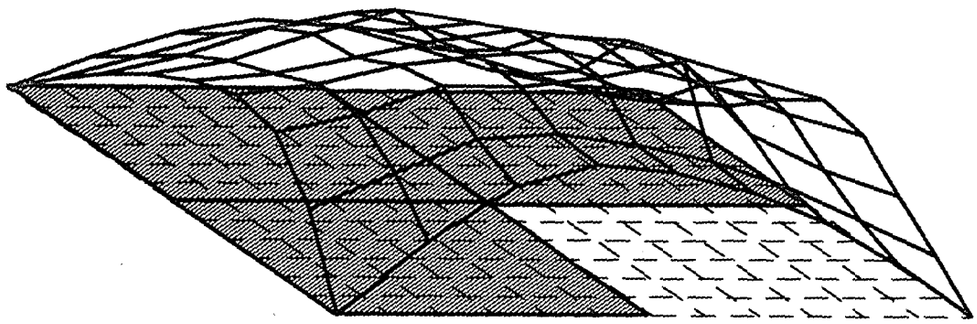

e) Panel Condition 5

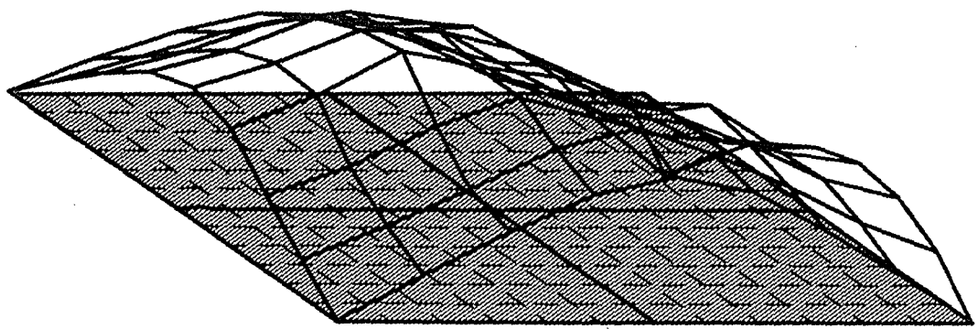

f) Panel Condition 6

Figure 5.3.2 d) Panel condition 4 e) Panel condition 5 f) Panel condition 6

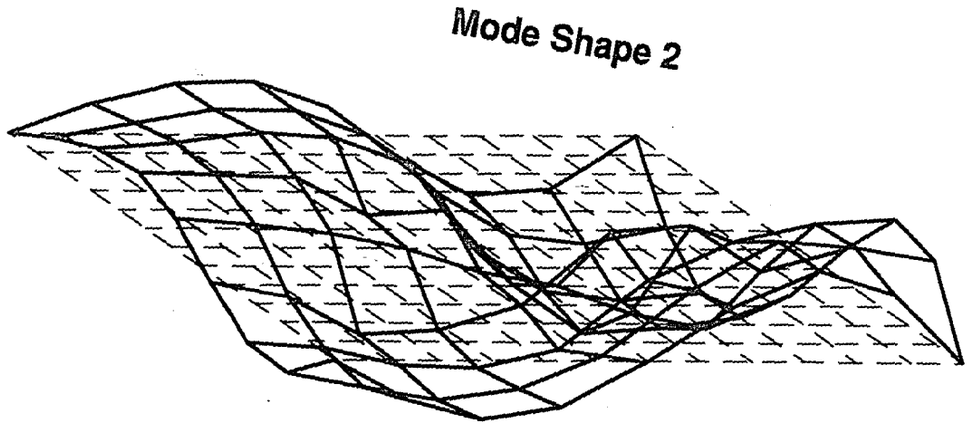

a) Panel Condition 1

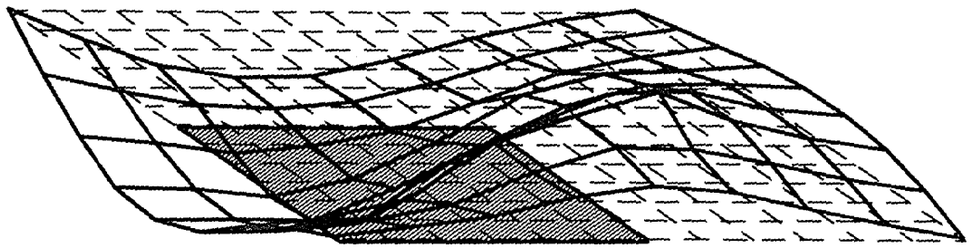

b) Panel Condition 2

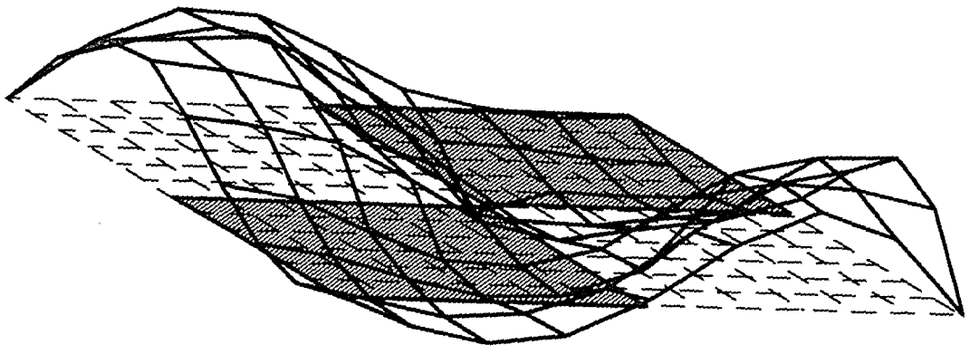

c) Panel Condition 3

Figure 5.3.3 a) Panel condition 1 b) Panel condition 2 c) Panel condition 3

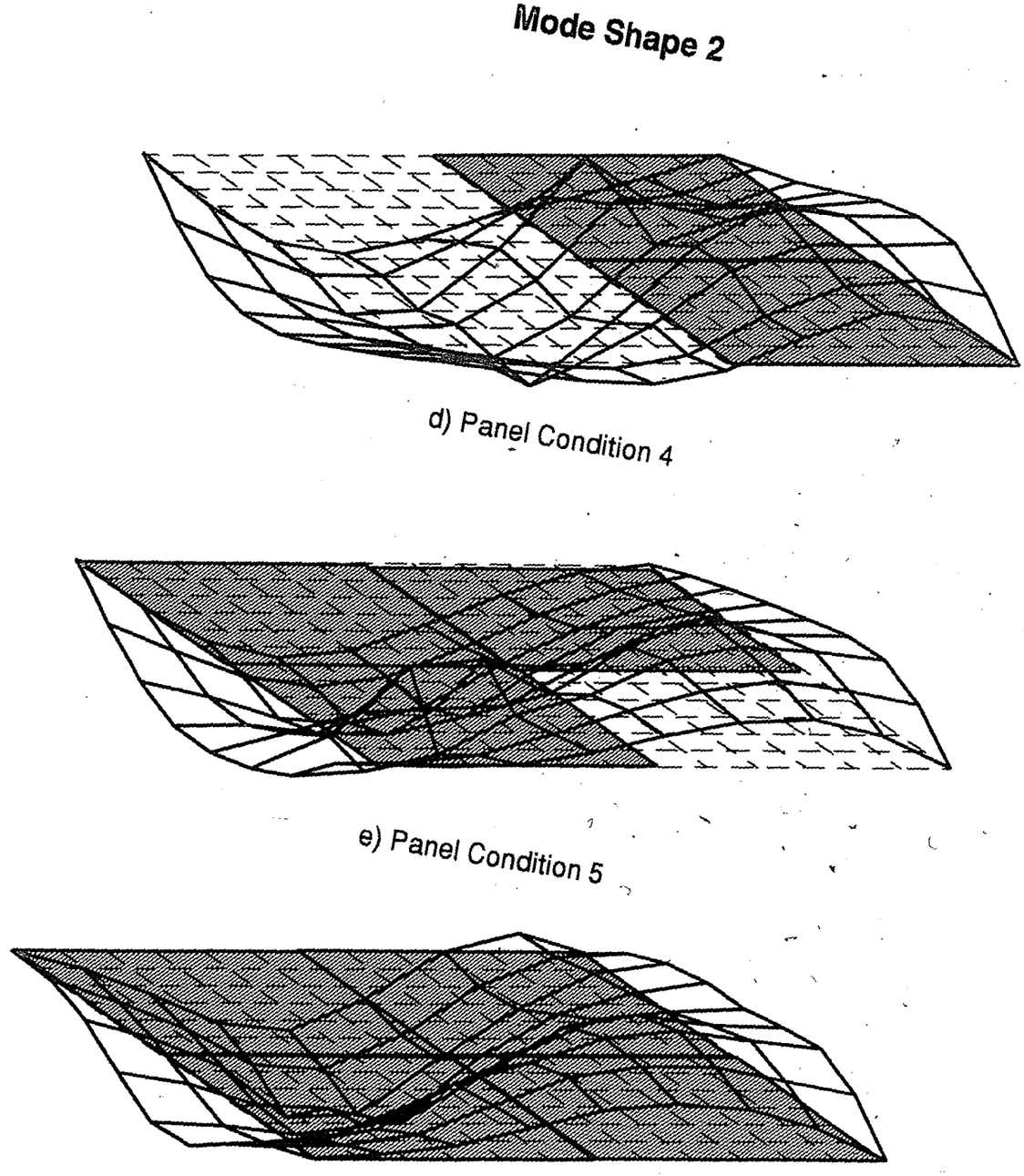

Figure 5.3.3 d) Panel condition 4 e) Panel condition 5 f) Panel condition 6

CHAPTER 6: CONCLUSIONS

6.1 Rheological Behavior of ER Materials

An investigation of the linear viscoelastic behavior of an ER material was performed. It clearly appeared that the ER material behaved linear viscoelastically in the stress-strain curves, but it was just as obvious that the behavior was not so clearly linear in the phase-strain curves. The phase appeared to drastically change at strains below the stress-strain yield definition especially at lower electric fields. An attempt was made to qualify the trends in transition from linearity in terms of stress and phase yield strain with respect to electric field and frequency. Increases in electric field resulting in increases in yield strain were observed for both the stress and phase yield strain. Increases in frequency resulted in decreases in the stress and phase yield strain. A quantifiable phase shift within the linear region was not able to be done due to the insensitivity of the instrumentation. Although it was concluded that since the phase was so close to 0 degrees, that G' dominated the behavior at electric fields of 1.5 kV/mm or more if the excitation was to be considered in the linear regime. Within this linear regime the instrumentation was accurate enough to measure the "real component" of the magnitude of the complex modulus. It was observed that the quantitiy showed a squared dependence with electric field. In addition, it was observed that the complex shear modulus showed little dependence upon frequency. The repeatability of these results over an expanded time frame showed that the material was behaving reliably.

Many of the previous investigations that were done measure G' and G" not taking into account the non-linearity of the material at all. In addition, the definition of linear behavior for many of the investigations was based on the deviation of sinusoidal stress as a function of time. This definition did not take into account the phase criteria. At some

electric fields it appeared that material behaved extremely non-linear with respect to phase. If either of these was the case, then the G' and G" results were flawed.

The results of this investigation warrant a more accurate study of the linear behavior of ER materials at small strains. The further efforts of this continuing investigation will focus on measuring the phase more accurately at smaller strains using more sensitive instrumentation. The purpose of the continuing effort will be to define a range of linear behavior for ER materials and examine the behavior in this range with respect to electric field, frequency, and eventually temperature.

6.2 Modeling of ER based Structural Beams

Both RKU and the Mead and Markus models were valid theories in predicting the resonance response of ER structures. The prediction of structural damping was not accurate due to the inaccuracies in both determining rheological properties of the materials, and the inherent experimental errors.

The accuracy of the models significantly depended upon the construction of the experimental structures. The most dependent variables to the accuracy were found to be the effects of the sealant, the accurate determination of material properties in both experiment and theory, and the uniformity of the sandwich layer. Previous investigations showed linear resonant-electric field relationships but it has been shown that the relationship was more parabolic as predicted by theory. The author attributes this to fabricated structures that were more consistent with the theoretical assumptions.

From an applications standpoint the use of ER adaptive structures for vibrational damping was not dependent upon the actual damping of ER materials, but rather the ability for the structure to change stiffness. The most dramatic reduction in amplitude observed in Figure 4.4.1 was the result of a change in resonant frequency.

The resonant frequency was modeled using both the RKU and Mead and Markus models. The models were able to predict the resonant frequencies. In those models it was observed that the resonance depended very little on the damping effects of the ER material as was seen in equations 4.2.26 and 4.2.3.27. Hence, for practical applications, it may be necessary only to consider the effects of G' when the material has a loss factor of less than 0.1. Control schemes could be developed based on this information.

6.3 Mode Shape Control Using Multi-electrode Panels

The use of a multi-electrode panel for vibration control was investigated in the final phase of the study. It was found that the resonance of the plate structure was significantly altered by varying the different panel conditions. The resonance increased as the number of panels was turned on as seen in Figure 5.3.1.

The effect of mode shape based control using and multi-electrode ER based structures was less conclusive. The first modal shape did not visibly change for the six different panel conditions. The second modal shape did visibly change for panel conditions 3 and 4. Panel conditions 3 and 4 had two activated electrodes; diagonally across from each other, and next to each other respectively. The displacement of the various locations on the activated panels was much less than the displacement on the non-activated panels as shown in Figures 5.3.3c and 5.3.3d. This reduction in amplitude of the activated panels caused the alteration of the modal shape.

The results of these experiments warrants further investigation into mode shape based control using ER based adaptive structures. The procedure and instrumentation used in measuring the mode shapes was not sensitive enough to accurately observe the variations in modal shape caused by the activation of the different electrode panels. The

application shows promise to increase the robustness of ER based adaptive structure applications in vibration damping.

6.4 Future Investigations

The results of this study show that ER based adaptive beam structures are potentially applicable for semi-active vibration control. The results also show that further investigation for the eventual physical realization of this application must be accomplished apriori. The further investigation, as pointed out in the preceding sections, are related to the understanding of the ER materials rheology, modeling and control, and the effectiveness of multi-electrode structures

The development of a better rheological testing apparatus for ER materials must be developed. The device must be able to increase the frequency range to at least 1000 Hz., and provide a controlled temperature environment similar to many of the real world applications. The sensitivity of a device specifically for measuring materials with small phase angle must be improved. More investigations on the reliability, and material behavior should be done to push this application from a pure R & D environment to commercialization.

A control scheme for ER based adaptive structures needs to be developed. This investigation has shown that two prior theories used in modeling the dynamic response of 3 layer composite structures are useful. The next step is to investigate possible sensors used in the structure, and a control algorithm. The current research being done at Lehigh involves the use of fiber optic embedded sensors and neural networks for control. Fiber optic sensors are being used because of their ability to function in environments with high electric fields unlike resistance based strain gages. Neural networks are being

utilized due to the non-linearities of the structural response and intrinsic robustness of the methodology.

The first control algorithm for a single location-single frequency system has been devised. The control scheme developed will minimize the vibration at one location on a beam structure in simply supported boundary conditions for a single excitation frequency. Figure 6.4.1 shows what the electric field should be for optimal response in the presence of a given forcing frequency between 0 to 250 Hz. The flat part of the optimal electric field curve on Figure 6.3.1 is the limit of the power supply rather than the actual optimal electric field. A neural network has been created to simulate these results and the actual creation of a ER based adaptive structure is in progress.

The research intends to devise control algorithms for multiple location-single frequency, and multiple location-multiple frequency systems. The complexity of these algorithms is related to the dynamics of the ER based structures. If a single location-single frequency control scheme is incorporated it is possible that the response of other locations and at other frequencies will dramatically increase. For example, if a structure exhibits simply supported mode 1 behavior and the amplitude at the midpoint is minimized by pushing the frequency response to simply supported mode 2, then the quarter point locations will dramatically increase. The structure has minimized the midpoint while maximized the quarter points. Another example is that if the response at one frequency is minimized by shifting the frequency response to the right via an electric field, the response at other frequencies could be enhanced. This is more clearly observed in Figure 4.4.1.

The investigation also intends to devise algorithms for the application of multi-electrode ER based structures. The use of mult-electrode structures in increasing the

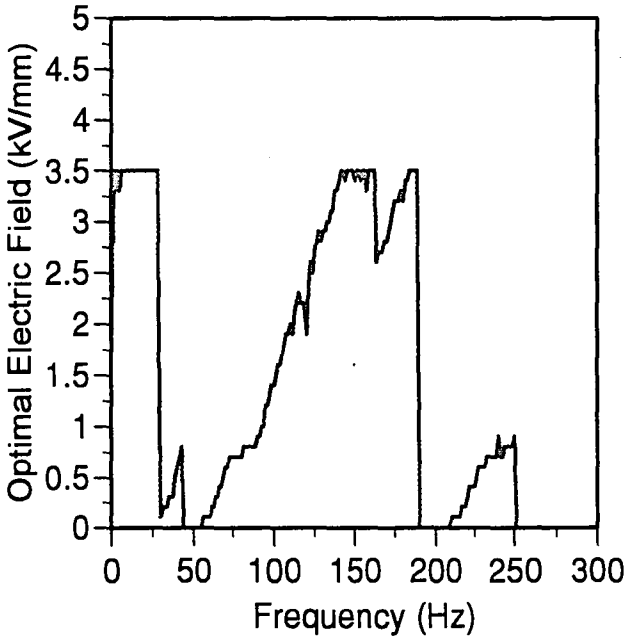

Figures 6.4.1 Optimal Electric Field to Minimize Vibration at One Location on a Structure

robustness of semi-active vibration control has been proven in the present study. There needs to be more investigation into the applicability of these structures; specifically, research in the use of different electrode configurations and geometrys and how they affect the frequency response and modal shapes. A experimental system that is more sensitive in measuring mode shapes needs to be developed. Control schemes for multi-electrode structures will follow after a more thorough feasibility analysis.

ER based adaptive structures have been shown to be an potential solution to many vibration problems. Significant research has been done in the present study related to the rheology, modeling and control, and feasibility. From this investigation the directions of further efforts to create real structures have been clearly defined.

BIBLIOGRAPHY

1. Block, H. and J.P. Kelly, *Electro-rheology*. J. Phys. D: Appl. Phys., 1988. **21**: p. 1661-1677.

2. Gast, A.P. and C.F. Zukoski, *Electrorheological Fluids as Colloidal Suspensions*. Advances in Colloid and Interface Science, 1989. **30**: p. 153-202.

3. Jordan, T.C. and M.T. Shaw, *Electrorheology*. IEEE Transactions on Electrical Insulation, 1989. **24**(5): p. 849-878.

4. Weiss, K.D., J.P. Coulter, and J.D. Carlson. *Electrorheological Materials and Their Usage in Intelligent Material Systems and Structures, Part I: Mechanisms, Formulations and Properties*. in *Recent Advances in Adaptive and Sensory Materials and Their Applications*. 1992. Blacksburg, Virginia: Technomic Publishing Co., Inc.

5. Winslow, W.M., *Induced Fibration of Suspensions*. Journal of Applied Physics, 1949. **20**(12): p. 1137-1140.

6. Klingenberg, D.J. and C.F.Z. IV, *Studies on the Steady-Shear Behavior of Electrorheological Suspensions*. 1990. : p. 15-24.

7. Hill, J.C. and T.H. Van Steenkiste, *Response Times of Electrorheological Fluids*. Journal of Applied Physics, 1991. **70**(3).

8. Stangroom, J.E., *Electrorheological Fluids*. Physics Technology, 1983. **14**: p. 290-296.

9. Jordan, T.C., Shaw, M.T., McLeish, T.C.B., *Viscoelastic Response of Electrorheological fluids. II. Field Strength and Strain Dependence*. Journal of Rheology, 1992. **36(3)**: p. 441-463.

10. Tao, R. and J.M. Sun, *Three-Dimensional Structure of Induced Electrorheological Solid*. Physical Review Letters, 1991. **67**(3): p. 398-401.

11. Halsey, T.C., *The Structure and Dynamics of Electrorheological Fluids*. Proceeding of the Conference on ER Fluids, 1991. : p. 37-52.

12. Klass, D.L. and T.W. Martinek, *Electroviscous Fluids. II. Electrical Properties*. Journal of Applied Physics, 1967. **38**(1): p. 75-80.

13. Klass, D.L. and T.W. Martinek, *Electroviscous Fluids. I. Rheological Properties.* Journal of Applied Physics, 1966. **38**(1): p. 67-74.

14. Wong, W. and M.T. Shaw. *The Role of Water in Electrorheological Fluids.* in *Electrorheological Fluids.* 1989. Raleigh, North Carolina: Technomic Publishing Company, Inc.

15. Block, H., *et al.*, *Materials and Mechanisms in Electrorheology.* Langmuir, 1990. **6**(1): p. 6-14.

16. Filisko, F.E., *Rheological Properties and Models of Dry ER Materials.* Proceedings of the International Conference on Electrorheological Fluids, 1991. : p. 116-128.

17. Vinogradov, G.V., *et al.*, *Viscoelastic Behavior of Electrorheological Suspensions.* Inzhenerno-Fizicheskii Zhurnal, 1986. **50**(4): p. 605-609.

18. Shulman, Z.P., E.V. Korobko, and Y. Yangovskii, *The Mechinism of the Viscoelastic Behaviour of ER Suspensions.* Journal of Non-Newtonian Fluid Mechanics, 1989. **33**: p. 181-196.

19. Block, H., Rattray, P., Watson, T., *Semi-Conducting Polymers as ER Fluid Substrates.* Proceedings of the International Conference on Electrorheological Fluids, 1991. : p. 93-115.

20. Hartsock, D.L., R.F. Novak, and G.J. Chaundy, *ER fluid requirements for automotive devices.* The Journal of Rheology, 1991. **35**(7): p. 1305-1326.

21. Lingard, S. and W.A. Bullough. *Tribological Aspects of Electro-Rheological Fluid Behaviour with Respect to Non-Polar Base Liquids.* in *Electrorheological Fluids.* 1989. Raleigh, North Carolina: Technomic Publishing Company, Inc.

22. Duclos, T.G., *Design of Devices Using Electrorheological Fluids.* 1988, Society of Automotive Engineers:

23. Yen, W.S. and P.J. Achorn, *A Study of the Dynamic Behavior of an Electrorheological Fluid.* Journal of Rheology, 1991. **35**(7): p. 1375-1384.

24. Coulter, J.P., Duclos, T.G., Acker, D.N., *Electrorheological Materials in Structural Damping Applications.* Accepted for publication Journal of Sound and Vibration, .

25. Gamota, D.R. and F.E. Filisko, *Dynamic mechanical studies of electrorheological materials: Moderate frequencies*. Journal of Rheology, 1991. **35**(3): p. 399-425.

26. Gamota, D.R. and F.E. Filisko, *High Frequency Dynamic Mechanical Study of an Aluminosilicate Electrorheological Material*. Journal of Rheology, 1991. **35**(7): p. 1411-1425.

27. Coulter, J.P., K.D. Weiss, and J.D. Carlson. *Electrorheological Materials and Their Usage in Intelligent Material Systems and Structures, Part II: Applications*. in *Recent Advances in Adaptive and Sensory Materials and Their Applications*. 1992. Blacksburg, Virginia: Technomic Publishing Co., Inc.

28. Rogers, C.A. *Workshop Summary*. in *U.S. Army Research Office Workshop on Smart Materials, Structures, and Mathematical Issues*. 1989. Virginia Polytechnic Institute and State University: Technomic.

29. Carlson, J.D., J.P. Coulter, and T.G. Duclos, *Electrorheological Fluid Composite Structures*, in *U.S. Patent #4,923,057*. 1990.

30. Coulter, J.P. and T.G. Duclos. *Applications of Electrorheological Materials in Vibration Control*. in *Electrorheological Fluids*. 1989. Raleigh, North Carolina: Technomic Publishing Company, Inc.

31. Gandhi, M.V., B.S. Thompson, and S.B. Choi, *A New Generation of Innovative Ultra-Advanced Intelligent Composite Materials Featuring Electro-Rheological Fluids: An Experimental Investigation*. Journal of Composite Materials, 1988. **23-December, 1989**: p. 1232-1255.

32. Gandhi, M.V. and B.S. Thompson, *A New Generation of Revolutionary Ultra-Advanced Intelligent Composite Materials Featuring Electro-Rheological Fluids*, in *Smart Materials, Structures, and Mathematical Issues*, C.A. Rogers, Editor. 1989, Technomic Publishing Co., Inc.: Lancaster, Pennsylvania. p. 63-68.

33. Gandhi, M.V. and B.S. Thompson. *Dynamically-Tunable Smart Composites Featuring Electro-Rheological Fluids*. in *Fiber Optic Smart Structures and Skins II*. 1989. Boston, MA: SPIE-The International Society for Optical Engineering.

34. Choi, S.B., M.V. Gandhi, and B.S. Thompson. *An active vibration tuning methodology for smart flexible structures incorporating electro-rheological fluids: A proof-of-concept investigation*. 1989.

35. Coulter, J.P., T.G. Duclos, and D.N. Acker. *The Usage of Electrorheological Materials in Viscoelastic Layer Damping Applications.* in *Damping 89.* 1989. Palm Beach, Florida:

36. Choi, Y., A.F. Sprecher, and H. Conrad, *Response of ER Fluid-Filled Laminate Composites to Forced Vibration.* •Journal of Intelligent Material Systems and Structures, 1992. **3**: p. 17-29.

37. Choi, S.B., Thompson, B.S., Gandhi, M.V., *Vibration Tuning of Smart Cantilevered Beams Featuring Elecrto-Rheological Fluids.* 1992 Submitted for publication. .

38. Choi, S.B., B.S. Thompson, and M.V. Gandhi. *An Experimental Investigation on the Active-Damping Characteristics of a Class of Ultra-Advanced Intelligent Composite Materials featuring Electro-Rheological Fluids.* in *Damping 89.* 1989. Palm Beach, Florida:

39. Gandhi, M.V., B.S. Thompson, and S.B. Choi, *A Proof-of-Concept Experimental Investigation of a Slider-Crank Mechanism Featuring a Smart Dynamically Tunable Connecting Rod Incorporating Embedded Electro-Rheological Fluid Domains.* Journal of Sound and Vibration, 1989. **135**(3): p. 511-515.

40. Spurk, J.H., Huang, Z., *Electrorheological Material Under Oscillatory Shear.* Recent Advances in Adaptive and Sensory Materials and their Applications, 1992. : p. 593-604.

41. Thurston, G.B. and E.B. Gaertner, *Viscoelasticity of Electrorheological Fluids During Oscillatory Flow in a Rectangular Channel.* Journal of Rheology, 1991. **35**(7): p. 1327-1343.

42. Shulman, Z.P. *Viscoelastic Behaviour of Electrorheological Fluids.* in *Electrorheological Fluids.* 1989. Raleigh, North Carolina: Technomic Publishing Company, Inc.

43. Brooks, D., *et al., Visco-elastic Studies on an Electro-Rheological Fluid.* Colloids and Surfaces, 1986. **18**: p. 293-312.

44. Ross, D., E.E. Ungar, and E.M. Kerwin, *Damping of Plate Flexural Vibrations by means of Viscoelastic Laminate.* Structural Damping, 1959. **ASME**: p. 49-88.

45. Nashif, A.D., D.I. Jones, and J.P. Henderson, *Vibrational Damping.* 1985, John Wiley & Sons.

46. Mead, D.J. and S. Markus, *The Forced Vibration of a Three-Layer, Damped Sandwhich Beam with Arbitrary Boundary Conditions*. Journal of Sound and Vibration, 1969. **10**(2): p. 163-175.

47. Mahjoob, M.J., H.R. Martin, and F. Ismail. *Distributed Vibrational Control Using Electrorheological Fluids.* in *International Modal Analysis Conference.* 1993. Florida:

48. Chrzan, M.J., Coulter, J.P., *A Numerical Investigation of Electrorheological Material Behavior*. Proceedings of the International Conference on Electrorheological Fluids, 1991. : p. 175-194.

49. Meirovitch, L., *Analytic Methods in Vibrations*. Macmillian, New York, 1967.

50. Coulter, J.P., K.D. Weiss, and J.D. Carlson, *Engineering Applications of Electrorheological Materials*. Journal of Intelligent Material Systems and Structures, 1993. **4**: p. 248-259.

VITA

David L. Don was born August 2, 1968 in Pasadena, California to parents of Dr. Sherman Don and Gloria Chang. After graduating from Atholton High School in June 1986, the author began his undergraduate studies at the University of Maryland at College Park, Maryland. The author completed his undergraduate studies at Lehigh University in Bethlehem, Pennsylvania with a Bachelor of Science degree in Mechanical Engineering. He continued his studies as a National Science Foundation funded research assistant at Lehigh University under the direction of Dr. John P. Coulter. In June 1993, the author received has Master's of Science degree in Mechanical Engineering. Presently, the author plans to gain practical engineering experience in industry and eventually continue his studies towards a Doctor of Philosophy degree in Mechanical Engineering.

END

OF

TITLE